

**DLR-IB-RM-OP-2018-161**

**Viscosity Perception of Virtual  
Fluids rendered by a Hand  
Exoskeleton**

**Masterarbeit**

Annika Schmidt



**DLR**

**Deutsches Zentrum  
für Luft- und Raumfahrt**

## MASTERARBEIT


# VISCOSITY PERCEPTION OF VIRTUAL FLUIDS RENDERED BY A HAND EXOSKELETON

Freigabe:

Der Bearbeiter:

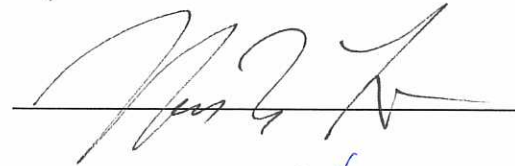
Unterschriften

Annika Schmidt



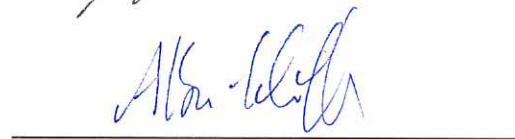
Betreuer:

Dr. Neal Y. Lii



Der Institutsdirektor

Prof. Alin Albu-Schäffer

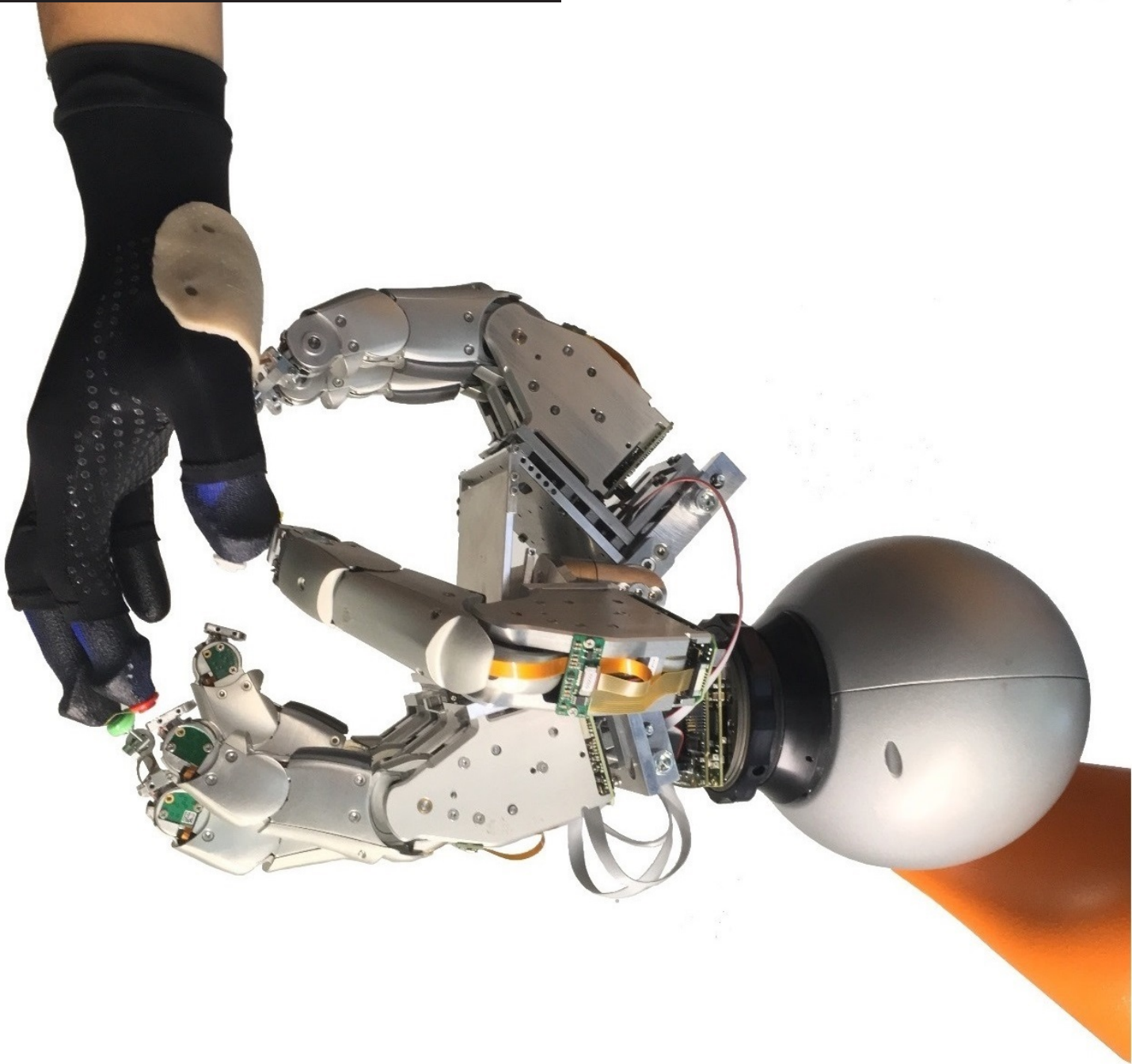


Dieser Bericht enthält 91 Seiten, 71 Abbildungen und 5 Tabellen

# Viscosity Perception of Virtual Fluids rendered by a Hand Exoskeleton

Annika Schmidt

Technische Universiteit Delft



# VISCOSITY PERCEPTION OF VIRTUAL FLUIDS RENDERED BY A HAND EXOSKELETON

THESIS

by

**Annika Schmidt**

in partial fulfillment of the requirements for the degree of

**Master of Science**

in Mechanical Engineering  
(Track of Bio-Mechanical Design)

at the Delft University of Technology

September 6th, 2018

Supervisors:	Prof. Dr. ir. D. Abbink Dr. N. Y. Lii	TU Delft DLR
Thesis committee:	Prof. dr. ir. D. Abbink Dr. J. Hartcher-O'Brian Dr. H. Boessenkool Dr. N. Y. Lii	TU Delft TU Delft TU Delft DLR

*This thesis is confidential and cannot be made public until September 6th, 2019.*

An electronic version of this thesis is available at <http://repository.tudelft.nl/>.



# PREFACE

This master thesis is the final project submitted for the degree of Master of Science in Mechanical Engineering, Track of Bio-Mechanical Design at Technical University Delft, Netherlands. It is developed at and in cooperation with the Robotic and Mechatronics Institute of the German Aerospace Center (DLR) in Oberpfaffenhofen, Germany.

The main objective of this work was the development and validation of a rendering algorithm for viscous fluids, that can run on very high update rates ( $\approx 1$  kHz), to be implemented in a novel hand exoskeleton as dexterous haptic device developed by the DLR. This work is original to the best of my knowledge, except where acknowledgments and references are made to previous work.

The first part of this report consists of a scientific conference paper summarizing the main findings, conclusions and recommendations of my work. The second part consists of appendices which include details about the hardware, considered fluid dynamics, algorithm implementation and the user studies to allow future students and researchers to perform post research on the output of this study.

I would like to thank everyone who contributed to this project. In particular my thank goes to my supervisors Prof. Dr. ir. David Abbink, whose constructive feedback and asking the right questions helped me to get a deeper understanding of the performed research and Dr. Neal Y. Lii, who did not only give me the chance to get hands-on experience on novel robotic systems, but also taught me some valuable life lessons. A special thank you goes to all members of the MODEX Lab of the DLR, above all Almost-Dr. Aaron Pereira for many helpful suggestions when I was stuck on a problem and Benedikt Pleitinger for repetitive help in fixing the exoskeleton fingers in record time throughout my experiment. In addition, I would like to thank Niels Terleth for the endless patience in discussing flow phenomena of all kinds and mental support when nothing made sense. Last but not least, I want to thank my parents for giving me the opportunity to always pursue my goals in various geographical locations.

*Annika Schmidt  
Delft, August 2018*

# PAPER

# Viscosity Perception of Virtual Fluids rendered by a Hand Exoskeleton

Annika Schmidt, Aaron Pereira, Thomas Baker, Benedikt Pleitinger, Thomas Hulin, Zhaopeng Chen, David A. Abbink, Neal Y. Lii

**Abstract**—Enabling haptic interaction with non-solid materials, such as liquids or sediments, could expand possibilities for exploration of virtual or remote environments, which would e.g. enable training divers and astronauts in simulators. To allow application of natural investigation procedures in such scenarios, haptic interfaces with several degrees of freedom (DOF) are necessary, which allow the interaction with a variety of solid objects as well as different surrounding mediums. The goal of this work is to develop an algorithm for a high-DOF hand exoskeleton as haptic interface connected to five points on the human hand, that enables the perception of virtual fluids by rendering the fluids' prominent proprioceptive characteristic (viscosity). To allow simultaneous rendering of virtual solid objects of varying stiffness, a high update rate should be maintained. To quantify human perception of the rendered fluid, two user studies are carried out. The first investigates the ability to perceive fluids of low viscosity such as water, while the second deals with the discrimination ability for higher viscous virtual fluids. For virtual fluids with low viscosity, it is found that a linear relationship exists between the rendered and perceived viscosity with a scaling factor of 2. Fluids with high viscosity ( $> 10 \text{ Pa s}$ ) can be discriminated well, achieving similar values for the Weber fractions ( $w = 0.3$ ) as are found in real interactions with fluids. The results of both experiments prove that properties of fluids rendered using simplified models to allow high update frequencies (833 Hz) can still be discriminated by human users.

**Index Terms**—human machine interaction, multi-finger force feedback, proprioception, drag forces, fluid dynamics.

## 1 INTRODUCTION

HAPTICS allow humans to feel and physically interact with systems in an immersive way by stimulating the human's proprioceptive and tactile senses via a haptic interface [1]. Such interfaces can be as simple as force-reflecting joysticks. However, dexterous haptic devices, often summarized under the term "hand exoskeletons", can enable truly intuitive and realistic interaction with a virtual environment by allowing humans to use the hands naturally. Such robotic devices are coupled to the human hand and follow hand and finger motions. Each finger can receive independent force feedback to help perceiving the virtual reality in a more natural way. A variety of exoskeletons are available [2, 3, 4], which allow interaction with solid bodies, e.g. allowing the user to investigate the shape and stiffness of a virtual object. While this suffices for many applications, it does not make use of the full potential of haptic technology. In order to fully explore an unknown environment, not only solid objects should be rendered, but also other mediums, such as fluids or sediments. However, the perception of such materials differs and tactile senses might be more important, since the feeling of wetness is a unique characteristic property of fluids [5]. Another important characteristic of fluids is dynamic viscosity, which describes the relationship between shear rate and shear stress. Removing tactual cues by using a spatula instead of the finger directly to investigate the viscosity of a fluid shows that the discrimination ability of

humans is similar for both procedures [6]. This indicates the dominating importance of proprioception for the perception of viscosity. Since viscosity is also commonly occurring property in mechanical systems (alongside inertia and friction), it can also be perceived in the interaction with a haptic interface. Jones and Hunter showed in 1993 that the human perception of such mechanical viscosity is very similar to the one of dynamic viscosity in liquids [7]. This allows to actively render a fluid's dynamic viscosity on a haptic interface. Attempts to implement haptic rendering of virtual fluids on endpoint devices have been made [8, 9, 10, 11, 12], but the capabilities are still limited. When using one-point virtual probes, interaction possibilities with virtual fluids are limited to motions like stirring [10, 11, 12] or moving the liquid in some sort of container [9]. This kind of fluid interaction does not suffice when aiming to carry out complex or dexterous tasks such as sweeping sediment or plunging the hand into a liquid. Additionally, with exception of the work by Dobashi (500 Hz) [10], all haptic simulations run on low rendering frequencies (30 - 120 Hz). This might be a sufficient update rate for fluid interactions only, but make it impossible to incorporate stable and crisp contact with stiff bodies, for which a frequency of 1 kHz is accepted to be sufficient [1].

This paper proposes a haptic rendering algorithm for a hand exoskeleton with multiple interface points running on very high update rates (833 Hz) to allow interaction and perception of virtual fluids and stiff bodies alike. To validate the human perception abilities for rendered fluids of varying viscosity two human-in-the-loop experiments are carried out: firstly, a fluid with familiar properties (water) is rendered, to compare the human perception of the virtual fluid with the feeling of the physical counterpart and sec-

- A. Schmidt and D. A. Abbink is with the Department of Mechanical, Maritime and Materials Engineering, Delft University of Technology, Delft, Netherlands.
- A. Schmidt, A. Pereira, T. Baker, B. Pleitinger T. Hulin, Z. Chen and N. Y. Lii are with the German Aerospace Center, Oberpfaffenhofen, Germany

only, a wider variety of viscosity is rendered to investigate the discrimination abilities of virtual fluids. Eventually the overall findings are discussed and future implementation possibilities are considered.

## 2 RELATED WORK ON HAPTIC FLUID RENDERING

For a long time the focus of haptic rendering has been the realistic perception of virtual solid bodies, mainly considering compliance. In recent years the rendering of frictional effects and some textures has become possible [1], however, haptic rendering of interaction with liquids has barely been investigated. With increasing computing power it is possible to further expand the capabilities of current haptic devices. Most devices deliver only force feedback, making the perception of wetness impossible, since this stimulates the human's tactile sense. Viscosity, however, relates velocity to force and can be felt by the human operator through force feedback [5]. A method to compute the appropriate fluid forces was first proposed by Baxter and Lin in 2004 [8]. Their work suggests using a numerical method based on Navier-Stokes equations of fluid motion. In this Computational Fluid Dynamics (CFD) simulation the boundary of the haptic probe is discretized. This method calculates the forces quite accurately, but is limited to small amounts of fluid and simple probe shapes due to the resource intensive calculations, and runs only at 60 Hz. By adding a force filtering technique, Baxter and Lin were able to increase the rate to commonly used 1000 Hz of a haptic loop while only introducing minor artefacts. This was found to be acceptable for fluids, but could not incorporate rigid body contact in the same simulation, since it would lead to instability. Another numerical approach was introduced by Cirio et al [9]. Applying a Smoothed-Particle Hydrodynamics (SPH) simulation, both fluid and solid bodies are represented by particles with forces occurring opposite to the particle's movement at the contact point. With this method a 6 DOF haptic interaction with fluids of variable viscosity with arbitrary shaped bodies was possible at a frequency of 60-120 Hz. This is also computationally expensive and due to the low frequency again limited to solely interacting with fluids. Additionally, unconditional stability could not be guaranteed.

Other techniques that allow more efficient rendering of fluids in real-time use pre-calculated or pre-recorded data. Dobashi et al. [10] decompose the dynamics of the fluid into a linear and nonlinear part. The linear flow is rapidly calculated using linearized Navier-Stokes equations. The complex and highly nonlinear flow around the emerged rigid body is pre-computed. Both parts are then combined for real-time haptic interactions, enabling the algorithm to work at 500 Hz. However, requiring pre-computations for every interaction scenarios limits general applicability. Instead of using computed models of the fluid behavior, Höver et al. recorded data of arbitrary manipulation of an object in multiple viscous fluids [11]. This data was then interpolated, so that the user is not only limited to the same pre-recorded motions in the virtual fluid. It could be shown that with this method, the interaction forces of the recorded fluids could successfully and realistically rendered. However, the method is limited to interaction with pre-recorded materials

and the dimensionality of the interpolation domain for more complex shapes increases considerably, once more leading to expensive computations.

Vines et al. apply simplifications and approximations to the flow. The fluid surface is modeled as a mass-spring network of connected particles, which enabled the rendering of waves [12]. For the perception of the inner flow, the haptic probe is represented as a particle in the fluid simulation. Forces arising from the viscosity and inertia effects of the fluid were calculated with simplified formulas to be proportional to the velocity and position respectively [13]. This reduces computing power, but leads to lower level of perceived realism.

## 3 HAPTIC INTERFACE DESCRIPTION

The haptic interface used in this research work is a novel hand exoskeleton developed by the German Aerospace Center (DLR). The new system combines the multisensory fingers previously developed at the DLR [14], of which a maximum of six can be mounted on a platform. The fingers can be arranged in different positions, forming a reconfigurable haptic interface that can be adjusted to fit various applications. In the current set up, five robotic fingers are arranged on the platform to form an exoskeleton opposing the human hand [15], similar to the principle introduced by the Gifu University [16]. A key difference is that two of the robotic fingers connect to the palm of the human hand, while the remaining three attach to the thumb, index and middle finger as can be seen in Fig. 1. In the following sections, those points will be referred to as *palm points* and *finger points*. The attachment to all points is realized through a magnetic clutch for which the human user has to wear a custom made glove and finger sleeves. This ensures easy detachment in case of high forces from the exoskeleton. Each robotic finger has four joints, of which two are coupled,

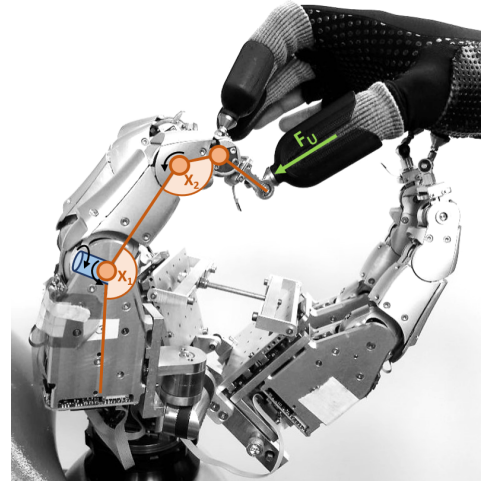


Fig. 1. Novel hand exoskeleton used as haptic interface attached to two palm points of the human user's hand, as well as three finger points (thumb, index and middle).  $X_1$  (base) and  $X_2$  (distal) represent the joint angles of the two active extension joints (orange). Together with the angle measured in the abduction joint in the base (not shown), the position vector  $X$  is given which can be measured by position encoders.  $F_U$  stands for the force applied to each robotic finger by the human.

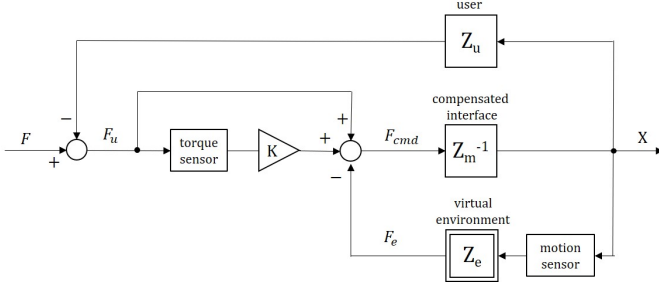


Fig. 2. The block scheme of impedance interaction with feed-forward compensation implemented for each individual robotic finger on the novel haptic interface, where  $F$  describes the applied forces and  $X$  the joint positions.

resulting in three degrees of freedom (DOF) per finger. Since each robotic finger is defined through a known kinematic chain, the position of the attachment point on the human hand in space can be calculated. The inclusion of the palm points prevents ambiguity of the human hand position, which enables the tracking of the human hand [17] without additional hardware such as the cyberglove [18]. To extend the workspace and enable the user to move around in space, the exoskeleton is mounted on a KUKA Light Weight Robot (LWR) [19]. This device has been shown to be a powerful haptic interface by itself, and can also be used to give additional haptic feedback in this setup [20,21]. The control of the LWR is described in [22], while the control of the exoskeleton is based on the work carried out by Chen et al. [23,24]. The identical modular robotic fingers are each treated as a separate system and individually controlled. The high level control loop for each individual robotic finger is depicted in Fig. 2. It runs at update frequency of 833 Hz. The human user  $Z_u$  and the virtual environment  $Z_e$  act as an impedance, while the haptic interface is modelled as admittance. The angles of the active joints  $X$  can be measured through position encoders in each robotic finger [14], which are used to calculate forces in the virtual environment  $F_e$ . Torque sensors in each controllable robotic finger joint measure the resultant force of the human user  $F_u$ , which allows adding a feed-forward term to reduce the perceived inertia. Together with the applied forces of the user and the rendered forces from the virtual environment, the total forces  $F_{cmd}$  to be applied to the haptic interface are determined. The forces are converted to torques, incorporating additional friction compensation [25]. Finally, the torques move the robotic fingers joints.

Considering this, the impedance felt by the human user is

$$\frac{X}{F} = \frac{1}{Z_u + \frac{Z_m}{1+K} + \frac{Z_e}{1+K}} \quad (1)$$

This shows that the feed-forward gain reduces the perceived dynamics of the haptic interface, however, the rendered forces are also reduced. This could be compensated through an additional gain applied to the forces of the virtual environment as explained by Gil and Sanchez [26]. Nevertheless, it is referred from implementing it, as tests have shown that noticeable dynamics of the robotic remain. These include friction and inertia, but also mechanical viscosity of the system. This mechanical viscosity is perceived by humans

similarly to the viscosity of fluids [5]. In contrast to most haptic experiments, this work aims to render the viscosity of virtual fluids. Thus the mechanical viscosity is added to the rendered one, therefore acting as a gain of unknown value. For this reason, no additional gain is added in the control model. The human user does not only interact with the exoskeleton, but also with the LWR. This allows execution of a motion similar to stroking through a fluid, feedback is not only given to the human hand, but rather the total hand arm system. For this reason, the sum of the forces acting on the hand, are additionally forwarded to the LWR, which leads to perceivable viscosity forces in the human arm, which should make the interaction more realistic.

## 4 STUDY 1: PERCEPTION OF VIRTUAL WATER

This experiment investigates if the viscosity of water with simplified flow properties can be rendered on high update rates, while being perceivable as stable and realistic by the human user. It assesses how the human user perceives the virtual fluid compared to the real one and how disturbing the dynamics of the haptic interface are to the humans perception.

### 4.1 Viscosity Rendering

Calculating all forces acting during the interaction with a fluid is a complex task, especially when taking into account turbulence, waves and particle interactions. Resource intensive computations are required, which makes rendering at very update frequencies impossible. Therefore, this work follows the approach of Vines et al. [12] to simplify the fluid properties and limit the rendering to the minimum necessary, namely the fluid viscosity. However, in contrast to past implementations of fluid rendering where only single point-probe haptic interfaces were used, the use of a hand exoskeleton in this study allows the human user a wider variety of investigative movements. Accounting for all such movements complicate the scenario and thus the calculations. Therefore, in this first attempt the interaction is limited to one motion, which is defined to be a sweeping motion through the fluid, similar to what can be observed when investigating real fluids. The fingers of the human are assumed to be close together with the maximum frontal area of the hand pointing in the direction of motion. For this motion no lift forces occur on the hand [27] and lift can thus be neglected. Further, buoyancy is not considered, since water is of similar density to the human body [28]. Therefore, in this simplified scenario the main contribution of forces is through drag components. Those are defined to always act against the direction of motion and their magnitude can be calculated using the drag equation [29]

$$F_D = \frac{1}{2} \rho v^2 A C_D \quad (2)$$

where  $\rho$  is the density, taken to be  $1000 \text{ kg/m}^3$  and  $v$  the velocity of the flow or the body moving through the flow, which can be measured through encoders on the haptic interface.  $A$  refers to a reference area, which can be taken to be the maximum projected area of the human hand, here set to be  $0.0148 \text{ m}^2$  as proposed by Sato and Hino [30].



$C_D$  refers to the drag coefficient, which has been determined for the human hand in various studies [27] finding a relationship to the angle of attack for the flat hand with extended fingers. Even though the magnitude range varies depending on the applied procedures and methods of measurement, a distinctive curve shape can be observed. Fitting a sinusoid to an exemplary drag coefficient curve [30] leads to the relationship

$$C_D = -0.3105 \cdot \cos(2\alpha) + 0.5794 \quad (3)$$

where  $\alpha$  is the angle of attack, which can be determined in the haptic interface from encoders. Substituting the coefficient relation in equation 2 leads to an analytic expression for the drag forces, which should correspond in magnitude to the literature [27, 31]. This expression is implemented in the control loop of the hand exoskeleton and divided over the robotic finger in proportion to the amount of area the forces at each attachment point act on. The finger points are assumed to act on the entire finger, and the palm points act on the palm in equal measure (ring and little finger, and the body beyond the wrist, are not considered). This leads to 10% of the drag force being applied on thumb, index and middle finger, and 35% on both of the palm points.

## 4.2 Methods

This experiment investigates the relationship between the given viscosity and the perceived viscosity by the human user when taking into account the residual system dynamics of the haptic interface. Pilot studies found 0-4 to be a sufficient scaling range for this investigation. To remove regression bias, a combination of magnitude estimation and magnitude production is applied. During the estimation part, the user is presented with scaled forces and has to estimate the intensity of the stimulus, where 100 % defines the feeling of water. Three trials are carried out, within each 9 scaling factors (0-4 in steps of 0.5) are presented in pseudo-randomized order. During the production part of the experiment, the human user is asked to set the given stimulus until the virtual fluid can be perceived to have the viscosity of water (100 %), starting from a scaling factor in the range of 0-4. Each scaling factor is used as starting point once, leading to a repetition of 9 times, and the order is randomized. In a second and third trial, the user repeats the procedure adjusting the stimulus to be perceived as 50 % and 200 % viscosity of water, respectively. Whether the participants started with the magnitude estimation or production was randomly assigned.

The setup for this experiment is shown in Fig. 3. The human user faces the robotic interface with the right hand attached to the exoskeleton. After some minutes of exploring free space to get familiar with the system dynamics, three example trials are given to ensure the participants understood the task. For the experiments, the participants are asked to carry out a horizontal sweeping motion while imagining a wall of virtual fluid to be in front of them. The stroke amplitude and velocity are not specified, but left the user's discretion, to enable a more natural interaction. The verbal answers of the participants are noted by the experimenter, while system data, such as occurring and rendered torques as well as hand and finger trajectories are

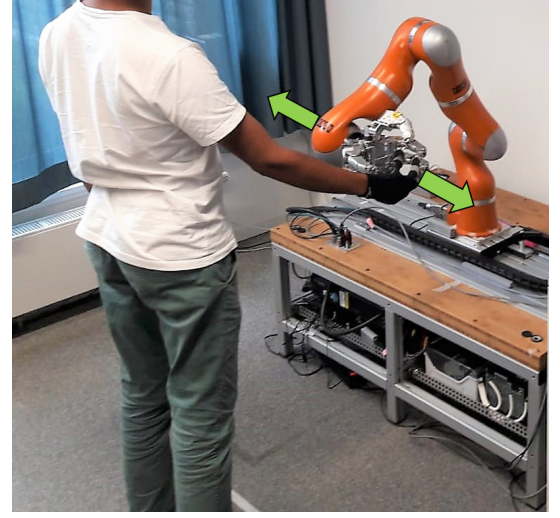


Fig. 3. Testing setup for the user studies with the participant being positioned in front of the robotic device. The human hand is attached to the hand exoskeleton, which is mounted on a KUKA LWR. The green arrows indicate the specified direction of motion to investigate the virtual fluid.

recorded with a sampling time of 1 kHz. Additionally, the experiment is recorded with a camcorder for the purpose of reviewing the human-robot interaction later on. To analyze this experiment, a curve is fitted to the results of all participants for magnitude estimation and production. To find the overall relationship between the given stimulus and the perceived viscosity, the mean data is calculated for both experiment parts and fitted with a power function of the form

$$S = kI^a \quad (4)$$

where  $S$  is the sensation magnitude, here the perceived viscosity by the human user, and  $I$  the set intensity of a stimulus, determined through the scaling factor. The exponent  $a$  describes the relationship between the two, while  $k$  is an arbitrary constant, that determines the scale unit.

## 4.3 Participants

13 right-handed people (four female) between the ages of 21 and 29 took part in the study. All had an engineering background. Seven had interacted with a haptic interface before, of whom two had significant knowledge in the field of haptics.

## 4.4 Results

It was possible to render the virtual viscosity such that it was perceived to be stable by all participants, where no unwanted vibrations or perturbations could be felt. However, due to the remaining dynamics of the haptic interface it was not possible to directly compare the viscosity to real water, as the perceived mechanical viscosity in free space already exceeded the viscosity perceivable in the physical fluid. Therefore the participants were verbally instructed to take into account the inherent dynamics of the system and indicate when the virtual fluid was identifiable to be water compared to the feeling of free space. Nevertheless,

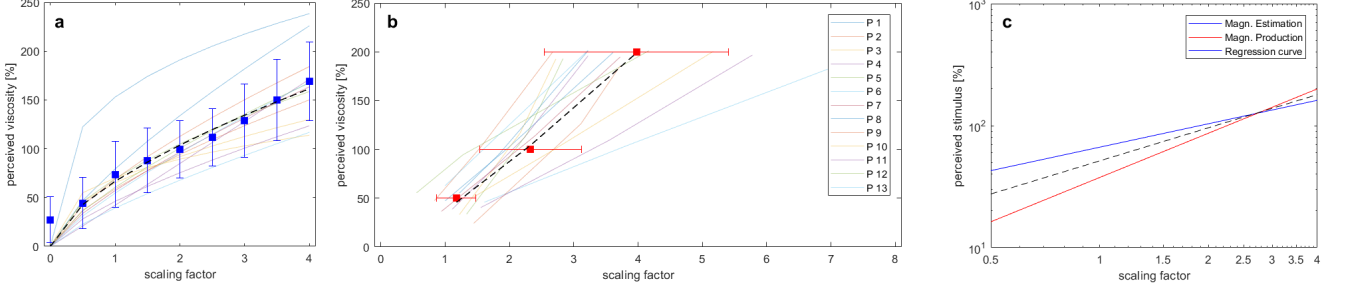


Fig. 4. Results of Study 1, showing the relationship between the perceived viscosity of virtual water to the set scaling factor in magnitude estimation (a) and production (b). Each colored line corresponds to the results of one participant. The curves are fitted with a power function to obtain the general relationship. The squares depict the averaged values ( $n = 13$ ) with the error bars indicating the standard deviation. (c) shows the comparison of the fitted power functions of the two procedures in with a fitted regression curve.

consistent results could be obtained from all participants, as indicated in Fig. 4. Although neither the stroke amplitude nor moving velocity were specified, overall similar investigation procedures were found between the participants with little variation in stroke width ( $0.2600 \pm 0.0559$  m) and maximum hand velocity ( $0.4409 \pm 0.0830$  m/s). It appeared that the hand movement is led by the palm, pushing the attached exoskeleton fingers when moving forward, and pulling during the backward motion. The thumb, index and middle finger of the human seem to not be extensively used, but only counteract the motion of the palm, spreading outward when pushing forward and being flexed inward, when moving backward.

The analysis of the psychometric data also reflects a consistent behavior throughout the participants. To show that the findings per participant are causal, a regression analysis is carried out for the magnitude estimation. This shows moderate to strong correlations for all participants, except the first. The curve of this person appears to be offset from the main trend, but is not disregarded as the video review does not show abnormalities and the difference might just relate to variation in individual perception. For the magnitude production, again similar curves can be found for all participants, but a varying steepness can be seen. However, for all participants, the ratios of the set scaling factors appeared to be constant, i.e. when the participants set a higher stimulus intensity for the perception of 50 % water viscosity, they also set the stimuli proportionally higher for 100 % and 200 % perceived viscosity. A relatively constant value was found throughout the participants for the ratio between 100 and 50 % virtual water viscosity ( $1.97 \pm 0.34$ ) and 200 and 100 % ( $1.78 \pm 0.55$ ). Fitting a power function curve between the averaged points per participant for magnitude estimation (ME) and magnitude production (MP) leads to the following relationships:

$$S_{ME} = 0.6663 \cdot I_{ME}^{0.6386} \quad (5)$$

$$S_{MP} = 0.3761 \cdot I_{MP}^{1.206} \quad (6)$$

Comparing the two curves shows the effect of the expected regression bias [32]. To account for this, another curve is fitted between the curves obtained through the different procedures, leading to a general relationship between the given and the perceived stimulus of:

$$S = 0.5145 \cdot I^{0.9021} \quad (7)$$

This indicates a near-linear relationship between the given and perceived intensity of the viscosity stimulus. However, it shows that a factor of 2 has to be applied to the calculated drag forces.

#### 4.5 Revision

This first user study showed that it was possible to render virtual viscosity at high update rates (833 Hz) without introducing perceivable disturbances. Although the comparison with physical water could not be made due to the remaining dynamics of the robotic system, all participants were able to perform the experiment. By taking into account the mechanical viscosity, it was possible to find a scaling factor with which the virtual fluid could be identified to be water, even though this perception might not match the perception experienced in the physical fluid. Consistent results for psychometric data and exploration procedures throughout the participants could be observed. This shows the ability to render perceivably stable viscosity, despite quadratic dependency on moving velocity. To further investigate the human capabilities compared to the interaction with real fluids, a second user study is carried out. However, for this it is necessary to reconsider the force equation, as the relationship used for the drag coefficient has only been shown to be valid for water.

### 5 STUDY 2: VIRTUAL VISCOSITY DISCRIMINATION

The experiment in Sec. 4 shows, that perceivable viscosity can be rendered at high update rates. A second experiment investigates the human capabilities for viscosity discrimination in comparison to that found for real fluids.

#### 5.1 Viscosity Rendering

Bergmann Tiest et al. observed that humans are only able clearly discriminate viscosity differences above  $2 \text{ Pa} \cdot \text{s}$  [6], which is a viscosity significantly higher than water at  $0.001 \text{ Pa} \cdot \text{s}$ . Since the relationship used for the drag coefficient is only valid for water, the formula may not apply to fluids with such high viscosity. Therefore the force equation needs to be adjusted. For this, the flow properties of higher viscous fluids are considered described by the Reynolds number [29]

$$Re = \frac{\rho v L}{\mu} \quad (8)$$

where  $L$  is a characteristic length of the emerged body and  $v$  its moving velocity.  $\mu$  and  $\rho$  describe the viscosity and density of the fluid, respectively. Toussaint proposed that the characteristic length of the human hand be the chord length ( $\approx 0.1$  m) [33]. For investigating motions with the hand the velocity can be assumed to be  $< 1$  m/s. For viscous fluids,  $\mu$  is in a range of  $2 - 100$  Pa s, while  $\rho$  can be assumed to be around  $1000$  kg/m<sup>3</sup> as applicable for many viscous silicones [34]. This leads to a Reynold's number of 1-10. Since Taamneh [35] showed the flow around ellipsoidal bodies to be perfectly laminar for  $Re \leq 24$ , the flow in the scenario in question can be approximated as Stokes flow, which allows simplifications of the drag coefficient [29]:

$$C_D = \frac{24}{Re} \quad (9)$$

Substituting this in equation 2 gives a new analytical expression for the drag force, which can be used to render fluids of higher viscosity.

## 5.2 Methods

The setup for this user study is identical to the one described for the first experiment (Fig. 3). Inspired by the research carried out by Bergmann Tiest et al. [6] the method of constant stimuli is applied to identify the human discrimination abilities of viscosities. The virtual fluids are rendered using the relationship described by equation 9, where  $\mu$  was set to be identical to that of the fluids tested by Tiest et al. for viscosity group D and E, but an additional step is added below and above the reference viscosity to get a better estimation of the psychophysical curve progression (Tab. 1).

TABLE 1

Summary of the applied viscosities in Pa s as proposed by Tiest et al. [6] for group D and E, with  $T_i$  being the test stimuli ( $T_4$  and  $T_5$  added to Tiest's viscosities) and  $R$  being the reference of each range.

Range	D	E	Range	D	E
$T_1$	1.093	10.100	$T_5$	2.203	17.505
$T_2$	1.237	11.158	$T_6$	2.553	18.950
$T_3$	1.646	13.830	$T_7$	3.185	23.200
$T_4$	1.7495	14.945	$T_8$	3.883	29.335
$R$	1.853	16.060			

A two-alternative forced-choice procedure is used, where the rendered reference viscosity is presented first, followed by a test viscosity, which must be judged to be thicker or not. Each test stimuli is presented once per trial in a random order and five trials are carried out for both viscosity groups. The order in which the groups are presented is assigned to the users at random. To quantify the discrimination abilities the percentage of times that each test stimulus is perceived thicker than the reference is determined. Ideally, for lower test stimuli than the reference this percentage should tend toward 0 % and for higher ones towards 100 %. Between the extreme points a psychometric curve can be fitted, where the steepness of the curve indicates the discrimination threshold. As proposed by Tiest et al., the fitted function is

$$f(x) = 50\% + 50\% \cdot \operatorname{erf}\left(\frac{\log(x/p)}{\sqrt{2}\log(w+1)}\right) \quad (10)$$

where  $\operatorname{erf}$  is the error function,  $p$  the reference viscosity and  $w$  the weber fraction as a free parameter.

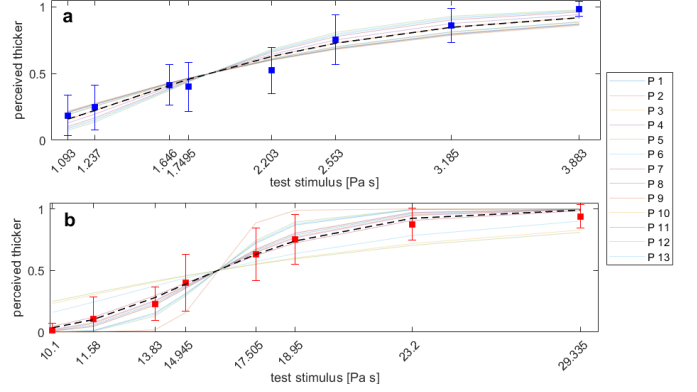


Fig. 5. Results of Study 2 giving a fitted psychometric curve defined through the Weber fraction for viscosity group D (a) and E (b) for all participants ( $n = 13$ ) and for the mean data with the error bars indicating the standard deviation.

## 5.3 Participants

13 right-handed people (four female) between the ages of 20 to 35 participated in the study. All were different from the ones in the experiment in Sec. 4, but again all had an engineering background and eleven had interacted with a haptic interface before. However, only three had significant knowledge in the field of haptics.

## 5.4 Results

Similar to the first experiment in Sec. 4, the results for all participants seem to be consistent, for the psychometric data as well as applied exploratory procedures. The average stroke amplitude over the participants ( $0.5534 \pm 0.1150$  m) was significantly greater than observed in the first experiment ( $n=11$ , t-test,  $p < 0.001$ ). For the maximum hand velocities no prominent difference to the prior findings can be seen ( $0.4130 \pm 0.0610$  m/s). However, a significant drop in the maximum mean velocity applied to investigate the viscosities in group D ( $0.4513 \pm 0.0625$  m/s) to the one in group E ( $0.3748 \pm 0.0644$  m/s) can be seen ( $n=11$ , t-test,  $p = 0.01$ ). Considering the recorded joint angles of the exoskeleton fingers and the video recordings, the motion of the human hand matches that described in the first experiment.

Fitting the psychometric curve to the data obtained from the perception answers with equation 10, for each participant the Weber fraction is determined. It can be found that the Weber fractions for viscosity group D are significantly higher ( $n = 13$ , t-test,  $p < 0.001$ ) than for group E. Averaging the data of all participants and then fitting the curve, as seen in Fig. 5, leads to a Weber fraction of  $w_D = 0.6974$  for group D and  $w_E = 0.2928$  for group E.

## 6 DISCUSSION

For both user studies consistent results for all participants could be observed. In the first experiment, the results of the magnitude estimation as well as magnitude production could be fitted with a power function. As expected, the steepness of the magnitude estimation curve was lower than for the magnitude production, caused by the regression



bias described by Stevens [32]. Accounting for this bias yields a relationship, which indicates that the calculated forces should be increased by a factor of 2 for the user to be able to identify the virtual fluid to be water with the used haptic interface. This is probably caused by the high residual system dynamics. The mechanical viscosity felt in free space already exceeds the viscosity of real water, so the comparison between the rendered and the physical fluid was not possible. However, taking into account this limitation, humans seem to be able to identify a virtual fluid to be water with a rather consistent scaling. The mechanical viscosity might therefore be acting similar to an offset. Furthermore, the relationship found yields an exponent of  $\approx 1$  indicating a linear relationship between the presented and perceived viscosity in this range. This does not correspond to the findings reported by Bergmann Tiest et al. in 2014 [5] for the interaction with real fluids, where the exponent was found to be 0.3-0.4. However, in that work only interaction through stirring in fluids with higher viscosity are considered; a comparison to the perception of fluids using the whole hand, is not possible, as this has not been investigated until now. Looking at the exponent of other hand related perceptions, such as pressure on palm or vibration (60 Hz) on fingers, an exponent around 1 can also be found [36]. Investigating the human capabilities further through the method of constant stimuli, also taking into account the rendering of higher viscous fluids, shows that the weber fraction for the identification of fluids with a rendered viscosity range of 1-4 Pa s is significantly lower than for viscosities in the range of 19-30 Pa s. Comparing this to the weber fractions obtained for real fluids in the same viscosity ranges by Bergman Tiest et al. [6] shows an concurrence for the later group. In the range of 1-4 Pa s, however, Bergmann Tiest et al. also found a weber fraction of 0.3, while this work yielded a value 0.7. A reason for this might be, that this viscosity range appeared to be close to the mechanical viscosity of the robotic system, which made discrimination harder. Additionally, in the work of Bergmann Tiest et al., the fluids were explored by stirring the fluid with the finger or a spatula in a small container, while here the whole hand could explore the virtual fluid without walls. Therefore, the arm motion played a bigger role instead of only the wrist. Furthermore no literature was available to quantify the forces acting on the human hand in fluids with high viscosity. Therefore, a comparison needs to be regarded critically. Nevertheless, the findings of this study suggest that humans have similar discrimination capabilities in the perception of virtual fluids as they do for real fluids.

To further investigate the rendering of virtual fluids, the dynamics of the robotic systems should be improved by adding force sensors on the human side, enabling comparison to real fluids. Since the fluid properties were severely simplified and the investigation limited to one hand motion, the effect of added complexity should be investigated, accounting for human perception as well as the stability of the rendered environment. To guarantee safety, a stability analysis should be carried out, especially considering the quadratic dependency on the velocity for rendered water. Furthermore, the rendered forces for more viscous fluids should be verified through simulations or experiments to

ensure the correct magnitude of forces. A more extensive user study with a higher sample size is desirable.

Throughout both user studies a similar exploration procedure and hand motion was observed for all participants, despite only vaguely defining the desired trajectory. It was found that the hand motion was led by the palm, which appears to validate the assumption in the design of the novel feature of the used exoskeleton of the importance of attachment points on the human palm [15]. The use of the palm allows for richer sensations and seems to be useful to interact with virtual fluids. The human fingers, however, barely move when investigating the virtual fluid, suggesting the rendered viscosity could be perceived equally well using a less complex rigid end effector. However, when adding virtual solid objects to the environment the complexity of a dexterous haptic interface is needed for intuitive manipulation. The ability to render virtual objects submerged in fluids, can be a useful tool to improve control of underwater robotic systems, such as the humanoid diving robot Ocean One, recently developed by the Stanford University [37]. Reflecting fluid forces to the human operator, especially viscosity and wave interactions, can help to accordingly plan and carry out motions. Additionally, the rendering of fluids can be used in simulators for divers or astronauts, which could reduce training costs. On top of that, geologists wish for devices that allow to feel sediments in remote areas to better estimate material properties of unknown substances. Since the flow behavior of sediments is comparable to that of (viscous) fluids [38], progress in the rendering of fluids might also benefit this research.

## 7 CONCLUSION

This paper showed that an algorithm can be implemented in a hand exoskeleton with multiple endpoints to render virtual fluid viscosity at update frequencies high enough to render solid objects as well (833 Hz), by applying sufficient simplifications of the flow properties. Rendered viscosity seems distinguishable from the mechanical viscosity of the system, especially for virtual fluids with larger viscosity.

The first user study showed a near-linear relationship between the rendered and perceived viscosity with a scaling factor of 2. This scaling difference could have multiple reasons and should be investigated in more detail. It was found that the high residual system dynamics of the haptic interface prevent the direct comparison between virtual water and the physical counterpart, but nevertheless consistent results could be obtained for all participants. This indicates that even if the perception of rendered viscosity is not identical to the viscosity in a real fluid, a virtual medium can still be identified as liquid and even be matched to desired stimulus when instructed to take into account the additional mechanical viscosity of the system.

The second user study showed a Weber fraction of 0.3 for the discrimination of virtual fluids with a viscosity between 10 to 30 Pa s, indicating similar discrimination capabilities of the human as observed for real fluids in this range. For viscosities in the range of 1-4 Pa s this could not be verified, most likely because of the close proximity of the magnitude of the rendered forces to the inherently felt system dynamics.

Throughout both experiments, similar exploratory movements are observed for all participants, in which the hand motion is led by the palm and the individual fingers move noticeably less. This validates the palm points as a novel feature of the exoskeleton to be an important addition for rich interactions with more complex virtual environments. This is the first step towards an immersive haptic experience of the full spectrum of material properties.

## REFERENCES

- [1] B. Hannaford and A. M. Okamura, *Haptics*. Springer, 2016, pp. 1063–1084.
- [2] O. Halabi and H. Kawasaki, “Five fingers haptic interface robot hiro: Design, rendering, and applications,” in *Advances in Haptics*. InTech, 2010.
- [3] I. Sarakoglou, A. Brygo, D. Mazzanti, N. G. Hernandez, D. G. Caldwell, and N. G. Tsagarakis, “Hexotrac: A highly under-actuated hand exoskeleton for finger tracking and force feedback,” in *Intelligent Robots and Systems (IROS), 2016 IEEE/RSJ International Conference on*. IEEE, 2016, pp. 1033–1040.
- [4] X. Gu, Y. Zhang, W. Sun, Y. Bian, D. Zhou, and P. O. Kristensson, “Dexmo: An inexpensive and lightweight mechanical exoskeleton for motion capture and force feedback in vr,” in *Proceedings of the 2016 CHI Conference on Human Factors in Computing Systems*. ACM, 2016, pp. 1991–1995.
- [5] W. M. B. Tiest, “Tactual perception of liquid material properties,” *Vision research*, vol. 109, pp. 178–184, 2015.
- [6] W. M. B. Tiest, A. C. Vrijling, and A. M. Kappers, “Haptic discrimination and matching of viscosity,” *IEEE transactions on haptics*, vol. 6, no. 1, pp. 24–34, 2013.
- [7] L. A. Jones and I. W. Hunter, “A perceptual analysis of viscosity,” *Experimental Brain Research*, vol. 94, no. 2, pp. 343–351, 1993.
- [8] W. Baxter and M. C. Lin, “Haptic interaction with fluid media,” in *Proceedings of graphics interface 2004*. Canadian Human-Computer Communications Society, 2004, pp. 81–88.
- [9] G. Cirio, M. Marchal, S. Hillaire, and A. Lecuyer, “Six degrees-of-freedom haptic interaction with fluids,” *IEEE Transactions on Visualization and Computer Graphics*, vol. 17, no. 11, pp. 1714–1727, 2011.
- [10] Y. Dobashi, M. Sato, S. Hasegawa, T. Yamamoto, M. Kato, and T. Nishita, “A fluid resistance map method for real-time haptic interaction with fluids,” in *Proceedings of the ACM symposium on Virtual reality software and technology*. ACM, 2006, pp. 91–99.
- [11] R. Hover, G. Kósa, G. Szekly, and M. Harders, “Data-driven haptic rendering from viscous fluids to visco-elastic solids,” *IEEE Transactions on Haptics*, vol. 2, no. 1, pp. 15–27, 2009.
- [12] M. Vines, J. Mora, and W.-S. Lee, “Haptic display of 3d liquids for interactive applications,” in *Games Innovations Conference, 2009. ICE-GIC 2009. International IEEE Consumer Electronics Society's*. IEEE, 2009, pp. 140–148.
- [13] —, “Real-time haptic display of fluids,” in *Proceedings of the 2nd Canadian Conference on Computer Science and Software Engineering*. ACM, 2009, pp. 149–153.
- [14] H. Liu, K. Wu, P. Meusel, N. Seitz, G. Hirzinger, M. Jin, Y. Liu, S. Fan, T. Lan, and Z. Chen, “Multisensory five-finger dexterous hand: The dlr/hit hand ii,” in *Intelligent Robots and Systems, 2008. IROS 2008. IEEE/RSJ International Conference on*. IEEE, 2008, pp. 3692–3697.
- [15] N. Y. Lii, G. Stillfried, Z. Chen, M. Chalon, B. Pleitinger, and A. Maier, “Handexoskelett sowie roboterarm mit solchem handexoskelett,” Patent DE102 017 220 996.8, 23-11-2017, pending.
- [16] T. Endo, H. Kawasaki, T. Mouri, Y. Ishigure, H. Shimomura, M. Matsumura, and K. Koketsu, “Five-fingered haptic interface robot: Hiro iii,” *IEEE Transactions on Haptics*, vol. 4, no. 1, pp. 14–27, 2011.
- [17] A. Pereira, G. Stillfried, T. Baker, A. Schmidt, and N. Y. Lii, “Reconstructing human hand pose and configuration in a fixed-base hand-arm-exoskeleton,” *Robotics and Automation Letters*, 2019, in preparation.
- [18] CyberGlove-Systems, 19-01-2018. [Online]. Available: <http://www.cyberglovesystems.com/cybergasp/>
- [19] G. Hirzinger, N. Sporer, A. Albu-Schaffer, M. Hahnle, R. Krenn, A. Pascucci, and M. Schedl, “Dlr’s torque-controlled light weight robot iii—are we reaching the technological limits now?” in *Robotics and Automation, 2002. Proceedings. ICRA’02. IEEE International Conference on*, vol. 2. IEEE, 2002, pp. 1710–1716.
- [20] T. Hulin, K. Hertkorn, P. Kremer, S. Schätzle, J. Artigas, M. Sagardia, F. Zacharias, and C. Preusche, “The dlr bimanual haptic device with optimized workspace,” in *Robotics and Automation (ICRA), 2011 IEEE International Conference on*. IEEE, 2011, pp. 3441–3442.
- [21] M. Sagardia, T. Hulin, K. Hertkorn, P. Kremer, and S. Schätzle, “A platform for bimanual virtual assembly training with haptic feedback in large multi-object environments,” in *Proceedings of the 22nd ACM Conference on Virtual Reality Software and Technology*. ACM, 2016, pp. 153–162.
- [22] K. Hertkorn, T. Hulin, P. Kremer, C. Preusche, and G. Hirzinger, “Time domain passivity control for multi-degree of freedom haptic devices with time delay,” in *Robotics and Automation (ICRA), 2010 IEEE International Conference on*. IEEE, 2010, pp. 1313–1319.
- [23] Z. Chen, N. Y. Lii, T. Wimboeck, S. Fan, M. Jin, C. H. Borst, and H. Liu, “Experimental study on impedance control for the five-finger dexterous robot hand dlr-hit ii,” in *Intelligent Robots and Systems (IROS), 2010 IEEE/RSJ International Conference on*. IEEE, 2010, pp. 5867–5874.
- [24] Z. Chen, N. Y. Lii, T. Wimboeck, S. Fan, and H. Liu, “Experimental evaluation of cartesian and joint impedance control with adaptive friction compensation for the dexterous robot hand dlr-hit ii,” *International Journal of Humanoid Robotics*, vol. 8, no. 04, pp. 649–671, 2011.
- [25] L. Le Tien, A. Albu-Schaffer, A. De Luca, and G. Hirzinger, “Friction observer and compensation for control of robots with joint torque measurement,” in *Intelligent Robots and Systems, 2008. IROS 2008. IEEE/RSJ International Conference on*. IEEE, 2008, pp. 3789–3795.
- [26] J. J. Gil and E. Sanchez, “Control algorithms for haptic interaction and modifying the dynamical behavior of the interface,” in *2nd international conference on Enactive Interfaces*, 2005, pp. 17–18.
- [27] J. Van Houwelingen, S. Schreven, J. B. Smeets, H. J. Clercx, and P. J. Beek, “Effective propulsion in swimming: grasping the hydrodynamics of hand and arm movements,” *Journal of applied biomechanics*, vol. 33, no. 1, pp. 87–100, 2017.
- [28] I. P. Herman, *Physics of the human body*. Springer, 2016.
- [29] B. Lautrup, *Physics of continuous matter: exotic and everyday phenomena in the macroscopic world*. CRC Press, 2004.
- [30] Y. Sato and T. Hino, “A computational fluid dynamics analysis of hydrodynamic force acting on a swimmers hand in a swimming competition,” *Journal of sports science & medicine*, vol. 12, no. 4, p. 679, 2013.
- [31] M. A. Berger, G. de Groot, and A. P. Hollander, “Hydrodynamic drag and lift forces on human hand/arm models,” *Journal of Biomechanics*, vol. 28, no. 2, pp. 125–133, 1995.
- [32] S. S. Stevens, “Problems and methods of psychophysics,” *Psychological Bulletin*, vol. 55, no. 4, p. 177, 1958.
- [33] H. Toussaint and M. Truijens, “Biomechanical aspects of peak performance in human swimming,” *Animal Biology*, vol. 55, no. 1, pp. 17–40, 2005.
- [34] A. Wacker Chemie, “Solid and liquid silicone rubber-material and processing guidelines,” 2011.
- [35] Y. Taamneh, “Cfd simulations of drag and separation flow around ellipsoids,” *Jordan Journal of Mechanical and Industrial Engineering*, vol. 5, no. 2, pp. 129–132, 2011.
- [36] S. S. Stevens, *Psychophysics. Introduction to its perceptual, neural, and social prospects*. Transaction Publisher, 1975.
- [37] O. Khatib, X. Yeh, G. Brantner, B. Soe, B. Kim, G. Shameek, H. Stuart, S. Wang, M. Cutkosky, A. Edsinger et al., “Ocean one: A robotic avatar for oceanic discovery,” *IEEE Robotics & Automation Magazine*, vol. 23, no. 4, pp. 20–29, 2016.
- [38] H. M. Jaeger, S. R. Nagel, and R. P. Behringer, “Granular solids, liquids, and gases,” *Reviews of modern physics*, vol. 68, no. 4, p. 1259, 1996.

## APPENDICES

# CONTENTS

<b>A</b>	<b>Haptic Interface</b>	<b>1</b>
A.1	Human Interaction . . . . .	2
A.2	Hardware . . . . .	2
A.3	Control . . . . .	3
A.4	Limitations . . . . .	5
A.4.1	Friction . . . . .	5
A.4.2	Sensor Accuracy . . . . .	7
<b>B</b>	<b>Fluid Interaction Forces</b>	<b>9</b>
B.1	Fluid Forces . . . . .	9
B.1.1	Buoyancy . . . . .	9
B.1.2	Lift and Drag Forces . . . . .	10
B.2	Flow Characteristics . . . . .	10
B.3	Forces in Water . . . . .	12
B.3.1	Drag coefficient approximation . . . . .	13
B.3.2	Force Verification . . . . .	14
B.4	Forces in high viscous fluids . . . . .	16
B.4.1	Hand Shape Approximation . . . . .	17
B.4.2	Force Approximation. . . . .	19
B.5	Force distribution. . . . .	20
<b>C</b>	<b>Implementation</b>	<b>21</b>
C.1	Hand Simplification. . . . .	21
C.2	Collision Detection . . . . .	23
C.3	Fluid Forces. . . . .	24
C.3.1	Water Forces . . . . .	25
C.3.2	High Viscosity Forces . . . . .	26
C.3.3	Application to the Human Hand . . . . .	27
C.4	Force Reflection on LWR . . . . .	28
<b>D</b>	<b>User Studies</b>	<b>29</b>
D.1	Experimental Design . . . . .	29
D.1.1	Experiment 1: Magnitude Perception . . . . .	29
D.1.2	Experiment 2: Fluid Discrimination . . . . .	30
D.1.3	Post-Experiment . . . . .	31
D.1.4	Questionnaire Design . . . . .	31
D.2	Pilot studies. . . . .	32
D.2.1	Participants . . . . .	32
D.2.2	Results Pilot Experiment 1 . . . . .	32
D.2.3	Results Pilot Experiment 2 . . . . .	34
D.2.4	Pilot Questionnaire . . . . .	35
D.2.5	Discussion and Conclusion for Experiments . . . . .	36
D.3	Experiments . . . . .	37
D.3.1	Participants . . . . .	37
D.3.2	Procedure . . . . .	37
D.3.3	Results Experiment 1. . . . .	38
D.3.4	Results Experiment 2. . . . .	47
D.3.5	Results Post-Experiment . . . . .	52

D.4	Discussion . . . . .	52
D.5	Additional Experiment . . . . .	53
D.5.1	Experiment Setup . . . . .	53
D.5.2	Results . . . . .	53
D.5.3	Discussion . . . . .	55
<b>E</b>	<b>Critical Evaluation and Outlook</b>	<b>56</b>
E.1	Evaluation of the Haptic Interface. . . . .	56
E.2	Evaluation of the Fluid Interaction Force . . . . .	57
E.3	Evaluation of the Implementation . . . . .	58
E.4	Evaluation of the User Studies . . . . .	58
E.5	Conclusion . . . . .	59
	<b>Bibliography</b>	<b>60</b>
<b>F</b>	<b>Additional documents</b>	<b>63</b>
F1	Consent Form - Experiment 1 . . . . .	64
F2	Consent Form - Experiment 2 . . . . .	68
F3	Plan of Procedure . . . . .	72
F4	Questionnaire. . . . .	75

# A

## HAPTIC INTERFACE

The haptic interface used in this project is a hand exoskeleton developed and patented by the DLR [1, 2]. Similar to the HIRO exoskeleton [3], which was developed at the Gifu University in Japan, it is a grounded device positioned opposite the human hand instead of being attached to backside of the hand as more commonly seen [4–6]. Thus, the human user does not need to carry the weight of the haptic device and fatigue can be avoided.

The newly developed exoskeleton can be mounted as an end effector to any grounded device. During this project it is attached to a KUKA Lightweight Robot (LWR) 4+ (Fig. A.1). The mounting enables to extend the workspace and enhance the capabilities of the exoskeleton further, since the LWR has been shown to also be a powerful haptic interface by itself [7, 8]. When set in torque control mode, gravity is compensated to allow the human user to move around freely within the LWR's workspace. To support the perception of virtual objects, it is possible to additionally reflect rendered forces of the exoskeleton to the end effector point of the LWR. The exoskeleton has five interface points, but instead of connecting to all fingers of the human, only the thumb, index and middle finger are attached. The remaining two exoskeleton interface points connect to the palm. This makes the new exoskeleton the first of its kind to reflect forces to the palm instead of only considering the human fingers (Fig. A.1, right). Taking the palm into consideration is hypothesized to add to the realistic perception of virtual objects. In real interactions humans often involve the palm to investigate their environment with exploratory procedures [9]. This remains, however, to be investigated further.

In the following, the interaction possibilities of the human user as well as the hardware capabilities and the existing control structures are explained in more detail. Additionally limitations of the system are identified as important boundary conditions for the intended work in this research project.

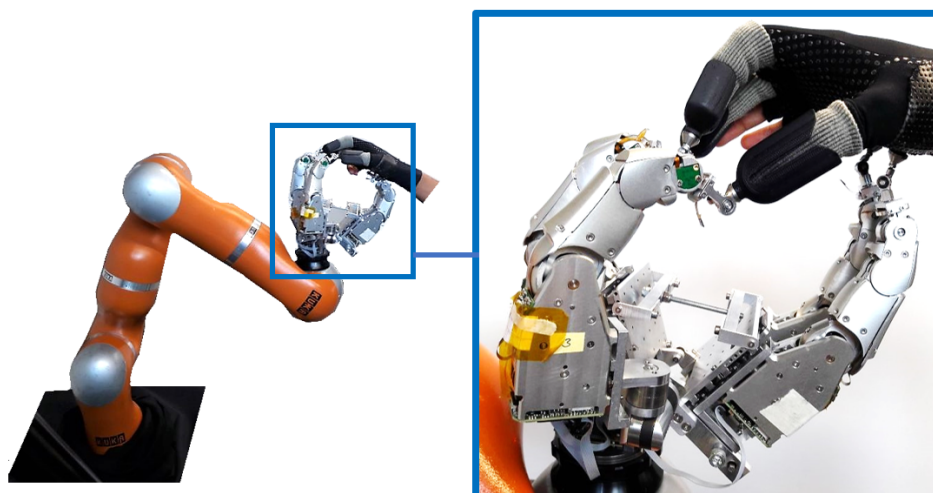


Figure A.1: KUKA Light Weight Robot (LWR) and hand exoskeleton as combined haptic user interface, to which the human user is attached via a magnetic mechanism.

## A.1 HUMAN INTERACTION

The human user is attached to the exoskeleton on five points on the hand. Three of the interface points attach to the finger tips of the thumb, index and middle finger, the remaining two to the palm. To ensure the safety of the user, the connection is a magnetic clutch, such that the human can easily detach by pulling away from the haptic interface in case of an emergency. At the beginning of this project, a custom made glove was available to attach to the interface. However, for users that did not fit the glove perfectly, the finger tips had a lot of play. This flexibility noticeably decreased the perception of the rendered forces. To avoid the decrease in perception, the glove was revised and a modified version fabricated. In this version, the magnets for the connection on the palm are attached to a fingerless glove as seen in Figure A.2. To better accommodate different finger lengths and shapes, individual dressings can be fit to each finger. The dressings consist of finger sleeves from AFH to which a 3D-printed cap is attached with the magnet glued to its end (Fig. A.2). The cap covers the proximal joint of each finger to achieve sufficient force transmissions as shown in first try-outs.



Figure A.2: Fingersleeves with magnetic tip to be worn on thumb, index and middle finger together with a fingerless glove with two additional magnets on the palm area.

## A.2 HARDWARE

The exoskeleton fingers (Fig. A.3) were initially designed for the modular multisensory DLR-HIT Hand [10]. To be used as haptic interface, a metallic cone is added to the tips as counterpart for the magnets on the human hand. Five of the modular fingers are arranged on two planes to build the exoskeleton. The planes are connected via a rotational joint and fixed in position with a setscrew. On the outside of each plane, two fingers are attached with the tips facing each other. The cupping angle between the two opposing sides can manually be changed to account for different hand sizes. Additionally, the robotic fingers can be adjusted horizontally along the planes. The robotic fingers on one side of the platform attach to the two palm points, the opposing ones to the index and middle finger. On each side next to the rotatable platform an additional finger can be mounted, which can be manually adjusted in three different axes. For the exoskeleton, the fifth finger is mounted such it connects to the thumb of the human user. Despite the robotic fingers resembling its natural model, in the used configuration the system is non-anthropomorphic.

Each of the robotic fingers has four joints, that are specified in Figure A.3. The basis has two intersecting joints to enable a flexion/extension motion as well as abduction/adduction of the robotic finger. The proximal and distal joint also enable flexion/extension, but are mechanically coupled to each other. Thus, each robotic finger has 3 degrees of freedom (DOFs). With five robotic fingers on the exoskeleton, the haptic interface has a total of 15 DOFs. The LWR on which the haptic device is mounted, has additional 7 DOFs, so that the combination of both system adds up to have 22 DOF. The finger incorporates position and torque sensors, so that the position of each joint (in degrees) and the torque applied to the finger can be measured. Details on dimensioning and the kinematic chain can be found in [10].

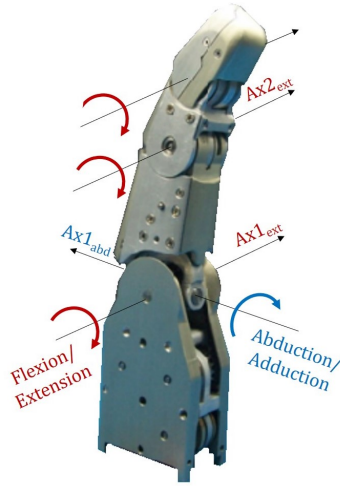


Figure A.3: One of the modular robotic fingers used to build the configurable exoskeleton used as haptic interface in this project. Each finger has four joints to enable the indicated motions. The distal and proximal one are coupled, leaving 3 DOF (modified from [10]).

## A.3 CONTROL

The exoskeleton is operated via an already available Simulink model (v2014b), individually controlling each of the robotic fingers. The model runs at a rendering frequency of 833 Hz. It is divided into four main parts as shown in Figure A.4: Command, High Level Control, Low Level/ Plant and an Output, consisting of Scopes and Visualization.

In the Command part the settings for each finger can be defined. A software stop can be enabled and the control mode can be chosen to be position or torque control. However, in this work the fingers are only operated in torque control.

In the High Level Control, the forces for virtual interactions are calculated. The interaction with some virtual solid objects with simple shapes is already possible through implementation of the God-object method [11]. A limit protection is implemented to preserve the hardware by preventing the fingers from reaching the mechanical stops. The coordinates and orientation of each finger tip in world space is known due to the fully defined kinematic chain up to the base of the LWR. The tip positions are identical to the one of the finger tips of the human hand. Based on the finger tip positions the position and orientation of the human hand can be calculated with inverse kinematics. The necessary transformations are defined through the kinematic model of the human hand as obtained through Magnetic resonance imaging (MRI) data in previous studies at the DLR by Stillfried et al in 2010 [12, 13]. Using inverse kinematics has the advantage, that the user does not need to wear a data glove to determine the hand's position in space [14]. Therefore, the human hand geometry and orientation can be used in the model to calculate occurring forces during a virtual interaction. The forces as well as the human hand information are send as outputs of the High Level subsystem.

In the Plant subsystem output and input data of the robotic hardware are processed. Here, the Low Level Control is implemented, in which e.g. the calculated forces are converted to torques to be applied to the joints of the robotic fingers. To account for the robot's dynamic behavior, mainly mechanical inertia and friction, a feed-forward gain and friction compensator as proposed in [15] are implemented. The total torque to be applied to each robotic finger is converted into a Pulse-width modulation (PWM) signal to be sent to the motors of the joints. The incoming signals from the robot are pre-processed and positions and velocities concerted into Cartesian space. The information obtained in the Plant subsystem are fed back to the High Level Control, closing the system's loop.

The commanded and measured torques, as well as the current position and velocity of each finger joint are presented to the human operator in scopes to monitor the robot's behavior. Additionally, the haptic interface can be visualized with the instantreality player developed at the Fraunhofer Institute for Computer Graphics Reserach (IGD) [16], seen in Figure A.4. Using the data sent and received from the robot, the motion of the individual robotic fingers can be shown as well as the commanded torques on each joint. Adding the information of the estimated human hand position obtained through the inverse kinematics, the human hand can also be visualized. The model of the hand is again using Stillfried et al.'s MRI data [12].



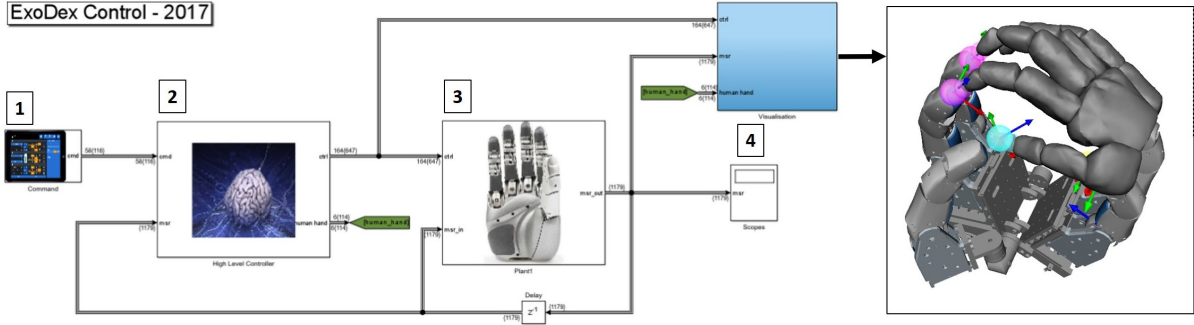


Figure A.4: Highest level of the used Simulink Control model of the exoskeleton with 4 subsystems: (1) Command, (2) High Level Control, (3) Low Level and Plant Control and (4) Scopes and Visualization (visualized in Instantreality).

A block diagram of the simplified control loop valid for each individual finger is shown in Figure A.5. It is based on the nomenclature in Gil and Sanchez' work [17].  $Z_u$  represents the impedance of the human user and  $Z_m$  the dynamics of the haptic interface. The model assumes the link between the user and the haptic interface to be rigid, which is valid for sufficiently compressed finger pulp of the human [17]. This leads to equal displacements of the human finger and the haptic interface.  $F_u$  defines the force exerted by the user on the haptic interface, which does not equal all occurring external forces  $F$ . The user's force can be measured through torque sensors in each joint. Applying a gain to those forces can compensate some of the dynamical behavior of the mechanical system and can help the human move the system.  $Z_e$  is the impedance of the virtual environment, through which interaction forces of virtual objects can be calculated. Implementing a subsystem to enable the calculation of fluid forces is the main modification of the control model during this thesis project. Necessary positions and velocities ( $X$ ) of the end points of the exoskeleton fingers are delivered by the robot's position to detect when the user's hand enters the virtual fluid. The position data of the exoskeleton fingers can be obtained through potentiometers and Hall sensors in the joints. This data can be converted to Cartesian space using the kinematics chain of the robot combination. The position data of each finger tip can be used to calculate the interaction forces  $F_e$  in the virtual environment. This force also includes the joint limit protection, which applies forces before the physical limit is reached to prevent the wear of the hardware. The forces from the virtual environment are opposing the acting forces of the user and are therefore considered as a negative signal. Together with the feed-forward term, this sums to the forces to be applied to the robotic system to move the robotic fingers as intended. The forces can be disturbed by the human interaction, resulting in the forces  $F_m$ , which are actually applied to the robot. The haptic interface additionally includes a friction compensation as developed by Le Tien et al [15] to further improve the dynamics of the system.

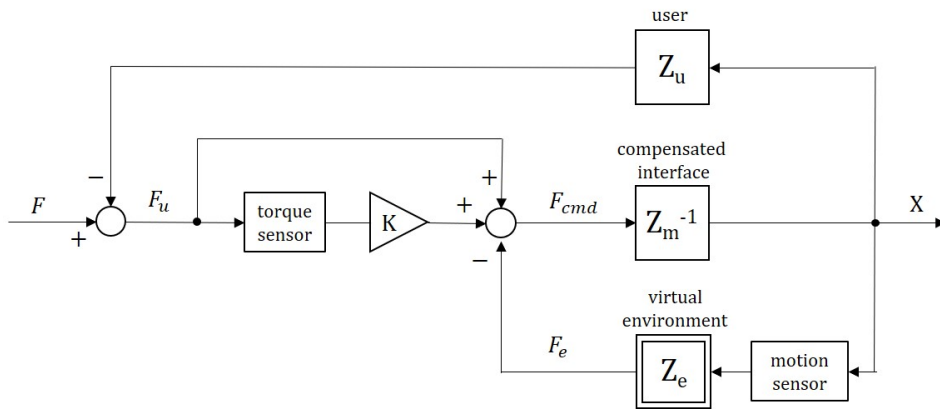


Figure A.5: Control loop of each robotic finger of the exoskeleton, set up with the nomenclature defined by Gil and Sanchez [17].  $Z_u$  and  $Z_e$  describing the impedance of the human user and the virtual environment, respectively.  $Z_m$  represents the dynamics of the haptic interface including the friction compensation. The input is the total external force  $F$  and the output the motion of the robotic finger joints  $X$ .

Setting up the transfer function, shows the impedance felt by the user to be:

$$\frac{X}{F} = \frac{1}{Z_u + \frac{Z_m}{1+K} + \frac{Z_e}{1+K}} \quad (\text{A.1})$$

The function indicates that the felt dynamics of the haptic interface  $Z_m$  are reduced to be  $1+K$  times smaller than the real one. However, if the calculated forces from the virtual environment  $Z_e$  are reduced by the same factor, meaning the forces are perceived to be weaker than calculated. To counteract this reduction, an additional gain of  $K + 1$  could be added. This gain is not added in this control model, since noticeable dynamics of the robotic system remain, which will be analyzed in detail in the following section. The system's dynamics include friction and inertia, but also mechanical viscosity of the system. Mechanical viscosity is perceived by humans similar to the viscosity of fluids [18]. Therefore the mechanical viscosity is adding to the simulated one of the virtual fluids, acting as a gain of unknown value. Thus it is assumed that the viscosity felt by the human user will already be higher than calculated, so no additional gain is added in the control model.

## A.4 LIMITATIONS

The modularity of the robotic fingers makes the system adjustable and allows different configurations to be used as haptic interface. However, this leads to many hardware components, which are powered and controlled individually. The modular design makes the system more prone to failure. Each finger is a very compactly packed system, in which the sufficient transmission ratios are realized through harmonic drives and belts. This causes friction and efficiency loss in each finger. These losses can clearly be felt by the human user despite control efforts, especially the friction in the robotic fingers. Additionally, the fingers only incorporate a torque sensor, which can be translated into applied forces with an appropriate inertia matrix. However, considering the complexity of the system, the accuracy of those measurements is questionable. To get a better picture of the limitations of the system, the friction and the torque sensor accuracy are investigated in short experiments, which are explained in the following.

### A.4.1 FRICTION

During operation without rendered forces, the robotic fingers are set in torque mode, in which gravity forces are compensated. This means the finger should remain motionless when at rest and ideally move as soon as applying external forces, e.g. through the human. However, in the reality some friction needs to be overcome before the robotic fingers move. To better approximate the capabilities of the system it is desired to measure the magnitude of the remaining friction, by gradually adding weight to the robotic finger tips until the system starts moving. For this purpose, a container is built that can be attached to the system with the same magnetic mechanism as used for the human user to connect to the exoskeleton (Fig. A.6). To add weight, the container is gradually filled with sugar.

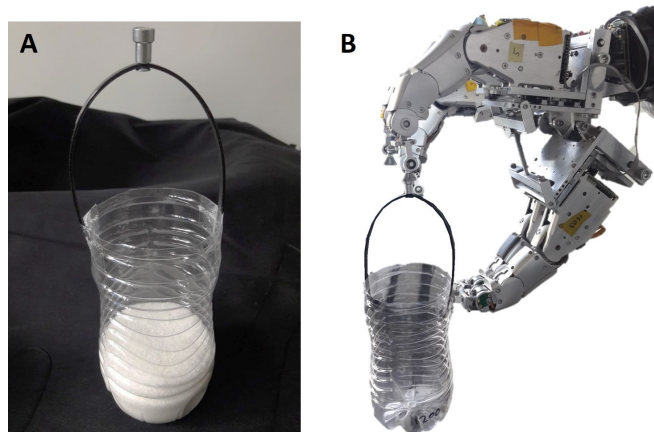


Figure A.6: Container built for friction and sensor accuracy testing (A), that can be attached to the exoskeleton via magnetic connection (B).

The focus lies on the analysis of the axes on the base joints, as those were observed to move the most when the human user interacted with the exoskeleton. The study takes into account the base axes for abduction ( $A_{abd}$ ) and extension ( $A_{ext}$ ). The distal and proximal extension joints showed to move before the one at the base. Only the higher occurring friction at the base was analyzed.

For the friction test, the robotic finger is in a horizontal position in torque control mode. The finger is rotated to  $270^\circ$  in steps of  $90^\circ$  to take into account each direction of the two axes on the base joint (Fig. A.7).  $A_{ext}$  is additionally tested in an inclined finger position of  $45^\circ$  as this is a commonly occurring pose during the interaction with the human user.

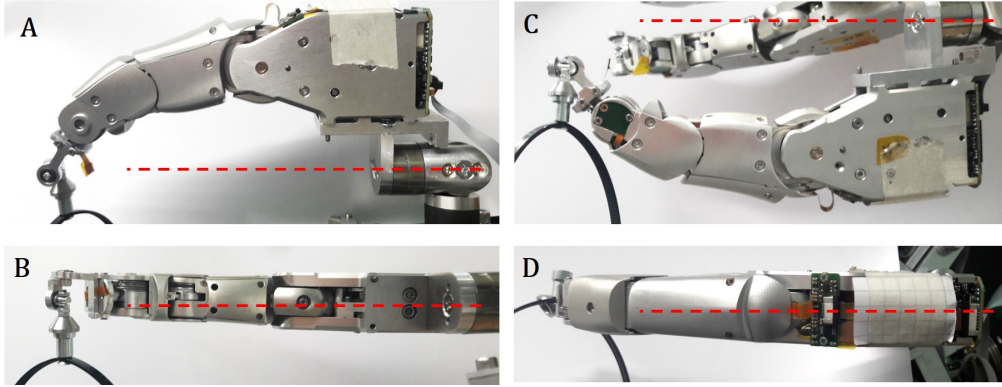


Figure A.7: Tested orientations of the finger for the friction experiment rotated around the indicated red axis a)  $0^\circ$ , b)  $90^\circ$ , c)  $180^\circ$ , d)  $270^\circ$

The experiment is carried out on one randomly chosen finger. As the fingers are identical in design, the results are assumed to be valid for all fingers. In each of the four tested poses in horizontal position as well as in the inclined position, the attached container is gradually filled with sugar until the robotic finger starts moving (10 replicates). Then the container is detached and the weight is measured with a precision scale. From the weight measurements the applied force to the robotic fingers can be calculated when taking into account gravity with  $9.81 \text{ m/s}^2$ . The mean and standard deviation of the found forces are plotted in Figure A.8.

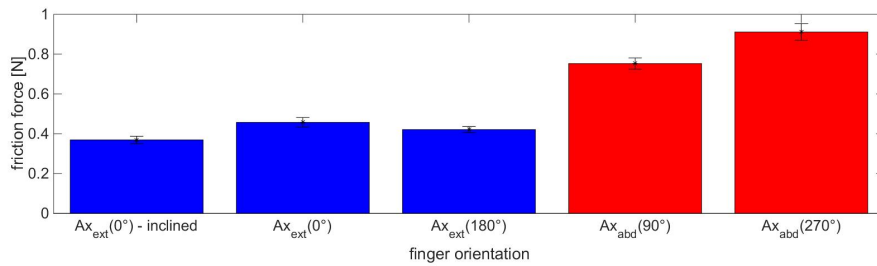


Figure A.8: Friction in the base joint for extension ( $A_{ext}$ ) and abduction ( $A_{abd}$ ), measured in four directions with the finger in horizontal position. The  $0^\circ$  orientation was also measured at a  $45^\circ$  inclined position.

It can be seen that independent of the orientation and position of the finger around  $0.4 \text{ N}$  had to be applied to axis  $A_{ext}$  before the finger started to move while for axis  $A_{abd}$  an average of  $0.83 \text{ N}$  are necessary. The reason lies probably in the motion mechanism of the robotic finger. As explained by Liu et al. [10], the base of the robotic finger houses two motors. For the extension motion in the base joint both motors move in the same direction, while for the abduction, the motors' motions are opposite. Consequently, the friction for the latter motion should be higher, as static friction needs to be overcome individually for each motor by moving in the same direction static friction only needs to be overcome once. This explains the factor of roughly 2 between the magnitude of friction in the two considered axes. The magnitude of friction is equally high for the extension motion when the finger is inclined as measured for the horizontal position. This measurement indicates that the gravity compensation is sufficiently working. Otherwise the measured force would be higher when the lever arm is shorter.

Those measurements indicate that a considerable amount of mechanical friction remains in the system despite counteracting control (feed-forward, friction compensation). In the current control it is not possible to compensate the friction further. An increase in feed-forward gain can lead to vibrations of the finger, which destabilizes the control loop. This limitation has to be taken into account for the further research on the exoskeleton. It is suggested, that the fluid forces to be rendered should exceed 1 N to get meaningful results.

#### A.4.2 SENSOR ACCURACY

Each joint of the robotic finger has a torque sensor. The torques measurements are important for the feed-forward control term and the friction compensation. It is desirable to have a high accuracy in those sensors, which is investigated in the second experiment. To investigate the sensor accuracy, a defined weight is added. Knowing gravity and the lengths of the phalanges, the weight can be translated to the applied torques in each joint. The expected torque values are compared to the sensor measurements. To apply the weight, the container from the previous experiment is used, again filled with sugar. The applied weights range from 50 to 250 g in steps of 50 g in between. Again, the finger is in a horizontal position. The  $0^\circ$  - orientation is set to apply torques to the joints for flexion and extension ( $A_{ext}$ , Fig. A.7a) and the  $90^\circ$  - orientation to measure the torque sensor data for the abduction/adduction joint ( $A_{abd}$ , Fig. A.7b). For this experiment, only one direction is tested as the measurements should be independent of the direction. Each of the weights is applied for 10 seconds and the torque sensor data is sampled at a rate of 1 kHz.

The obtained data is plotted in Figure A.9 together with the expected values for the two considered orientations. In the first orientation ( $0^\circ$ , Fig. A.9a), only the extension/flexion motion can be carried out in the distal and base joint (Fig. A.3). Therefore, only two sensors should be able to measure a change. In the second orientation ( $90^\circ$ , Fig. A.9b) only the the abduction motion in the base is possible, leading to one expected sensor measurement. However, it can be seen that the extension sensors on the base and distal joint show a clear increase, as well as a slight abduction measurements for the first orientation. The undesired detections are probably caused by unintended motion of the fingers. The robotic fingers were in torque mode, so they were able to move. Thus, it is suspected that a small displacement occurred in the axes, leading to unintended measurements. However, this should not have influenced the intended measurements as each sensor is independent. The unexpected increase of the abduction joint in the first orientation and the extension joints in the second one, is ignored in the following analysis.

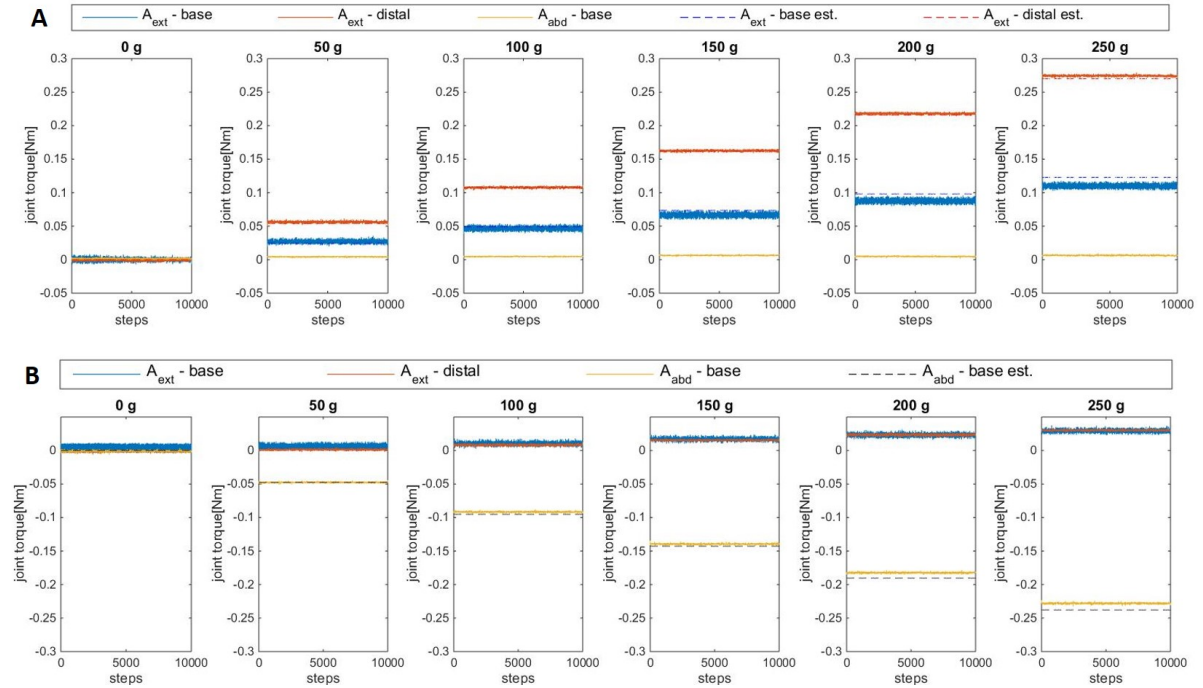


Figure A.9: Torque measurements for defined applied weights (50, 100, 150, 200, 250 g) to test the different axes of the robotic fingers. The finger is in horizontal position at (A)  $0^\circ$  and (B)  $90^\circ$ .

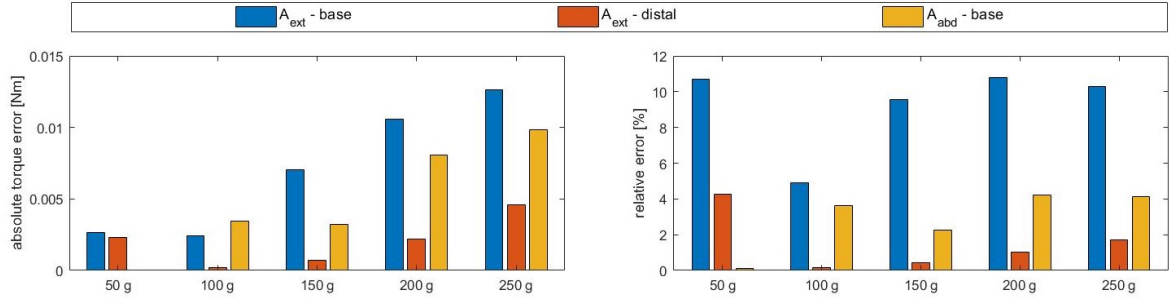


Figure A.10: Absolute error (left) and relative error (right) of the torque measurements for each axis. The torques are recorded for 10 s (1 kHz), obtaining 10000 measurements.

It can be seen that the measured torques in the extension joints for orientation 1 and the abduction joint for orientation 2 show the expected increase in magnitude. Nevertheless, with increase in applied torque, an offset error becomes noticeable. Investigating this error closer for the extension axes (base and distal) in orientation 1 and the abduction axis in orientation 2, shows a steady increase between 100 g and 250 (Fig. A.10, left). The high values at the extension joints for 50 g cannot be explained and might indicate a measuring error. Thus this measurement is neglected in the further error analysis. To relativize the error, it is divided by the expected torque applied through each weight, leading to a relative error (Fig. A.10, right). Not considering the measurement for 50 g, for every applied weight the sensor error in the base extension joint is the highest. The measuring error for the abduction joint is lower and for the distal joint it is considerably small. Averaging the relative error shows a mean error of 8.89 % for the base extension joint, 3.56 % for the base abduction joint and 0.83 % for the distal joint. While the error for the latter two joints might be acceptable, the first one is considerably large. This is a known problem of the system, caused by several reasons. The torque of each joint is measured through a strain gauge based joint torque sensors. To save space those sensors are implemented with a small offset to the axis. The offset causes an inherent a small error to the torque measurements. Additionally, the amplification factor could not be simulated, but was empirically determined for one finger. This is applied to all fingers, but because of non-ideal properties and slight variances in the real mechanical system an additional error might be introduced. Therefore, an error is inherent due to the limited ability of proper calibration of the torque sensor causing the obtained measurements errors.

This is a limiting factor for the control and is one of the reasons why rather high friction remains in the system. To account for this and improve the system, ideally a force sensor should be added on the tips of the robotic fingers. This sensor would eliver more reliable measurements of the forces applied by the human user. However, this problem cannot be fixed within this project. Despite the known large error of the torque sensors, the measurements are used in the low level control to generate a feed-forward force and for the friction compensation, which does improve the system, though not ideal.

# B

## FLUID INTERACTION FORCES

This project aims to investigate the interaction with fluids of varying viscosity. However, the calculation of fluid forces is complicated, as many changing variables play a role. Literature on the forces acting on the human hand are only available for the interaction with water due to the interest for competitive swimming. For this field, hand positions, orientations and resulting thrust in water have been investigated through experimental data and Computational Fluid Dynamics (CFD) simulations. It is therefore decided to first investigate the rendering of this specific fluid to simulate forces with a verifiable magnitude and approximative behavior. Additionally, every human has experience in the interaction with water, which is helpful for the later carried out human user study to compare the feeling of the rendered viscosity to the one of the physical stimulus. Later on it is desired to also render fluids with higher viscosity. Since one of the main goals of this thesis project is to render fluid interaction forces with very high update rates to still be able to interact with rigid virtual objects, it is not possible to carry out resource intensive calculations. For this reason, it is chosen to appropriately simplify the occurring interactions and only implement analytical equations. A similar approach was already applied by Vines, Mora and Lee [19, 20], however, there the goal was to realize low rendering frequencies to enable the algorithm to run on conventional computers for the purpose of gaming. Additionally, only the interaction with a spatula was considered, while for this work the human hand should interact with the fluid and feedback will be given to multiple points. For this purpose, first the occurring forces in a fluid interaction are analyzed and then appropriate simplifications are made for water and higher viscous fluids.

### B.1 FLUID FORCES

The forces acting on a body in a flow arise from buoyancy, drag and lift of the body. Each play a role, but differ in magnitude and direction. The sum of all occurring forces is then acting on the body. In the following, each type of force is analyzed and the implications on fluid perception are evaluated in order to develop a simplified analytical equations that can sufficiently render the forces in a fluid interaction. Additional forces that might occur, e.g. from waves or disturbances are not considered.

#### B.1.1 BUOYANCY

Buoyancy is force acting on a body emerged in a fluid opposing gravity. The magnitude of the buoyancy force depends on the density of the object. Objects with a higher density than the fluid will sink, while object with a lower density will float. Depending on the fat percentage of the body, the human has a density between 900 and 1050 kg/m<sup>3</sup> [21], which is close to the density of water (1000 kg/m<sup>3</sup>). This means, that the human body is in abeyance in water. Therefore, neither an dominant upward buoyant force nor gravity pulling down can be felt and thus, the calculation of both is neglected in this study. The same is valid for many fluids with higher viscosity, such as silicones or food products, which often also have a density in this range of magnitude [22, 23].



### B.1.2 LIFT AND DRAG FORCES

Additionally to buoyancy and gravity, the forces that act on a body emerged in fluid is the sum of drag and lift forces as seen in Figure B.1.

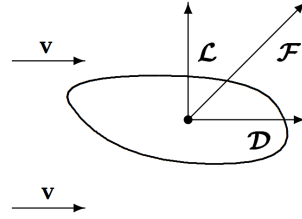


Figure B.1: Scheme of a body emerged in a fluid with velocity  $v$ , on which drag forces  $D$  act in direction of the flow and lift forces  $L$  perpendicular to it. The sum of both forces ( $F$ ) acts on the body. [24]

Drag forces result from friction occurring between the skin of the object and the fluid (skin drag) on one hand and pressure resistance due to pressure differences along the body (form drag) on the other hand. The force occurring from it are defined to act parallel to the direction of the fluid flow, but in the opposite direction. Lift forces are defined to act perpendicular to the drag forces, but the direction is strongly dependent on the form of the body and its orientation. This makes it hard to determine the vector along which the lift forces act. For simplification, it is decided to limit the way of interaction with the virtual fluid to one motion, which should suffice to prove the possibility of implementation of such forces. No research was found on applied human exploratory procedures in the interaction with fluids, but from experience it is known that humans tend to stir with a finger or drag the whole hand through water with the palm area facing the direction of flow. For the purpose of this study, in this scenario, the fingers are considered to be fully extended and without spread. It has been found that for this kind of motion, close to no lift forces occur [25], while drag forces are maximal. It is therefore decided to neglect lift forces and only consider the drag on the human hand during the interaction with a fluid. The direction is according to the definition chosen to be opposing the hand motion, which can be determined for each interface point through sensors in the haptic device. The magnitude of such forces can be calculated with the analytical equation

$$F_D = \frac{1}{2} C_D v^2 A \rho \quad (\text{B.1})$$

where  $\rho$  refers to the density of the fluid,  $v$  to the fluid velocity and  $A$  to a body specific area presented to the flow. No clear definition of this area is given, but different approaches for interactions of the human hand with water have been proposed by literature. Berger et al. defined it to be the total wetted area of the hand [26], but more commonly used are the projected area orthogonal to the flow direction [25, 27–29] or the maximum projected hand area [30–34].  $C_D$  refers to the drag coefficient. This is a body specific dimensionless number, that varies with the type of flow and the form and orientation of the body [24]. Therefore, first the flow characteristics for a human hand in water and higher viscous fluids are identified.

## B.2 FLOW CHARACTERISTICS

The patterns of a flow are characterized by the dimensionless Reynolds number ( $Re$ ). It describes the relation from inertial forces to viscous effects. In a turbulent flow inertial forces dominate, which leads to spinning vortices and instabilities. This is indicated by a high Reynolds number ( $\approx 10^5$  [35]). In flows with low Reynolds number, viscous forces play a more important role due to friction between the body and the fluid. Such flows are usually laminar and flow separation from the body occurs very late or not at all [24, 36]. The Reynolds number is expressed by

$$Re = \frac{\rho v L}{\mu} \quad (\text{B.2})$$

where  $\rho$  is the density,  $\mu$  the dynamic viscosity of the fluid and  $v$  the flow velocity. The parameter  $L$  refers to characteristic geometric size of the body in the flow, e.g. the diameter in case of a sphere.

The aforementioned drag coefficient  $C_D$  depends on the type of flow. Therefore, it is important to investigate the considered flow regimes for the human hand in water and viscous flow in order to find the appropriate drag coefficients to solve equation B.1 analytically in the haptic rendering loop.

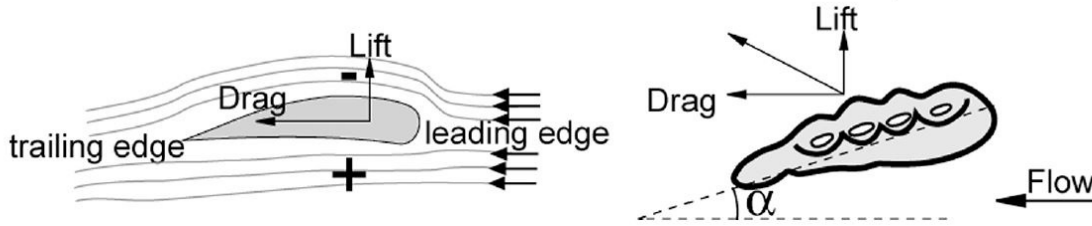


Figure B.2: Comparison of a hydrofoil and the human hand subjected to flow with acting lift and drag forces, which are dependent on the angle of attack  $\alpha$  [37].

For the investigation of the flow regimes, first the interaction with water is taken into account. There is no defined characteristic length for the human hand, but as the hand in a horizontal position in the flow compares to a wing profile (Fig. B.2), the width of the hand ( $= 0.1$  m) is chosen to be the characteristic length, as also proposed by and Troussaint and Truijens [37]. To assume a characteristic velocity, various studies on the human hand motion while swimming are considered, showing that the average hand velocity during swimming lie around 2 m/s [38–40]. This, however, describes a strong stroke, which is not the typical speed when investigating a fluid. For feeling a fluid, the flow velocities are likely to stay under 1 m/s, but are taken to be  $v = 1$  m/s as a maximum value. With the water's density of  $\rho = 1000$  kg/m<sup>3</sup> and dynamic viscosity of  $\mu = 0.001$  Pa s, the Reynolds number is found to be of the magnitude of  $Re = 10^5$ . This means that turbulences occur in the flow.

For the interaction with fluids of higher viscosity, the velocity and characteristic length remain the same. The viscosity and density, however can vary depending on the fluid. Most viscous fluids, the human interacts with in everyday life are silicones, oils and different kinds of liquid food, such as mayonnaise or honey. It is found that most liquid foods and oils [23] as well as silicones [22] have a density close to the one of water, so that for this case  $\rho$  is again chosen to be 1000 kg/m<sup>3</sup>. Furthermore, the viscosities of common liquid food products are found to be in the range of 1-100 Pa·s [36, 41]. Since it has been found by Bergmann Tiest et al., that humans can haptically only distinguish between viscosities above 2 Pa·s [42], in this study only the range between 2 and 100 Pa·s is investigated. Thus, for determination of the Reynolds number,  $\mu$  is chosen to be in this range. For the purpose of the study, all fluids are assumed to be Newtonian, having a constant viscosity. Substituting the mentioned values, it can be found that the Reynolds number for viscous fluids is between 1 and 10. At such low Reynolds number, inertia forces are marginal, so that the flow can be considered purely laminar, which will be explained in more detail in section B.4.

As mentioned, this identification of Reynolds' number and thus flow properties are important to determine an estimate for the drag coefficient in order to find an analytical expression for the acting drag forces on the human hand. A general relationship between the drag coefficient and the Reynolds number is given for a sphere [24] and is shown in Figure B.3 with the identified areas for the human hand in highly viscous fluids and water, respectively. It is to emphasize that the shown graph is only valid for an axisymmetrical sphere and is only meant to give an overview of the considered flow regimes and the behavior of the drag coefficient in such. For the rendering of the fluid forces in real time, the specific drag coefficient for the interaction with water and higher viscous fluids need to be found. The procedure of choosing and implementing this in the force formula is explained in the following sections.



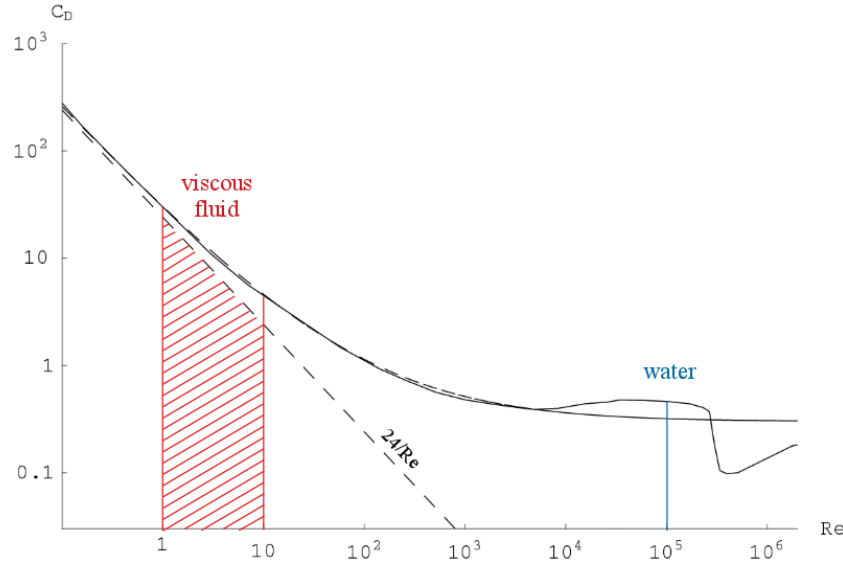


Figure B.3: Development of the drag coefficient  $C_D$  over the Reynolds number  $Re$  with the characteristic regime for the human hand in water (blue) and fluids with a high viscosity (red) (modified from [24])

## B.3 FORCES IN WATER

The locomotion of humans in water is of special interest regarding competitive swimming. Therefore, various studies have been carried out investigating the occurring forces on the human hand and arm caused by the interaction with water [25, 26, 29, 31, 32, 37, 38]. It was found that the forces acting on the human hand depend strongly on the angle of attack  $\alpha$ , which is defined as the angle between the flow direction and the plane of the hand (Fig. B.4a). This explains why the human feels more resistance when sweeping through the water with the palm facing the flow, instead of the hand's surface being perpendicular to the direction of motion. Next to the angle of attack, the sweepback angle (Fig. B.4b) and the pitch angle (Fig. B.4c) have been shown to have an influence on the occurring forces. However, to reduce complexity, the specific effects of those angles have been neglected in most studies. Based on that, this study will also only take into consideration the influence of the angle of attack. Regarding the defined motion of sweeping with the flat water, even this effect might be neglectable, but is implemented to enable a more realistic feeling assuming the human does not always move the hand perfectly perpendicular to the water.

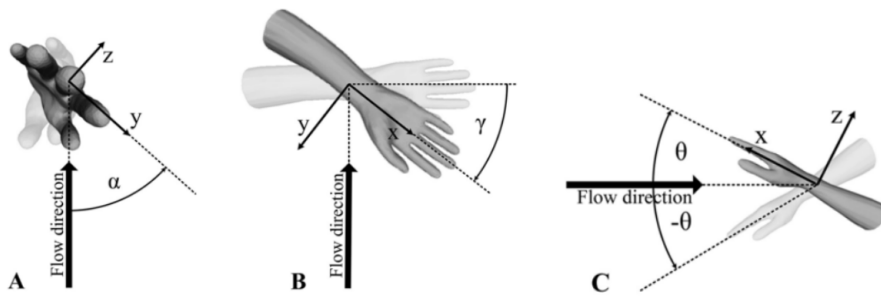


Figure B.4: Definitions of different hand orientations in swimming, where the x-y plane is define to lie in the hand palm and the z-axis pointing out from the backside of the hand: A) angle of attack  $\alpha$ , B) sweepback angle  $\gamma$  and C) pitch angle  $\theta$  [25]

As explained in section B.1, lift forces are neglected, thus solely equation B.1 is be implemented and solved analytically in real time. The choice of value for each variable is explained in the following. For water the density  $\rho$  of  $1000 \text{ kg/m}^3$  is set as a constant, while the velocity  $v$  of the human hand can later on be read out from position sensor data of the haptic interface. As seen in Figure B.3, the drag coefficient  $C_D$  should have a value around 1 for water. In this regime, however, a strong relationship with the angle of attack was found through

experimental and numerical (CFD) investigations. The findings of various works were recently surveyed by Houwelingen et al. [25]. Comparing the drag coefficient curves found through different methods showed similar results showing a consistent relationship between drag coefficient and angle of attack. To incorporate this in the haptic rendering, it is decided to fit a curve to the literature data to find the drag coefficient for the current angle of attack of the human hand attached to the haptic interface. This should add some realism to the very simplified force calculation in this project. The calculation of the angle of attack from the real time position tracking of the device is explained in Appendix C. The fitting of the curve for the drag coefficient is explained in the next section. For the characteristic area, different definitions for the hand have been mentioned. However, since the force will already vary with drag coefficient being dependent on the angle of attack of the human hand, it is decided to set the characteristic area  $A$  in equation B.1 to be constant. The area is chosen to be the maximum projected area of the human hand as proposed by various literature [30–34] and is also common practise for the investigation of forces on wing profiles [35]. For this, the hand is approximated to be ellipsoidal, the two radii being the chord length  $c$  and span  $s$  as depicted in Figure B.5. Measuring the hand of three individuals lead to an average hand area of  $0.0151 \text{ m}^2$ , which is close to the value used in the work by Sato and Hino ( $A = 0.0148 \text{ m}^2$ ) [39]. To better compare to results of this literature, this suggested value is used for the implementation of the analytic equation in the haptic device.

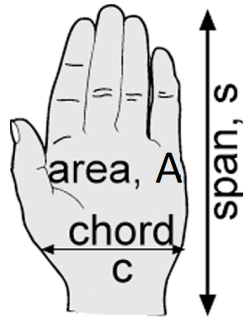


Figure B.5: Relevant parameters describing the approximated ellipsoidal area  $A$  of the human hand with the chord and span length being appropriate radii (after [25]).

To summarize the assumptions made for the force calculation, equation B.1 is rewritten with the substituted values:

$$\begin{aligned} F_D &= \frac{1}{2} C_D(\alpha) \cdot v^2 \cdot 0.0148 \cdot 1000 \\ F_D &= 7.4 C_D(\alpha) v^2 \end{aligned} \tag{B.3}$$

with  $v$  being the velocity of the hand determined through sensor data and  $C_D$  being a function of the angle of attack  $\alpha$  as explained in the following section.

### B.3.1 DRAG COEFFICIENT APPROXIMATION

The drag coefficient of the human hand has been investigated in numerous studies, and was found to be independent of the flow velocity  $v$  [26, 28, 31, 32]. This is important for the desired application as the velocity is given by the human user attached to the haptic interface and is therefore dynamically changing. However, the dependency on the angle of attack  $\alpha$  has been proven in multiple studies making use of experimental and numerical simulation techniques [25]. Since both methods are known to have their drawbacks, it is decided to compare the found results from each method with each other. It is desired that the boundary conditions for both methods are chosen to be similar. The research done by Sato and Hino in 2013 [39] analyzes the hydrodynamic forces acting on a swimmer's hand with a CFD simulation, in which the hand model is based on experimental data obtained through a study by Kudo in 2008 [33]. The experimental, as well as the numerical method led to very similar results in the determination of the drag coefficient  $C_D$  over the angle of attack  $\alpha$ . In the comparison by Houwelingen et al., those curves are shown to be between the extremes of the found drag coefficients of all compared authors [25]. Thus, they are assumed to be realistic mean values. To enable the calculation of the drag forces on the haptic device in real time, it is decided to fit a curve between the experimental and the CFD data (Fig. B.6).

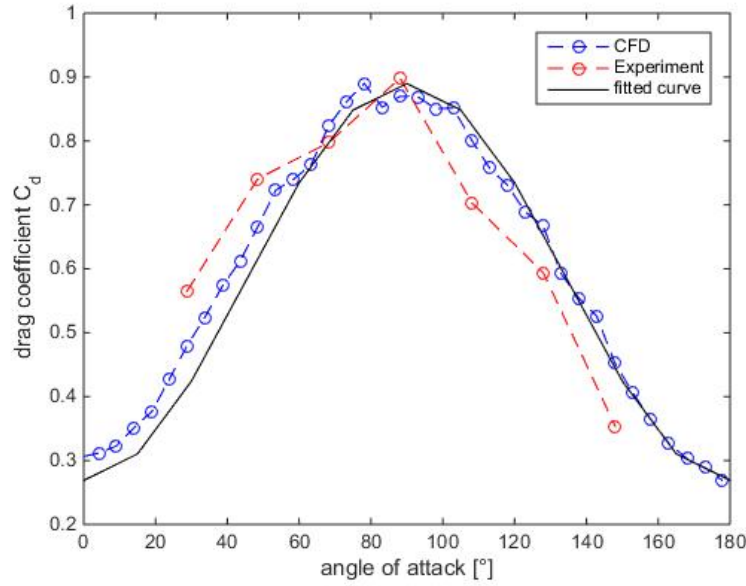


Figure B.6: Drag coefficient  $C_D$  of the human hand depending on the angle of attack as measured experimentally (red) [33] and numerically (blue) [39] with data taken from the same swimmers with a fitted function.

The drag coefficient  $C_D$  as function of the angle of attack  $\alpha$  is found to be

$$C_D = -0.3105 \cos(2\alpha) + 0.5794 \quad (\text{B.4})$$

Implementing this in equation B.1 and simplifying it leads to

$$F_D = 2.2977 v^2 (\cos(2\alpha) + 1.8660) \quad (\text{B.5})$$

The drag force is now only dependent on the angle of attack  $\alpha$  and the velocity of the human hand  $v$ . Both variables can be calculated using sensor information, so that the occurring drag force can be calculated in real time. This leads to fast and very inexpensive calculation of the drag force in the interaction of the human hand with water, which should enable stable rendering at very high frequencies ( $\approx 1$  kHz). For the application, the function is implemented in the Simulink model (see Appendix C).

### B.3.2 FORCE VERIFICATION

Before implementing the the found force equation from the the previous section in the haptic interface, it is desirable to investigate the validity of the calculated forces. Ideally this should be done by carrying out an experiment, in which the forces acting on the human hand are measured when dragging it through water. However, the hardware for this experiment is not available at the DLR during the time of this project, thus it is impossible to test this experimentally within given time. Nonetheless, due to the interest of the forces acting on the human hand for competitive swimming, much literature in this field is available and similar experiments have been carried out. Despite limited comparability due to varying hand and hardware properties, such literature is used to approximate that the magnitude of occurring drag forces range in the right order with the calculations done using the estimations explained in the previous section.

As mentioned the forces on the human hand during swimming have been investigated experimentally and numerically. One of the first investigations was carried out by Berger et al. in 1995 [26], where a hand arm model was dragged with 1 m/s through a water canal, as can be seen in Figure B.7. The forces on the hand-arm model were measured in three directions for various angles of attack using a six-component dynamometer with strain gauges. The obtained force curves can also be seen in Figure B.7. The forces in x-direction  $F_x$  were measured against the line of motion and respond therefore to the drag force, while  $F_y$  and  $F_z$  contribute to the lift force. This experiment verifies that the drag forces dominate when dragging the hand through water at moderate speed with the frontal hand area facing the direction of flow ( $0^\circ$  or  $90^\circ$  in B.7).

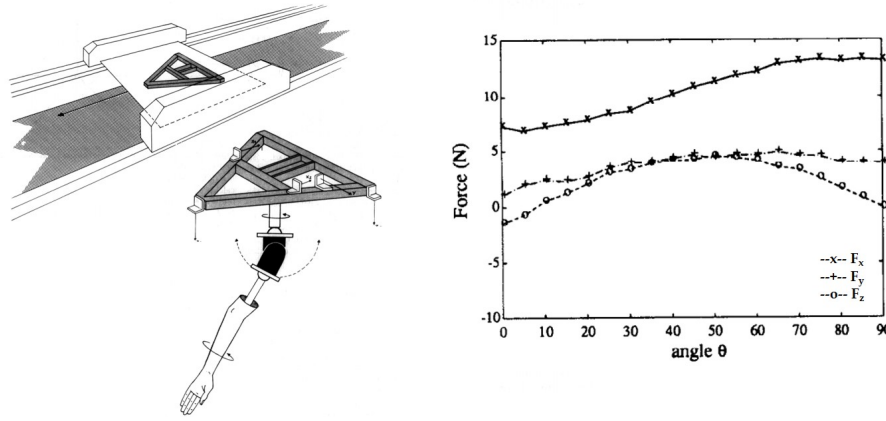


Figure B.7: Experiment setup by Berger et al. [26], in which a hand arm model was dragged through a water canal and the forces in all directions were recorded

The experiment was carried out with a towing velocity of 1 m/s. Substituting this in equation B.5 for different angles of attack leads to the curve seen in Figure B.8. It can be seen that compared to the forces measured by Berger, the calculated forces are considerably smaller, showing an offset of around 5 N. Looking at the drag coefficient curve from Berger, however, it can also be seen that a higher amplitude was defined than of the fitted  $C_D$  curve used for the force estimations. This relates to the difference in forces seen in this comparison.

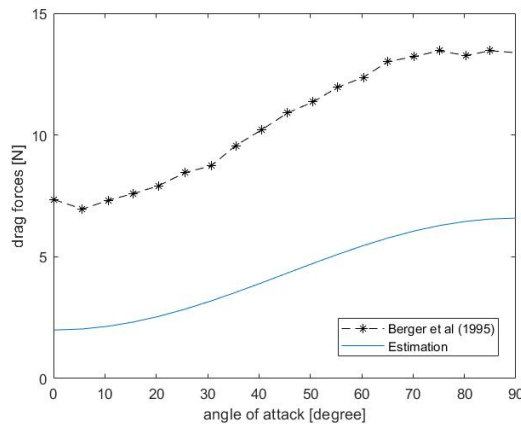


Figure B.8: Comparison of the drag forces measured by Berger et al. [26] and the ones calculated with the fitted drag coefficient curve over angle of attack of the human hand in water.

It is impossible to determine which drag force coefficient curve is more accurate. As explained previously, the findings of Sato and Hino [39] were chosen for the, as it found matching results through experiments as well as simulation and was more recent. However, Houwelingen et al. [25] have reviewed various literature in this field comparing drag coefficients found through numerical and experimental studies as shown in Figure B.9. Additionally the found fit is plotted in this graph. It becomes apparent that the used approximation for the drag coefficient is more on the conservative side, leading to lower forces, nevertheless showing the correct curve progression. The comparison between all those findings is very hard, as the results strongly depend on the hand shape and size, whether the influence of the arm was taken into account, the medium in which the measurement was carried out, the used reference area and many more uncontrollable variables. For example, Berger et al. [26] used initially the wet surface area to calculate the drag coefficient, leading to much lower coefficient values (see Fig. B.9). When applying the found forces however to the hand plane area as done by Schleihau, a more prominent curve can be observed, which is added to the overview. It becomes clear that the validity of different studies in this field is hard to verify. However, all found curves show identical progression properties. Therefore, the curve shape might be more important to render realistic force characteristics in the interaction of the human hand in water, while the difference in amplitude relates to the magnitude of forces, which could be corrected later on through a scaling factor.

Since the curve fit follows the correct shape in an appropriate range of magnitude for the drag coefficient, it is assumed that realistic forces can be calculated with the applied estimation. The reason for the more conservative pick of data for the fit can be explained with the aim to find a curve fit that would combine characteristics found through numerical and experimental studies, as both methods have advantages and drawbacks. For this, it was required that the boundary conditions and assumptions for both methods were identical to design a valid fit and only the research by Sato and Hino [32, 39] provided such information and were therefore chosen as the basis for the force estimations in this project.

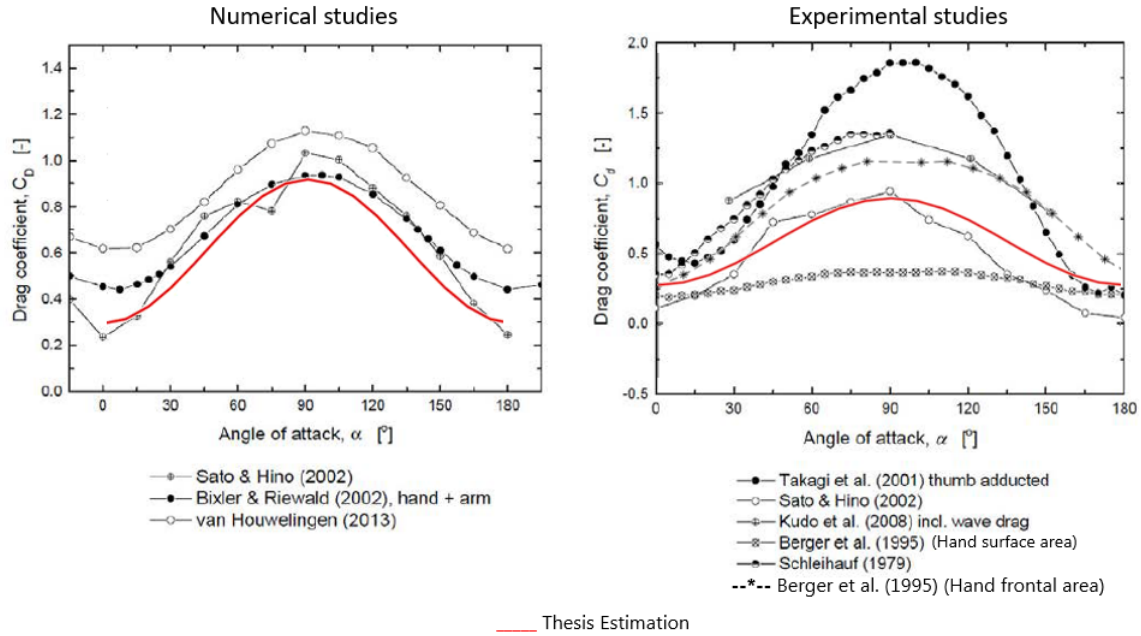


Figure B.9: Comparison of van Houwelingen et al. [25] of the drag coefficient determined by different numerical (left) and experimental (right) studies with additional data from Berger et al [26] and the fitted drag coefficient curve from this study.

## B.4 FORCES IN HIGH VISCOUS FLUIDS

As mentioned beforehand, this study should not only focus on the rendering of virtual water, but on various fluids. Especially higher viscous fluids are interesting as this might be a useful addition to the haptic exploration possibilities of remote or unknown environments. Especially, dry sediments or sludge behave more like viscous fluids than solid bodies [43], which adds new sensations and thus information for researchers. However, the forces occurring on the human hand during an interaction with viscous fluids have not specifically been addressed in the past. Nevertheless, some assumptions can be made for viscous fluids which simplifies the calculation of forces further. As shown in Figure B.3 moving through high viscous fluids with considerably low speeds, results in low Reynolds numbers. This means, that liquids in this regime, such as honey, show only insignificant effects of inertia and are dominated by internal friction [24]. This leads to a laminar flow with hardly any turbulences occurring. If the flow is perfectly laminar, referred to as creeping flow or Stokes' Flow [24], further simplifications can be made. However, the definition for such circumstances requires  $Re \ll 1$ . For the investigated case, in which the human hand is interacting with the viscous fluid, the  $Re$  number was found to be between 1 and 10 (Fig. B.3). However, it has been empirically shown that the assumptions hold for  $Re \lesssim 1$  and experimental investigations showed perfectly laminar flow for Reynold's numbers up to 24 [44]. In this project, therefore Stokes Flow is considered for the calculation of forces of viscous fluids acting on the human hand. The validity of applying this to the shape of the hand is further analyzed in section B.4.1.

Considering such flow of an incompressible Newtonian fluid around a sphere, Stokes formulated in 1851 the acting forces to be

$$F = 6\pi a \nu \mu \quad (\text{B.6})$$

where  $\mu$  refers to the viscosity of the fluid and  $a$  to the radius of the sphere with moving velocity  $\nu$ .

Since the sphere has no geometric direction, no lift forces are acting and only drag forces play a role. Skin drag contributes two thirds and one third of the forces occurs from form drag. For sufficiently small spheres in fluids with high viscosity, this Stokes' Law holds and is an easy way to approximate the acting forces. In this regime the drag coefficient of a sphere can be approximated with

$$C_D = \frac{24}{Re} \quad (\text{B.7})$$

The fit of this approximation to the drag coefficient on a sphere can be seen in Figure B.3. Accepting the error indicated in Figure B.3 for the regarded flow regime of the human hand in viscous fluids, the application of Stokes' assumptions are considered for the calculation of forces in fluids with high viscosity.

#### B.4.1 HAND SHAPE APPROXIMATION

In a simplified form, neglecting finger spread, the human hand can be described as an ellipsoid, where the defining lengths are chord length  $c$ , the span  $s$  and the thickness of the hand (Fig. B.5). No literature on the interaction of such a shape with a viscous fluid was found, but work done by Taamneh [44] and Richter and Nikrityuk [45] analyzed the drag coefficients of a prolate spheroid, which is an ellipsoid with two different radii rotated around the longer axis. This is considered the best available approximation for the human hand in a viscous flow, as shown in Figure B.10. The hand is not considered as a flat plate or disk, since it does not have blunt edges and thus it can be assumed that in viscous flow no direct flow separation on the corners occurs.

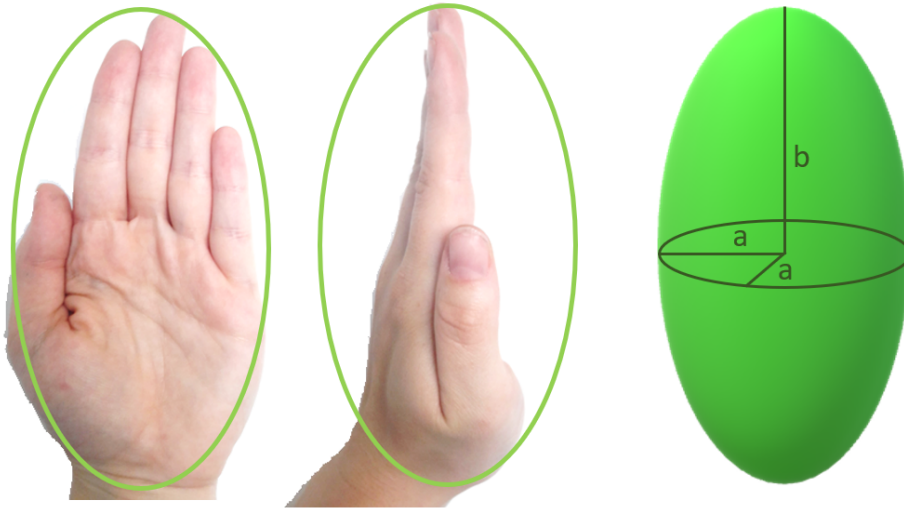


Figure B.10: Estimation of the human hand as a prolate spheroid with  $a$  and  $b$  being the two defining radii.

Richter and Nikrityuk found that for spheroids in various orientations, the flow is symmetric and transition to an laminar-unsteady flow regime only happens at Reynold's numbers of  $> 250$ . For lower regimes, even though flow separation might happen, no turbulence occurs, as can be seen in Figure B.11.



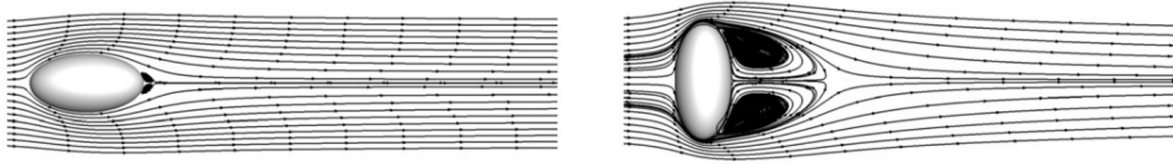


Figure B.11: Flow at  $Re = 100$  around a prolate spheroid at different orientations as obtained through simulation by Richter and Nikrityuk [45].

Similar to the findings for a perfect sphere, this indicates that viscous and drag forces dominate the interaction. This leads to the conclusion that Stokes Law might be a valid simplification to calculate the forces acting on the hand in a viscous fluid. The investigation for the drag coefficient of a spheroid shows an identical curve to the one known for perfect spheres, only shifted up for the vertical spheroid and down for the horizontal position in the flow (Fig. B.12). Since the hand is to be moved in the viscous fluid and both positions might occur, the drag coefficient curve of the sphere is actually recognized as an appropriate mean and therefore used for the further calculations in this project. This means that for the viscous fluid interaction, the angle of attack of the human hand does not need to be considered and a constant force is expected independent of the hand orientation. Similar to the findings of section B.3.2, the characteristics of the interaction with the fluid are proven to match, and only the magnitude might have to be adjusted when further investigating this case.

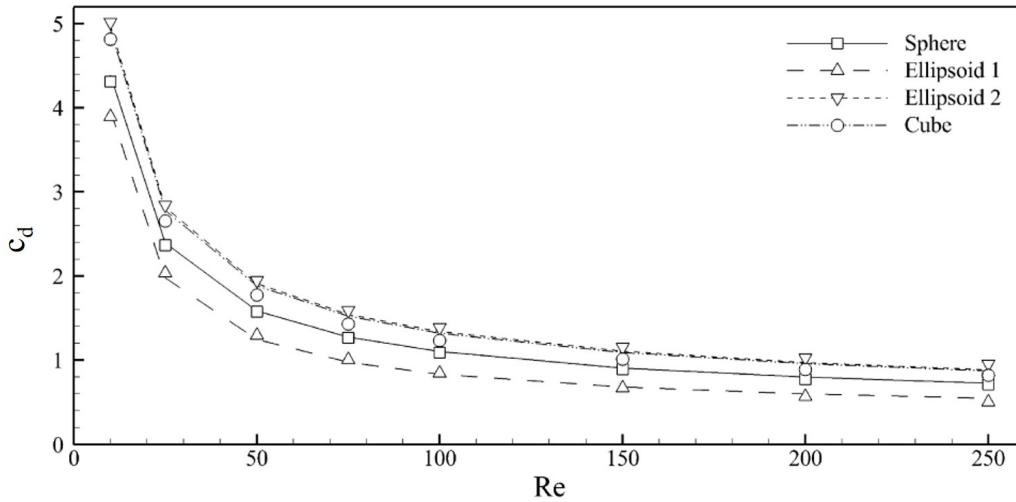


Figure B.12: Drag coefficient curve over Reynolds number as obtained by Richter and Nikrityuk [45] for a perfect sphere, an ellipsoid in horizontal (Ellipsoid 1) and vertical position (Ellipsoid 2) to the flow and a cube.

Therefore, the drag coefficient approximation for a sphere stated in equation B.7 is taken as an approximation for the human hand in this research, assuming the Stokes Law to be valid. As characteristic radius, the radius of the sphere is chosen that has the same surface as the approximated spheroid shown in Figure B.10. Assuming the two characteristic length to be the hand span  $s$  ( $\approx 0.2$  m) and the chord width  $c$  ( $\approx 0.1$  m) of the human hand as defined in Figure B.5, this leads to a Stokes radius of 0.064 m.

### B.4.2 FORCE APPROXIMATION

Assuming Stokes' Law to be valid for the interaction of the human hand with a viscous fluid, suggests the use of the curve approximation for the drag coefficient stated in equation B.7. Implementing the definition of the Reynolds number from equation B.2 and substituting this in equation B.1, leads to

$$F_D = 12 \frac{A}{L} v \mu \quad (\text{B.8})$$

Comparing this to equation B.6 and summing all known variables to a constants, leads for both formulas to the simplified expression of

$$F_D = c v \mu \quad (\text{B.9})$$

This shows the drag force to be proportional to the flow velocity and the fluid viscosity, which is known to be valid for arbitrary bodies in viscous fluids [24]. For equation B.6, implementing the defined characteristic radius of  $a = 0.065$  m, leads to a value for the constant of

$$c_{Stokes} = 6\pi a = 1.2322 \quad (\text{B.10})$$

For the second approximation (eq. B.8) the assumptions made in section B.2 and B.3 are assumed to still be valid, with  $A = 0.0148 \text{ m}^2$  and  $L = 0.1$  m. Implementing this, the constant for this analytical expression is found to be

$$c_{Approx} = 12 \frac{A}{L} = 1.7760 \quad (\text{B.11})$$

It can be seen that both constants are in a similar range. The validity of all the made assumptions cannot be proven, since no literature on this topic was available and neither experiments nor CFD simulations could be realized within this project time frame. However, the relationship defined in equation B.9 are known to be correct, thus a wrong constant will once more only result in a shifted magnitude range of the calculated forces, but should still lead to the correct behavior. Therefore, no validated pick can be made between the found constants  $c_{Stokes}$  and  $c_{Approx}$ . Due to the greater similarity with the equation used for the calculations of the water forces to remain consistency, in the following of this project, equation B.8 is chosen to be implemented in the Control model to render viscous fluids as described in Appendix C.



## B.5 FORCE DISTRIBUTION

Next to the correct calculation of the forces for the interaction with water and viscous fluid, the distribution of the forces on the human hand plays a role. In the real interaction, the fluid flows over and around the whole hand, resulting in a pressure distribution. Since the used haptic interface only has five interface points with the human hand as explained in section A, it is not possible to distribute the forces over the whole hand area. In order to still allow a realistic perception, the sufficient division of the forces across the interface points is analyzed. For this purpose it is assumed that the pressure distribution is evenly divided across the whole hand, as indicated by the results obtained through CFD simulations of Bilinauskaite et al. [29]. Since pressure is the distribution of force over area, the force is to be divided according to the percentage of area each interface point represents. With the used haptic interface, the ring and little finger of the human are not able to receive any force feedback, but it is still desired to reflect all of the calculated fluid forces to the user. Therefore, the area of those two fingers is neglected. The total area across which the force needs to be distributed, is then the area of the three remaining fingers (thumb, index, middle) and the palm area. The shape of each area is simplified as seen in Figure B.13. The percentage of the total force reflected on each interface point should then equal the percentage of each area of the total hand frontal area, not including the ring and little finger.

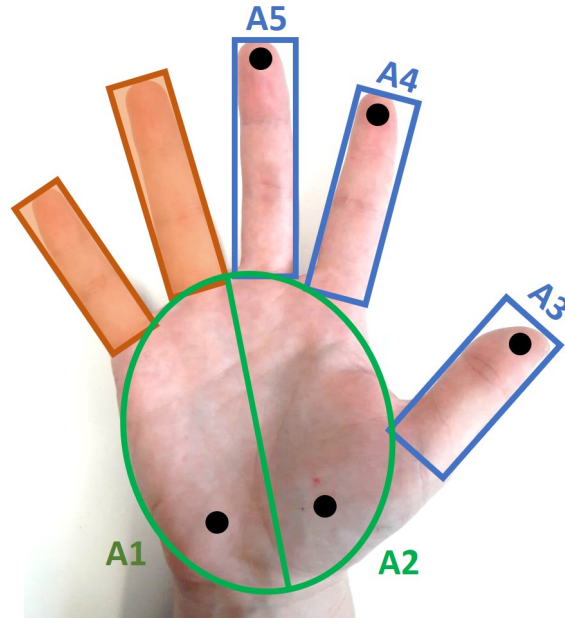


Figure B.13: Applied distribution of proportions of the human hand area for the force reflection through the haptic interface. The little and ring finger are not considered as they cannot receive force feedback.

To find the proportions of each area, the research by Garret (1971) is considered, who summarized anthropometric properties of the human hand [46]. Using the provided measurements and the simplified areas as seen in Figure B.13, leads to the following area percentages:

$$A_1 + A_2 = 64\%$$

$$A_3 = 10\%$$

$$A_4 = 12\%$$

$$A_5 = 14\%$$

Generalizing those findings, it is decided to reflect 10 % of the total calculated fluid forces on each of the interface points on the three attached fingers and 35 % of the force on each of the palm points.

# C

## IMPLEMENTATION

The overall control cycle is already explained in Appendix A. In Appendix B the analytical expressions are derived to calculate the simplified fluid forces exerted by water and viscous fluids. Combining those information, this Appendix describes the detailed implementation of the force rendering in the Simulink model. A model of the human hand is simplified to enable the fast calculation of length parameters. Further more a collision detection needs to be implemented to indicated, when the hand is immersed in a virtual liquid and forces need to be rendered. The calculation of the forces in water and viscous fluids is implemented separately and can be manually switched. Each component is explained in the following.

### C.1 HAND SIMPLIFICATION

The final calculations of the forces applied to the hand during the interaction with a fluid assume a constant value for the area  $A$  of the hand (Appendix B). In that case, it is not necessary to implement a hand model in the algorithm to find the current hand surface dynamically, but a constant can be set. Nevertheless in the process of deriving meaningful analytical expressions and first implementation tryouts, it was considered to use the projected area of the human hand as it is suggested by various literature [25, 27–29]. Therefore, a subsystem was added to the Simulink model to enable the calculation of specific hand parameters depending on the real time movements of the human user. This was eventually not used for the final calculations, but can be adapted when adding complexity to the derived equations later on, e.g. to add lift forces. Since the inverse kinematics for the human hand are already implemented in the control model, the transformation matrices for each joint of the human hand are known as defined by Stillfried et al. [12, 13]. The transformations allow to calculate the current pose of the hand and the angles of each human finger joint. The angles and pose are important to define the position of the hand in space, but do not suffice e.g. to find the projected shape. Instead, the whole hand geometry should be defined in the Simulink model. For the definition the human hand model data (22 DOFs) obtained by Stillfried et al. [12] is used, which consists of 17 bodies (Fig. C.1).

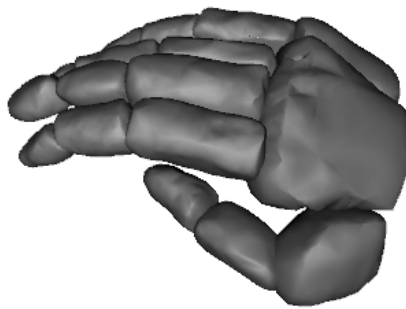


Figure C.1: Rendering of the human hand in Instantreality, based on the MRI data obtained through Stillfried et al [13].

Each of the 17 bodies is an individual point cloud and plotting all the points of this render leads to a total amount of 17683 points. Each of these points has to be translated and rotated using the appropriate transformation matrices obtained in [12] to arrange them to the complete hand model, as seen in Figure C.3A. Transforming all data points in the Simulink model during each step would slow down the algorithm considerably, effecting the ability to run in real time. A simplification of the hand model is desired to achieve high update frequencies. The complexity of the hand geometry should be maintained. For this purpose, the point clouds were first simplified to only include 50 points per body, which still lead to a total of 848 points (Fig. C.3B). To reduce calculation efforts further, finding a model with a minimum amount of points is desired. Therefore, each finger phalanx is simplified to a capsule, which can be defined through a line and a defined radius (Fig. C.2).

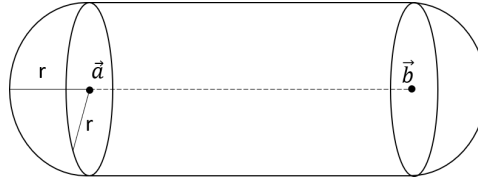


Figure C.2: Capsule defined by two points in space  $a$  and  $b$  and a constant radius  $r$ .

By defining two points per finger phalanx, a capsule can be matched to the body of each phalanx. The points are chosen such that the same radius can be applied for all finger parts. To unify the approach applying the same radius to the palm parts is desired. The minimum amount of points should be found for the palm parts, that are judged to sufficiently represent the body through manually matching to the original point cloud. Using an implemented matlab function (*reducepatch*) to reduce the point clouds, 7 points are found to be sufficient to define each palm part. In this way a hand model consisting of 73 points is achieved C.3C. The visualization of this hand with the added radius is seen in Figure C.4. Based on the current hand position of the human user, the joint angles of the hand are estimated with the inverse kinematics. Those angles can then be used to fully define the hand pose with the 73 data points by applying the appropriate transformation matrices. Due to the low amount of points, the calculations are possible without increasing the resource intensity of the algorithm. The coordinates of the hand points can then be used to find e.g. the projected hand area. By projecting all points to the plane perpendicular to the direction of motion, adding the defined radius allows to take the outer points as border and calculate the inner area. Similarly, other hand related sizes can be easily found.

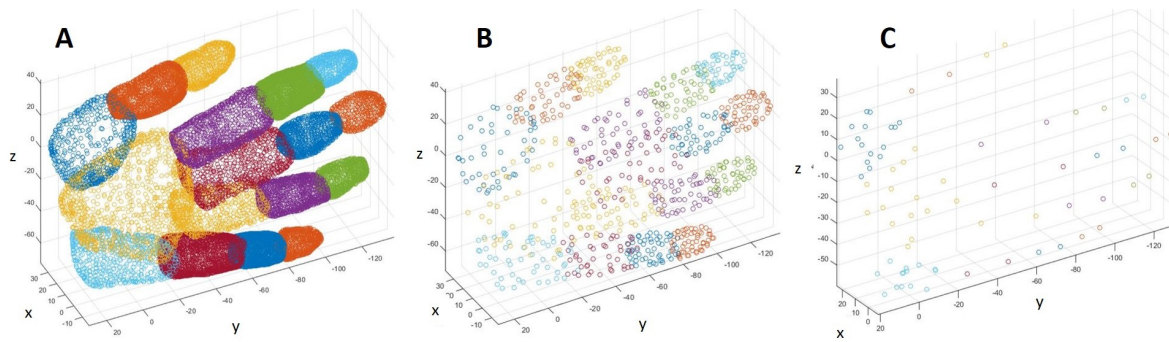


Figure C.3: Point clouds of A) original MRT data [13], B) data reduced to 50 points per body and C) data reduced to 73 points for the whole hand.

As mentioned in the beginning of this section, for the final implementation of the force calculation, the hand model is not needed since the hand specific values are set constant. Nevertheless, the simplification of the hand model was an important part in understanding the kinematics of the human hand. The achieved simplification is a useful tool to incorporate the human hand features, without slowing down real time calculations.

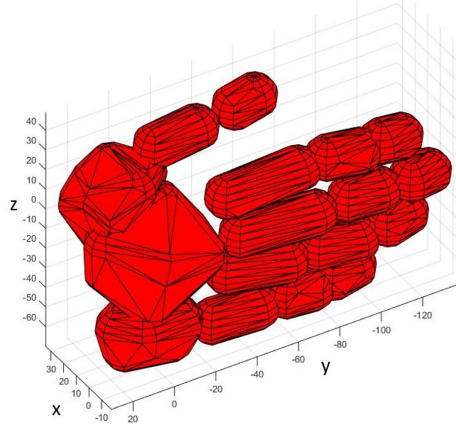


Figure C.4: Simplified model of the human hand fully defined through 73 points and an added radius of 0.01 m.

## C.2 COLLISION DETECTION

To interact with the virtual fluid, the human user has to immerse the hand in the fluid in the virtual environment. Therefore, a collision detection is necessary to give feedback about the state. The scenario is simplified to diving with the hand in a cylinder. The cylinder detection is enabled with the help of the God-object method. Defining the cylinder's position and orientation in the world frame by means of a transformation matrix is necessary. The coordinate system is defined to be positioned on the top of the cylinder with the z-axis pointing up (Fig C.5). The radius of the cylinder can be set freely by the user.

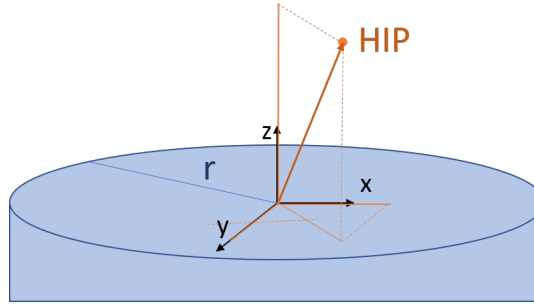


Figure C.5: Scheme of the space definition of the haptic interface point (HIP) on a virtual circular surface with radius  $r$ .

The position of the human finger tips are the haptic interface points (HIP). The HIPs can be measured with the available sensors of the exoskeleton and transferred into Cartesian coordinates in the world frame. Subtracting the position of the cylinder coordinate system from the HIP leads to a vector between those two. Projecting this vector on the z-axis of the cylinder leads to the penetration depth. When the HIP is below the surface of the cylinder, the value will be negative and then the penetration is true ( $= 1$ ). The possible penetration depth can be defined through a constant. Only when the distance between the HIP and the axis origin of the cylinder is smaller than the defined depth, the true value (1) remains. This means, being below the cylinder cannot be recognized as a collision. The vector between the cylinder coordinate system and the HIP is also projected along the x- and y-axis. Only if the length in both directions is smaller than the radius, a third true value (1) is sent. All the booleans are multiplied with each other. The multiplication ensures that only if all conditions are true, a total true statement for the penetration is sent. If any of the explained conditions is not fulfilled, the penetration is set to be false (0). This penetration information is multiplied with the calculated fluid forces, so only if the user is inside the cylinder, the forces are reflected to the user. The implementation in Simulink is seen below (Fig. C.6). This rendering is implemented for each of the robotic fingers separately. Adding a cylinder with open ends, in which the rigid body forces are reflected to the inside, the user can get the feeling of actually putting the hand in a bucket filled with a liquid. However, in the testing, the interaction is mostly simplified to the interaction with an infinite surface, in which only the first condition of the three mentioned above needs to be fulfilled. In this case penetration feedback is given as soon as the human dives through the surface remaining this signal everywhere below the surface.

Neglecting the force reflection of the bottom and walls is chosen, as people were asked to move around freely in the fluid. Unintended interactions with walls should be avoided, more so since the human did not get any visual feedback.

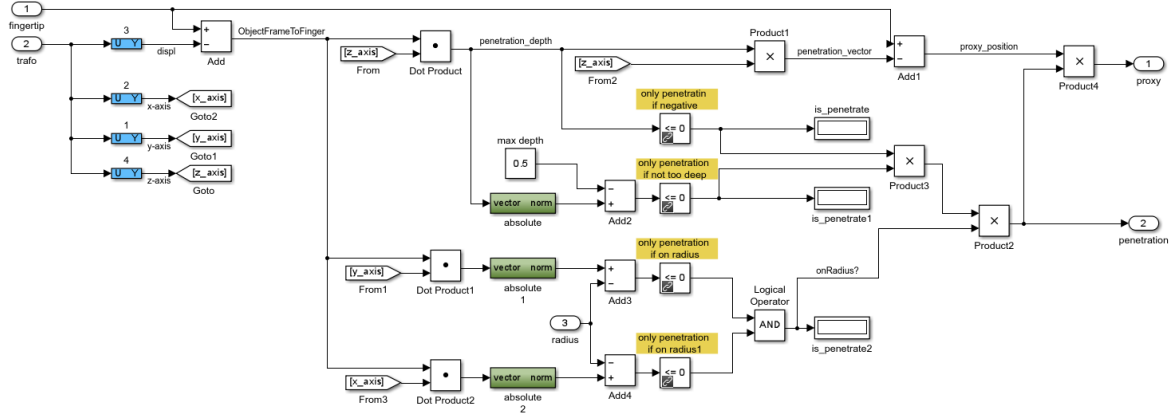


Figure C.6: Implementation of the virtual cylinder surface in the Simulink model of the haptic interface.

## C.3 FLUID FORCES

In this project the forces applied to the human hand when interacting with a fluid are to be rendered, while maintaining high update frequencies and a stable system. As explained in Appendix B, the rendering approach is split in two parts: the rendering of water and high viscous fluids. Both parts are implemented separately in the Simulink model and can be changed through a manual switch between the two (Fig. C.7). Both take the measurement and the calculated kinematics of the human hand as an input. Additionally, object information are needed, which in this case refers mostly to the viscosity of the fluid to be rendered. Also the boolean for penetration calculated as explained above is necessary, because only if the hand is inside the fluid, the forces should be reflected to the user. In the following, the implementation of each part is explained.

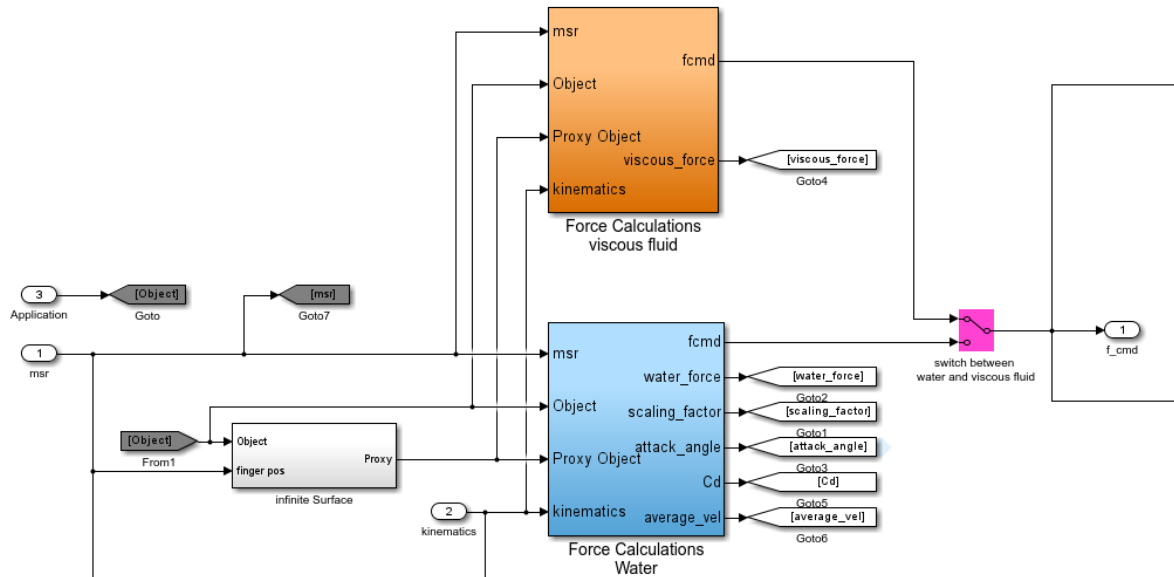


Figure C.7: Implementation of the force calculations for the interaction with water (blue) and high viscous fluids (orange) in the Simulink model.

### C.3.1 WATER FORCES

The calculation of the forces occurring through the interaction with water are implemented in the Simulink model with two subsystems, as can be seen in Figure C.8. Fluid forces depend mainly on the velocity, which can either be the velocity of the fluid flowing around a stationary object, or the velocity of a body assuming the fluid to be still. Since in the considered setup the whole hand is moving through the fluid, but each robotic finger receives the velocity separately, the velocity is averaged over the five fingers. This also takes into account the velocity of the LWR on which the haptic interface is mounted. The result is a vector describing the average velocity and direction of motion of the robot and thus the human hand. With this method, it is not possible to only consider the motion of one finger, especially when the LWR is not moved. However, due to the too high friction in the robotic fingers, the interaction with only one finger is not considered.

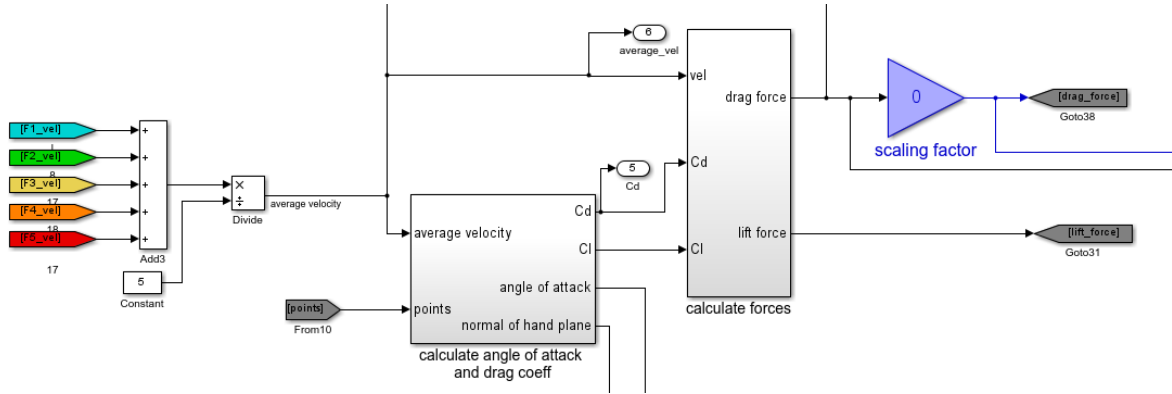


Figure C.8: Necessary subsystems for the calculation of the water forces in the Simulink model.

The velocity and the positions of the robotic finger tips in the world frame, which can be obtained through joint angle measurements and kinematics, are then used to calculate the drag coefficient  $C_D$  depending on the angle of attack of the hand of the human user. Because the kinematic model of the human hand showed at the time of the implementation to not be reliable enough and occasionally showed unrealistic poses, instead the robotic finger tip positions were used to estimate the plane of the hand. Thus, the human hand is treated as if all joints were fully extended and finger spread is ignored. If turbulences would be considered, this might not be acceptable, but for the simplified application it is deemed valid. The plane is found by using three of the attachment points of the human user as indicated in Figure C.9. Calculating the angle between this plane and the direction of motion, gives then the angle of attack  $\alpha$ . The correctness of this estimation was verified visually, by moving the hand on the interface in different orientations. As the drag coefficient  $C_D$  is a function of the angle of attack, the obtained angle can be used to calculate the coefficient as defined in equation B.4.

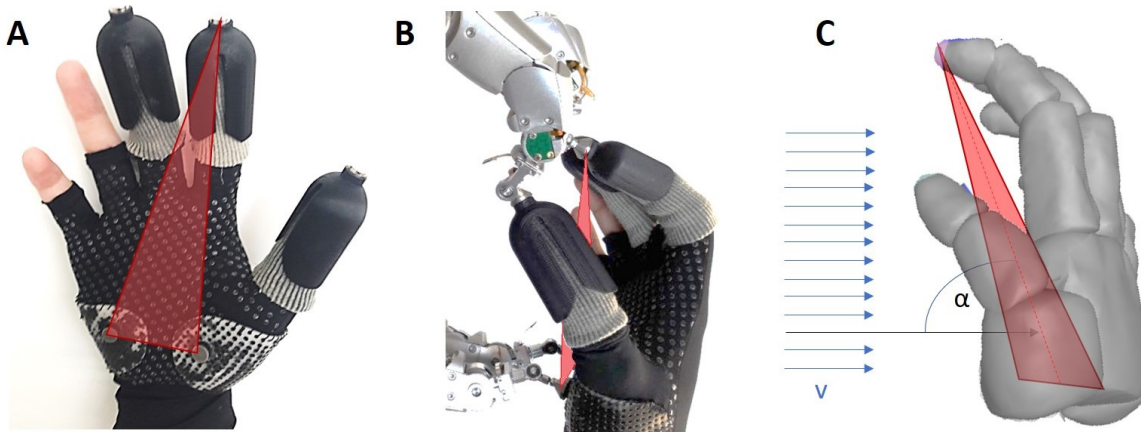


Figure C.9: Plane used to calculate the angle of attack  $\alpha$  in the human interaction with the virtual water. The plane is defined by the attachment points on the palm and the index finger (A), which are defined in space when attached to the exoskeleton (B).  $\alpha$  is then defined by calculating the angle between the plane and the flow direction  $v$  (C).



In the next subsystem, the drag coefficient is then used to calculate the drag force of the water on the human hand according to equation B.1. Considering the literature analysis of section B, the here calculated drag forces should be in the magnitude of the ones occurring in a real interaction with water. However, due to outer influences, such as the robots' dynamics, the correctness of the actually felt forces cannot be guaranteed. Additionally, the perception of the human user can vary, meaning that even if the forces are reflected correctly, they might have to be scaled in order for the human to be perceived realistically. Therefore, a scaling factor is included in this algorithm to investigate this. The forces are a scalar and the definition of the direction and application to the human user are explained in section C.3.3.

### C.3.2 HIGH VISCOSITY FORCES

Since the relationship of forces for viscous fluids is found to be different from the ones occurring in water, the viscous force calculation is implemented in a separate subsystem. Nevertheless, the same average velocity of the human hand attached to the haptic interface is used. In a first attempt of the implementation, it was tried to define the characteristic length to be dependent on the hand orientation in the flow (Fig. C.10) using the simplified hand model from section C.1.

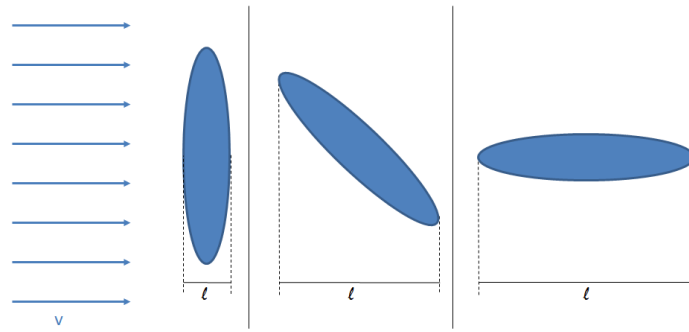


Figure C.10: Intended characteristic length  $l$  of the human hand in higher viscous fluids defined by the projected length on the direction of the fluid flow.

However, as derived in Appendix B, the forces occurring when interacting with a higher viscous fluid should be independent of the orientation, so that eventually the appropriate constant of  $L = 0.1$  m is used instead. With this length, the fluid forces are calculated according to equation B.9 in a subsystem (Fig. C.11). The calculated forces are then again of scalar size forwarded to the robotic fingers of the haptic interface as explained in the following.

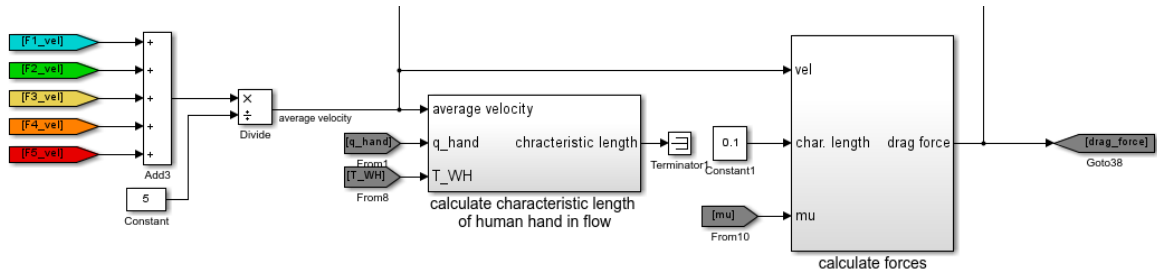


Figure C.11: Necessary subsystems for the calculation of the viscous forces in the Simulink model.

### C.3.3 APPLICATION TO THE HUMAN HAND

The calculated fluid forces have to be reflected to the human user by correctly applying the force to the robotic fingers. For this purpose, the total drag force, the individual velocity measured for each robotic finger and the collision information is needed (Fig. C.12). In each finger subsystem, the drag force is divided according to the distribution described in section B.5, so a gain of 0.1 is applied for thumb, index and middle finger while 0.35 of the force are applied to each of the palm parts of the human hand. By definition, the drag force is acting against the direction of motion and should be felt as such by the user. Therefore, the appropriate amount of force for each hand part is multiplied with the negative of the normalized vector of each robotic finger's velocity, defining the overall direction of the hand motion. This force is then multiplied with the penetration boolean explained in section C.2, which defines if the user's hand is inside the virtual fluid.

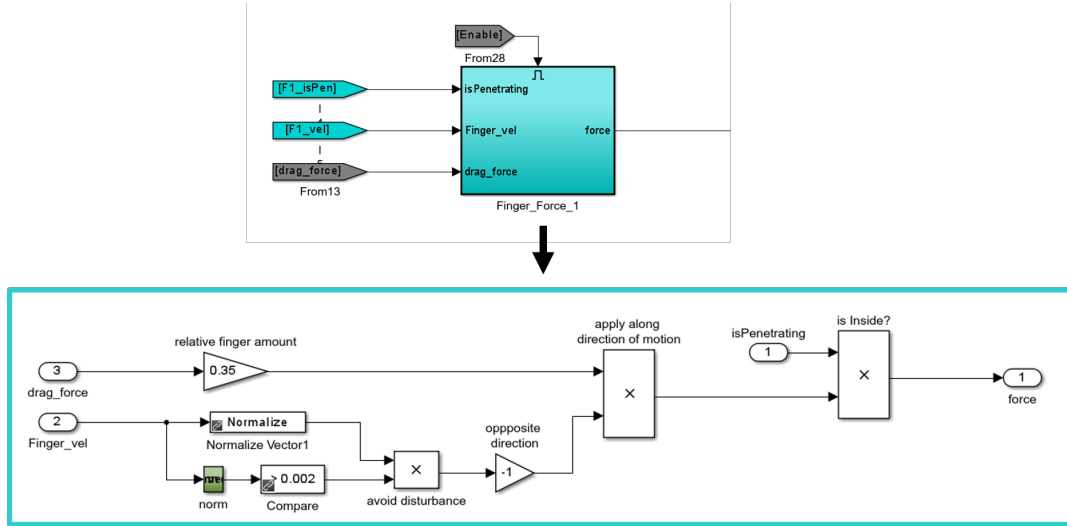


Figure C.12: Simulink subsystem to distribute and apply the calculated drag forces for one finger.

The force for each robotic finger is then forwarded to the low level control, where the force is converted into an appropriate joint torque by means of the Jacobian transformation (Fig. C.13). It is considered to implement a PID controller to match the calculated force with the one perceived by the human user. However, no noticeable improvement can be found for the rendered forces, most likely due to the large error in the torque sensor. Therefore, it is decided to not activate the PID controller to avoid instability. After the conversion of the calculated forces to torques, the torques of the joint limit protection for each robotic finger are added as well as the feedforward term. After further modification of the commanded torques through a friction compensation, the joint torques are converted to motor torques which are then applied to the hardware. Thus, the appropriate amount of the total calculated drag force is forwarded to the human hand through the five robotic fingers.

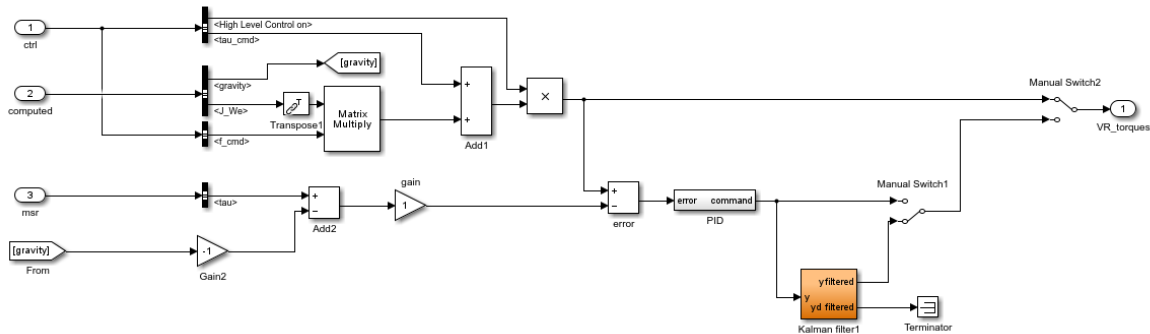


Figure C.13: Simulink subsystem to distribute and apply the calculated drag forces for one finger.

## C.4 FORCE REFLECTION ON LWR

As described in Appendix A, the remaining friction of the robotic fingers is quite high, making it hard or even impossible for the user to distinguish small force increases. Additionally, in the considered interaction, not only one human finger stirs the liquid, but the whole hand is dragged through it. The viscosity should therefore not only be perceived with the finger and hand, but actually with the whole arm of the human, as it is carrying out the main trajectory and defining the moving velocity to a substantial amount. For a more realistic feeling of interacting with a fluid, the forces should therefore not only act on the hand, but be also perceivable in the arm of the user. Therefore, it is decided to incorporate the LWR, which is used as a mount for the exoskeleton, in the force reflection to the user. An algorithm to forward the forces calculated in the robotic fingers to the LWR is already available. In this robot arm control the forces of each of the robotic fingers can be converted to act on the end effector of the LWR, which is the mounting point of the exoskeleton. The force to act on this point is found through transforming and summing force vectors of the individual robotic fingers. Then a six-dimensional vector can be calculated defining the forces and torques for each direction in space acting on that end effector point, as seen in Figure C.14. As the control of the LWR is further advanced, less friction and better dynamic behavior can be observed, which can distribute to the distinction of the perceived viscosity. Thus, the calculated fluid forces are not only proportionally reflected on each hand part, but additionally, the total drag force on the end effector point of the LWR. Those forces are acting in the same direction as defined for the robotic fingers, thus as intended against the direction of motion.

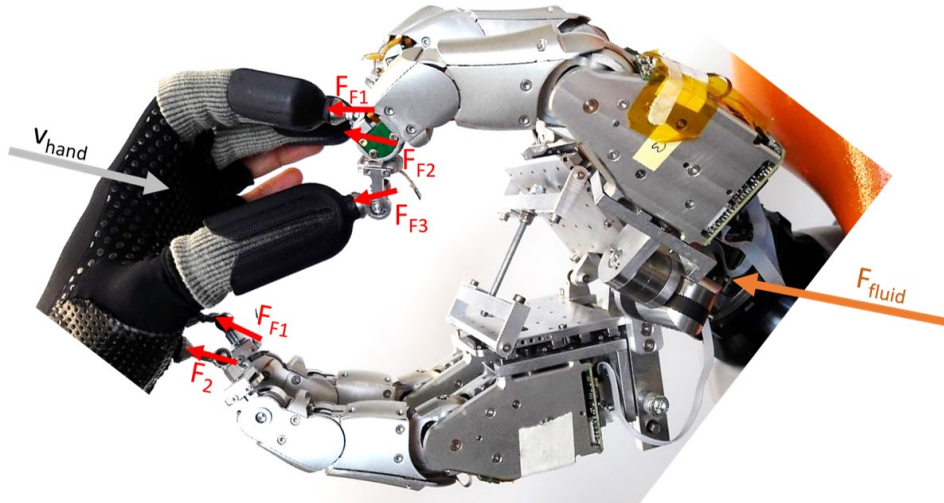


Figure C.14: Fluid forces acting on each finger and on the end effector of the Light Weight Robot against the motion direction of the human hand.

# D

## USER STUDIES

To investigate the human's perception of virtual fluids when only proprioceptive cues are given, a human user study is carried out within this research project. This user study is divided into two parts. The first part investigates, if humans are able to perceive a virtual fluid as water, despite remaining mechanical dynamics of the haptic interface. It aims to test the ability to perceive a rendered fluid, of which the physical properties are well known to the human. For this purpose, the relationship between the given and perceived stimulus are analyzed. This user study will be referred to as "Experiment 1" in the following. For the second part of the user study, a wider range of viscosity is rendered with an even more simplified force formula (Appendix B, Eq. B.8). It aims to find out how well humans can distinguish different viscosities of virtual fluids. In the following this part of the user study will be referred to as "Experiment 2". It was also desired to show that the applied algorithm cannot only render fluid properties, but also enable the interaction with solid stiff objects. To test the perception of rigidity, a small post-experiment is carried out after both experiments, where the human is asked to interact with a solid surface and describe the perceived feeling. In the following, the design and execution procedures are explained along with the results of the pilot study and the final experiments.

### D.1 EXPERIMENTAL DESIGN

The main goal of the user studies is to investigate and quantify the perception of a human user for the newly implemented haptic rendering algorithm for fluids. For neither of the experiments, the user is given a visual rendering of the virtual environment to limit the viscosity perception to haptic senses and avoid influence from other senses. To quantify the haptic perception, psychophysical methods are necessary, which are explained for each experiment below.

#### D.1.1 EXPERIMENT 1: MAGNITUDE PERCEPTION

The first experiment aims to investigate the way humans perceive rendered fluids and find a relationship between the given and the perceived stimulus. It is assumed that the implemented algorithm renders a realistic behaviour of viscosity, and comparison to literature indicate that the magnitude of forces are in a realistic range (see B.3.2). However, considering the used robotic system and its inherent dynamic behavior, it is to question, if those calculated forces are valid in the given setting. It is hypothesized that the forces need to be scaled for the considered system and application for the human to perceive the rendered fluid to be virtual water. To investigate this scaling factor, psychophysical methods are applied. A commonly used method is magnitude estimation, in which the participant is presented with a stimulus and then required to make a numerical estimation on the magnitude of the stimulus [47]. Stevens found in 1958 that a regression bias might be present in this method, which inhibits participants from giving extremely low or high answers and thus reducing the slope of the identified stimulus curve [48]. To account for this bias, a magnitude production procedure can be used additionally. This method can be described as the inverse of magnitude estimation, in which the participant is given a numerical value and has to increase or decrease a given stimulus until it is perceived to match the target value. The regression bias is assumed to be present in this method as well, however, leading to a increased slope of the stimulus relationship curve. Stevens suggested, that when applying both psychophysical methods, the systematic errors of the measurements cancel each other out.

Therefore, the participants are tested with both methods. Combining the results should then lead to a better estimate of an unbiased function [47]. To compare the findings of the magnitude estimation and production, Stevens proposed to fit a power function to the results of both methods [48]. The power function should be of the form

$$S = kI^a \quad (\text{D.1})$$

where  $S$  is the sensation magnitude, defined through the set intensity of a stimulus  $I$  and an exponent  $a$  describing the relationship between the two. An arbitrary constant  $k$  determines the scale unit. The stimulus  $I$  of which the intensity is varied, is described by the scaling factor in a specified range to be determined in the pilot study.  $S$  is the perceived viscosity by the human user. While attached to the haptic interface, the motion in free space with no rendered forces is defined to be 0 % viscosity. When the human perceives a given stimulus to feel like virtual water, the stimulus is defined to be 100 %. During the magnitude estimation the participant is presented with various stimuli of different scaling and is asked to determine a numerical value for each, judging the feeling of water to be 100 %. The presented scaling factors are pseudo-randomized per trial. 3 trials are carried out for each participant, leading to three repetitions of all presented scaling factors per person. For the magnitude production, the participant is asked to adjust the given stimulus, until it is perceived to have a defined viscosity. In the first trial, the stimulus should be adjusted to be 100 %, thus feeling like virtual water. In the second trial, the stimulus should be perceived to be 50 % and in the last trial 200 %. The amount of repetitions and range of scaling is determined through a pilot study, described in section D.2. Both methods, magnitude estimation and magnitude production, are tested on each participant with a short break in between to give the participant some rest. The order of methods is switched up, such that half the participants start with estimation and the other half with production to avoid further biases.

### D.1.2 EXPERIMENT 2: FLUID DISCRIMINATION

The second experiment should investigate, if humans are able to distinguish between different viscosities of virtual fluids as well as they are able for real ones. The discrimination is considered important for a meaningful application of haptic rendering of fluids. Only, To identify a fluid, e.g in a remote exploration or medical tele-operated palpation procedures, the human needs to be able to distinguish virtual feelings. The experiment was inspired by a study carried out by Tiest et al in 2013 [42], in which the human's capability to discriminate between fluids in different viscosity ranges were examined by means of the method of constant stimuli. Five different viscosity ranges were analyzed, defined in Table D.1. Each range consisted of six test stimuli and one reference stimulus. The fluids were investigated through stirring with a spatula or the human finger. Each test stimulus was compared to the reference. The participant had to indicate whether the test fluid felt "thicker" than the reference using a forced-choice procedure. Tiest et al. found that only for higher viscosity (above 1.8 Pa·s), discrimination can be described by a constant Weber fraction of 0.3, verifying previous results in this field. For lower viscosity ranges, discrimination is much harder to quantify. Due to this reason and the inability to render lower viscosity, because of high friction in the haptic interface (see Appendix A), it is decided to only investigate the two highest viscosity ranges.

Table D.1: Viscosity groups used in the experiments by Tiest et al. [42] for viscosity discrimination, highlighting the ranges that will be investigated in the user study carried out in the here presented research.

Range	A	B	C	D	E
T <sub>1</sub>	76	180	449	1093	10100
T <sub>2</sub>	98	243	606	1237	11580
T <sub>3</sub>	155	334	817	1646	13830
R	199	449	938	1853	16060
T <sub>4</sub>	243	555	1093	2553	18950
T <sub>5</sub>	363	740	1458	3185	23200
T <sub>6</sub>	555	1093	1853	3883	29335
Ratio	1.49	1.44	1.33	1.30	1.24

To obtain comparable results during this project, the second user study is set up similarly to the one carried out by Tiest et al. The participants are presented with a reference stimulus supposedly equal to the one used by Tiest. The rendered forces for higher viscous fluids could not be verified to be equal to the ones occurring in real fluids, since no appropriate literature was available. Nevertheless, the calculated forces are considered to be a good estimate. The viscosity  $\mu$  in the used equation B.8 (Appendix B.4) is changed accordingly to the

values mentioned by Tiest et al. In this project, only the viscosity ranges D and E (Tab. D.1) are tested, because lower viscosities could not be clearly distinguished by the human. The test stimuli and reference are presented alternately, repeating the reference in between each test. In each trial all test stimuli are presented once, in pseudo-randomized order. To determine the amount of trials, another pilot study is carried out (section D.2).

Both viscosity groups are to be tested on each participant with a short break in between to allow some rest. The order of the viscosity groups is switched up, such that half the participants start with viscosity group D and the other with group E.

The aim of the experiment is to determine the Weber fraction, which is a psychometric measurement, that relates the Just Noticeable Difference (JND) to a reference stimulus. It has been found that the Weber fraction is for most sensations constant throughout different ranges of references stimuli. For example, a Weber fraction of 0.1 means that a human can reliably detect a 10 % change in stimulus intensity referring to the reference [49]. For viscosity, Tiest et al. have found a Weber fraction of 0.3 for viscosities above 2 Pa·s. To compare the results obtained through this study with Tiest et al, the Weber fraction is determined with the same equation to fit a psychometric curve through data points [42]:

$$f(x) = 50 \% + 50 \% \cdot \operatorname{erf}\left(\frac{\log(x/p)}{\sqrt{2}\log(w+1)}\right) \quad (\text{D.2})$$

where  $x$  is the test stimulus and  $p$  the reference stimulus. The reference in viscosity group D is 1.863 and 16.06 Pa·s for group E. The Weber fraction  $w$  is a free parameter in the function and is to be adjusted to fit a function to obtained data points. The found weber fraction for the different participants and viscosity groups are then to be compare between each other and with the results obtained by Tiest et al.

### D.1.3 POST-EXPERIMENT

One of the goals of the haptic rendering algorithm developed and implemented during this thesis was the ability to run on high update rates to enable not only the rendering of virtual fluids, but of solid bodies with varying stiffness alike in the same control loop. To prove the possibility to render stiff solid bodies with the same algorithm, each participant is asked to participate in a short post-experiment after finishing the main part. During this post-experiment, a flat surface is rendered using the god-object method as first described by Zilles and Salisbury [11]. The participants are not given any visual cues, but are guided by the experimenter to an appropriate starting position above the surface with the hand facing down. The participants are then asked to slowly move downwards until they reach the surface. They are asked to describe the feeling and if they are able to identify this material to be solid. In comparison, at last a highly viscous fluid is rendered and the participants are once more asked to move downward and describe the feeling they experience.

This post-experiment is not validated by set experiment metrics, but only aims to obtain subjective impressions of the participants. The answers to that post-experiment are solely used as additional information.

### D.1.4 QUESTIONNAIRE DESIGN

It is anticipated to get additional information through a questionnaire at the end of the experiments. However, the questionnaire is to be kept short to avoid boredom of the participants and get more qualitative results. The books by Sudman et al. [50] and Robinson et al [51] are used for the design and appropriate phrasing of the questions. Three types of information are to be gathered. The first information type is required demographical data, such as age, gender and occupation of the participants. It is desirable to know if the users have background knowledge in the fields of haptics and/or experience in using a haptic interface, as this can influence the outcome of the experiments.

Second, information about the handling of the robotic system are to be obtained, since the user studies carried out within this project is the first in which the DLR's hand exoskeleton is used as a haptic input device. Therefore, it is considered useful to gather information about the feeling of safety and freedom while being attached to the device. Additionally, the ease of handling of the robotic systems is questioned, relating to the physical workload. All those questions are designed to be answered through a rating scale, with an even number of rating choices, to avoid a bias towards the middle.

Lastly, task related questions are asked to estimate the mental workload and the perceived realism of the haptic interaction, again to be answered through a rating scale. Open questions are added to give the participant a chance to give a more detailed opinion on the carried out task. The final questionnaire can be found in section F.4.



## D.2 PILOT STUDIES

To test the validity of the designed user studies, a pilot study was carried out for both experiments. Additionally, the range of the scaling factors are to be determined for Experiment 1 as well as the amount of repetitions for each experiment to limit the experiments to an appropriate length. The methods are applied as mentioned above.

### D.2.1 PARTICIPANTS

In the pilot study, a female (24 years) and two males (25 and 26 years) participated. All had background knowledge in engineering, but only one had background knowledge about the field of haptics and had used a haptic interface before. The first two pilot participants were asked to undertake both experiments, however, a long break was taken in between. The last participant was only needed for a repetition of the first experiment. The post-experiment was not carried out during the pilot study, since it only aimed to gain additional information.

### D.2.2 RESULTS PILOT EXPERIMENT 1

The pilot study was first carried out with two of the three participants. It was the goal of this study to simulate the viscosity of water to realize a comparable feeling in the virtual reality as in the physical world. For that reason, it was planned to define the feeling of real water as a reference. It was intended to do a direct comparison with one hand being attached to the robot and the other one stirring in a bucket of water. However, it became clear, that the friction and inherent mechanical viscosity of the robotic systems were too high to allow the participants a comparison with real water, because the forces occurring in free space were already above the ones perceived in water. In a first try it was impossible for the pilot subjects to match a viscosity. Despite control efforts to diminish those mechanical effects, it was not possible to improve the feeling further. Therefore it was decided to not present both stimuli, real and virtual water, at the same time, but instead successively. To diminish tactile sensations, which cannot be rendered with the available hardware, the participant was asked to wear thick rubber gloves while stirring in water. After that, magnitude production was carried out, where the pilot participants were asked to increase or decrease randomly presented stimuli, until they could identify the perceived viscosity to water in a virtual environment. This was repeated 18 times with the initial scaling factor ranging from 0 to 4. In the beginning, this was a hard task, that took both participants approximately 30 minutes to complete. The resulting boxplots for this magnitude production can be seen in figure D.1. It can be seen, that both pilot participants set the scaling factor to on average the same magnitude when asked to match the viscosity to 100 %, meaning the virtual fluid was perceivable to be water. Even though some outliers can be observed, it seems to be possible for different individuals to define a common stimulus range, in which the virtual fluid can be perceived as water.

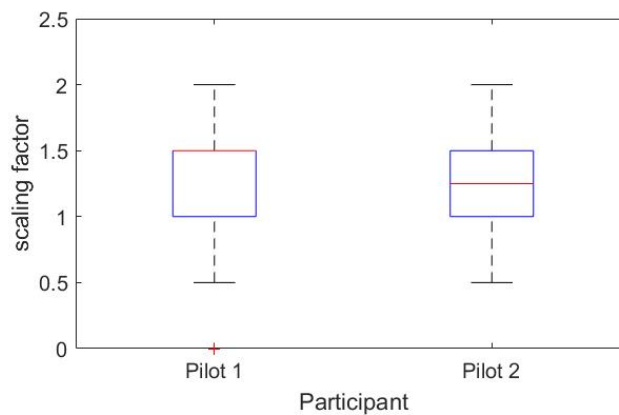


Figure D.1: Boxplot of the answers of two pilot participants during magnitude production (n=18) setting the scaling factor at which the viscosity was perceived to match the feeling of virtual water (= 100%).

However, the pilot participants were not able to carry out the second part of the experiment, being the magnitude estimation. After discussing the problem with the participants, it turned out, that the participants still tried to compare the feeling of the viscosity to the one of real water. For the aforementioned reasons of the remaining friction in the robotic system, this was an impossible task. It was therefore found, that the task had to be defined better. Hereinafter, the focus should not be to match the physical viscosity of water, but find the viscosity, for which the participant could identify the virtual fluid to be water, taking into account the dynamical behaviour of the mechanical system. The free space was therefore set as a reference, having a viscosity of 0 %. It was noticed that the participants had to be informed that because of the remaining dynamical behaviour, it was not possible to match the viscosity to real water, but should rather be compared to the feeling of free space. This feeling is comparable to moving the whole robot in a fluid instead only the hand. Considering this information and a more careful phrasing of the experiment task, the experiment was repeated, using one of the previous pilot participants and a third one, that had not yet participated, because the first pilot was unavailable. With those participants, the experiment was repeated, one starting with magnitude estimation, the other one with magnitude production. With the more detailed description of the task, the pilot participants were able to complete both parts of the experiment. For the magnitude estimation seven randomly distributed stimuli, being scaling factors between 0 and 4 were given, while for the magnitude production, the participants had to adjust the viscosity to feel like 100 %, 50 % and 200 %, each repeating seven times. The results are shown in figure D.2.

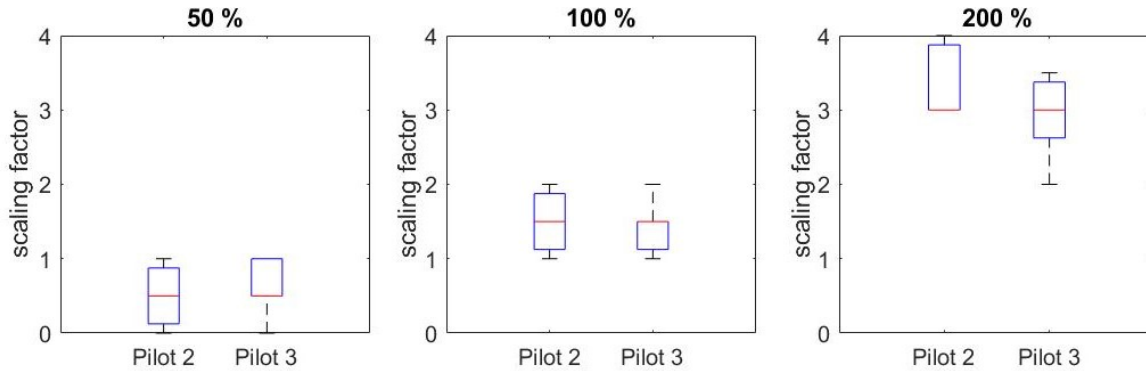


Figure D.2: Boxplots of the improved magnitude production pilot study for two pilot participants for the virtual fluid to have 50 % (left), 100 % (middle) and 200 % (right) of the viscosity of water ( $n = 7$ ).

It can be seen that for both pilot participants constant results without too much deviation can be obtained in the magnitude production, also for the 50 % and 200 %. The results of both participants lie in the same range, which indicated that a general relationship between the presented and the perceived stimulus can be found. In this second try, the participants were also able to carry out the magnitude estimation. Figure D.3 shows the results for the magnitude estimation of the different presented stimuli in comparison to the average set stimuli in the magnitude production.

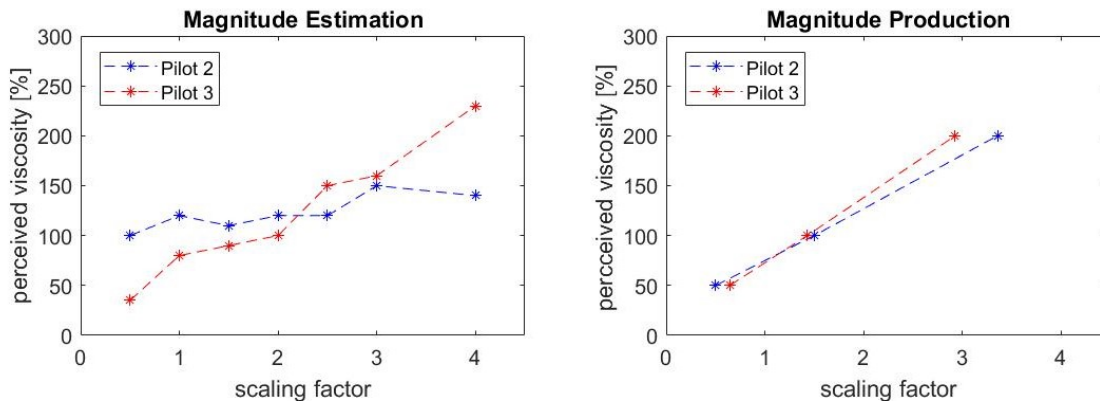


Figure D.3: Comparison of the averaged data obtained through the two pilots of the improved pilot study for magnitude estimation (left) and magnitude production (right).

For both methods a clear trend can be observed. Fitting a power function through the obtained points in both methods, leads to the plot shown in figure D.4. As expected, the function obtained by the magnitude production shows a steeper slope. Since only limited amount of data points is available through the pilot study, the correctness and meaningfulness of the displayed relationship cannot be judged. Therefore the obtained curves are not discussed in detail here, but the results seem promising and meet the expectations. Thus, the pilot study proves the experiment design to be valid.

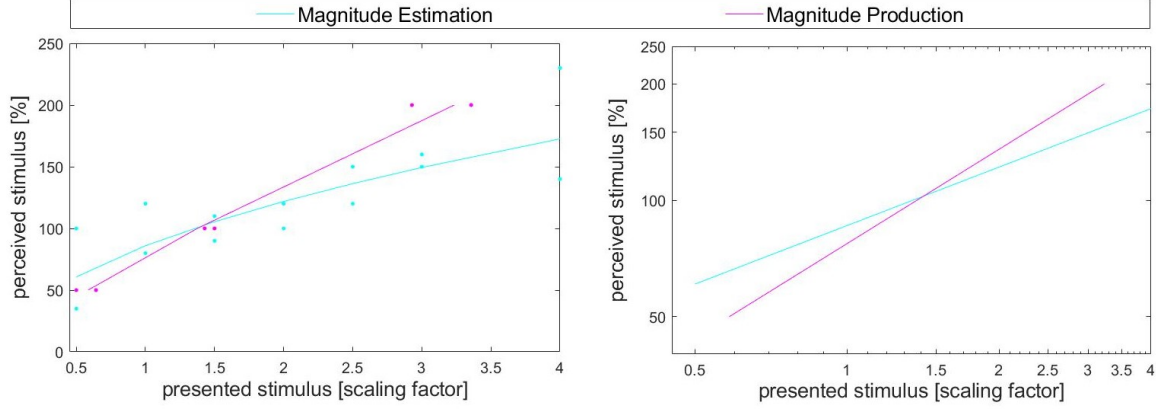


Figure D.4: Comparison of the fitted power function for magnitude estimation (cyan) and magnitude production (magenta) and a normal (left) and log-scale (right).

### D.2.3 RESULTS PILOT EXPERIMENT 2

The second experiment was inspired by the research carried out by Tiest et al. [42] and aimed to produce comparable results. Hence, the procedure was better defined and could be applied to the user study. However, in the experiment found in the literature, the participants investigated the viscosity of the fluids through steering with a spatula or the index finger, while the study carried out in this study intends the interaction with the whole hand. This has multiple reasons, mainly being hardware restrictions that would not allow a fine enough discrimination in this experiment due to the aforementioned high friction forces in the fingers of the haptic interface. Additionally, the interaction with the whole hand is desired, to enable manipulation of objects in fluids in a virtual environment. For this reason, the pilot participants are asked to imagine that their whole hand is emerged in a viscous fluid. In the beginning of the experiment the user can get used to the robotic system by exploring free space. Then the reference stimulus is presented, followed by the first test stimulus. The user is not presented with visual information, and does not need to dive in or out of a container, but keeps repeating the same motion, while the experimenter changes the viscosity. The hand-arm motion is defined as in Experiment 1 as a swiping motion in front of the user. Just like in the model experiment by Tiest, the user can ask to switch back and forth between the reference and test stimuli. Three trials in each of the two tested viscosity groups are carried out, where in each six test stimuli are presented once. The viscosity of all stimuli are set to match the ones mentioned by Tiest et al (Tab. D.1). As explained in section D.1 The pilot participants are asked to answer the question whether the test stimulus feels thicker than the reference, so that the answer is "yes" or "no". For the evaluation, a "yes" is interpreted as a "1", while "no" counts as a "0". Adding the answer value per the amount of answers given leads then to a relative frequency between 0 and 1. Plotted over the presented viscosity, results in the graphs shown in Figure D.5.

For group D as well as E, both pilot participants could identify the three low stimuli to lie below the reference viscosity. However, it can be seen that the answers given for viscosity group E, which relates to higher viscous fluids, seem to be more distinct, for pilot 1 even displaying the ideal characteristic curve of an experiment applying the constant stimuli method. This indicates that the participants are better able to distinguish between the viscosities, but could also indicate that the viscosity differences are too high to lead to meaningful results.

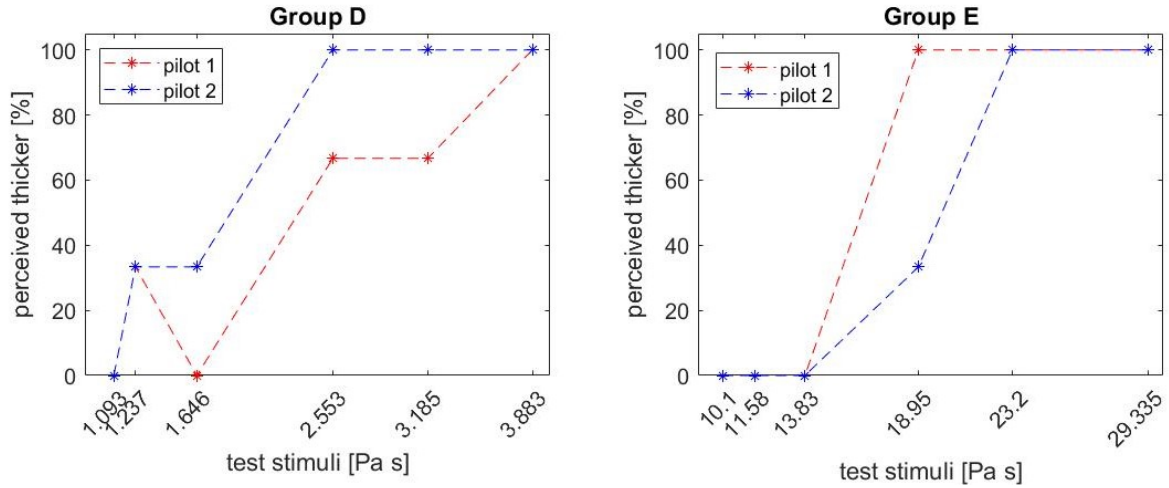


Figure D.5: Results of the two pilots for viscosity Group D (left) and E (right) with the y-axis indicated the relative amount of answers in which the participant perceived the presented test fluid to be thicker than the reference.

In a following step the answers of the two participants were averaged for each group and a curve was fitted according to equation D.2 to find the Weber fraction. The resulting curves are shown in Figure D.6. The Weber fraction for group D is found to be 0.5, while it is 0.15 for group E. Once more those results are not more closely analyzed in this section due to the ambiguity of the small sample size. However, the pilot study showed again the procedure and analysis to be valid, giving promising results to be investigated during the final experiment.

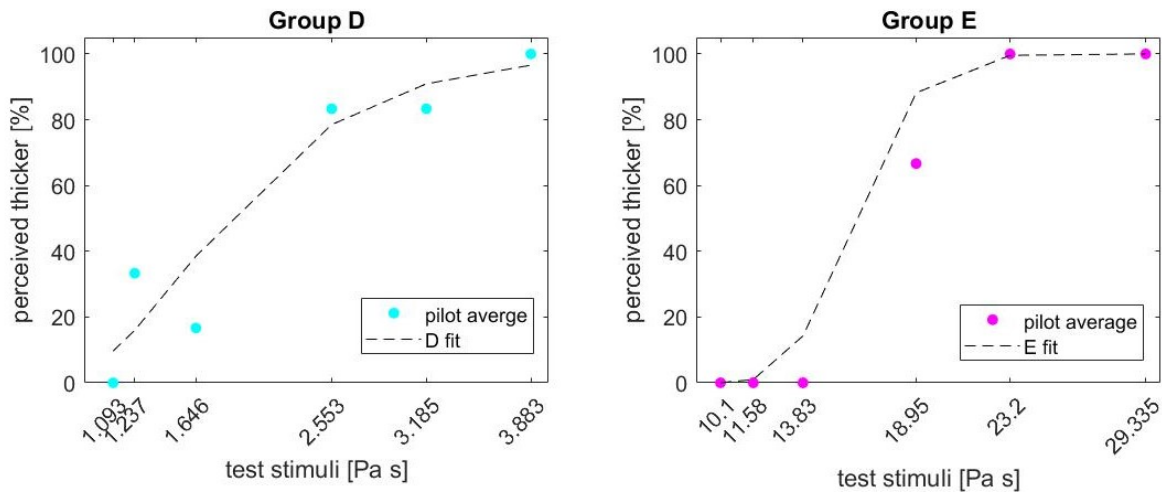


Figure D.6: Fitted psychometric curve to the results obtained with the method of constant stimuli for viscosity group D and E.

#### D.2.4 PILOT QUESTIONNAIRE

The questionnaire given to the pilot participants is in essence identical to the final questionnaire which can be found in section F.4. The differences are that the scales for questions 6 to 9a are only divided into six steps and question 9b in the final questionnaire is missing. This was adjusted after the pilot participants indicated, that the range for the rating questions was not big enough and a question about necessary sensations was missing. The given answers are not analyzed in detail, as this pilot study was only designed to prove the validity of the planned experiments and identify flaws as the one mentioned above.

### D.2.5 DISCUSSION AND CONCLUSION FOR EXPERIMENTS

The pilot studies of both experiment predict meaningful results and validate the intended procedures and methods. Nevertheless, valuable improvements are found for each of the studies that are summarized for each experiment.

#### *Experiment 1*

It is noticed, that high friction remains especially in the joints of the exoskeleton fingers, which makes exploration only using the human fingers impossible, because viscosity differences are hard to distinguished. Therefore the whole arm is to be used, also moving the LWR. But even then, the remaining dynamical behaviour is not good enough to allow a comparison to real water. Therefore, the motion in free space while being attached to the robot needs to be explicitly mentioned to the participants and is defined to be 0 % viscosity. Based on this, the users should indicate when they can perceive the virtual fluid to have the viscosity of water, which rather compares to the use of the robot underwater instead of just moving the hand through a liquid. However, further improvements on the hardware are not possible.

The pilot study indicated, that the magnitude production is easier for the participants than the magnitude estimation, which relates to the aforementioned dynamical behaviour of the robotic systems that does not allow a direct comparison with real water. However, it is found that when explained to take into consideration the robot's behaviour and set the free space to be 0 % viscosity, the users are able to carry out both methods. The explanation and phrasing to explain this is therefore defined and included in the time of procedure. The order of the applied methods is randomly alternated per participant. As initially planned, the participants are given a bucket of water to stir in at the beginning of the experiment, but since the pilot study revealed that a direct comparison is not possible, the necessity of this procedure is questionable. It is therefore decided to apply this priming procedure only to half of the participants to investigate if the immediate contact before the experiment has any influence on the results. The participants that are asked to feel the water in advance are wearing a thick rubber glove to diminish tactile sensations. They are instructed to concentrate on the viscosity of the fluid, especially paying attention to the difference of viscosity between water and air.

For the experiments it was decided to range the scaling factor between 0 and 4, as 4 was the highest set stimulus in the magnitude production. An appropriate step size between the presented scaling factors was found to be 0.5, leading to nine possible stimuli. For the magnitude estimation three trials are carried out, in which each every stimulus is presented once. For the magnitude production, also three trials are carried out, in which the participants have to adjust the stimulus to be perceived as 100 %, 50 % and 200 %, respectively. In each trial each of the nine possible stimuli is presented once as a starting point. For both methods the order of presented stimuli is pseudo-randomized. As both tasks are found to be very tiring for the participants, a break is taken in between. The repetitions are limited to the mentioned amounts to restrict the user study to not exceed a duration of approximately hour, since the user study indicated that after that the concentration and thus results decrease.

#### *Experiment 2*

In the second experiment, the high friction of the robotic system is found to play a less significant role, since the test stimuli as well as the reference are well defined and both include the inherent dynamic behaviour, which makes comparison between the two easier. The value of the test stimuli is applied as defined in the experiment by Tiest et al., but one additional step is added below and above the reference viscosity to get a better estimation of the psychophysical curve progression.

It is considered to lock the LWR in some of the joints to limit and specify the intended motion of the users. However, it is desired that the participants can apply exploratory procedures close to the ones they would use when investigating a real fluid. In that case, the motion and speed of movement can vary per person. It is therefore decided to enable all possible degrees of freedom. Only the rough hand-arm motion of the participants is specified to be a back and forth swiping motion in front of the body and in a horizontal direction. The speed, height and exact trajectory is to be defined by each participant individually to allow a more natural interaction with the haptic interface. For none of the experiments, a visualization is shown to the participants, since the focus should lie on the haptic perception and not be influenced by other sensations.

Considering and implementing all those adjustments, the final user study is carried out as described in the next section.

## D.3 EXPERIMENTS

According to the results obtained from the pilot study, the user study experiments are adjusted and carried out accordingly. The recruited participants, as well as the applied procedure and set up are presented in the following. The results are presented and discussed.

### D.3.1 PARTICIPANTS

A total of 26 right-handed participants (18 male, 8 female) between 20 and 35 years are recruited for the user studies carried out within this project, of which all have an academic background in various fields of engineering. The participants are randomly divided into two groups keeping the male-to-female ratio equal. Thus, 13 people participate in Experiment 1 and Experiment 2, respectively (9 male, 4 female).

The average age of the participants of Experiment 1 is 24 years. Two of the participants indicated in the questionnaire that they had advanced knowledge in the field of haptics, while two others mentioned basic knowledge in this field. Seven of the participants of Experiment 1 had used a haptic interface before of which three had experiences with numerous types. The participants of Experiment 2 are on average 27 years old. Here, three indicate deeper knowledge in the field of haptics and two more basic knowledge. All but two participants had used a haptic interface before, five of those various types.

Prior to the experiment, all participants gave their informed consent. Participation was voluntary and no financial compensation was given.

### D.3.2 PROCEDURE

For each participant a slot of two hours is reserved to have enough time before and after the approximately one-hour long experiments. Prior to the experiment, the form of consent is sent to the recruited participants with details about the experiment to be read in advance to prepare for the user study (see [F.1](#)). On the day of the experiment, the participant is invited to the laboratory at the DLR, in which the haptic interface is installed. The set up is identical for both experiments and can be seen in figure [D.7](#). The area where the experiments take place is separated from the rest of the room to offer a quiet and private environment for the participants. Before the experiment starts, the participants are once more explained the procedures and possible risks and the consent form is to be signed. Since the participants will wear headphones during the user study to limit disturbing noise and distraction, hand signs are explained to communicate with the experimenter. As a reminder the signs are printed out and hang in the view of the participants. As determined in the pilot study [D.2.5](#), before the user study starts, half the participants of Experiment 1 are asked to stir in a bucket of water while wearing a rubber glove to set a reference. When the procedures and hand signs are clear, the user is lead to a marked position in front of the robot and the right hand is attached to the haptic hand exoskeleton mounted on the LWR. The experimenter sits next to the participant controlling the hand exoskeleton and LWR, having the emergency stops always within reach to ensure the participants' safety in case of a system failure. The experiments are recorded with a camera (Casio Exilim). Additionally all occurring forces of each finger are read out, as well as the hand trajectories and velocities of the users and the applied scaling factor and viscosity. The rendering algorithm runs at a frequency of 1 kHz with the maximum ring buffer time for the recordings (1,000,000). Before the start of the experiment, the user is able to move around in free virtual space without any rendered forces to get a feeling for the behaviour of the robotic systems. The participants are informed that free space equals a viscosity of 0 %. This is to be set as a reference for Experiment 1, where considering the felt dynamic behaviour in free space, the magnitude of the viscosity of a fluid to be perceivable as water is to be found. For both experiments, the participant is asked to carry out a wiping motion in front of his body, where the height can be chosen by the user. The stroke amplitude and velocity are not specified, as an ideally natural exploration is desired. For that reason, none of the joints of the LWR are locked in position, leaving the exact motion up to the choice of the participant. Once the participants are accustomed to the use of the robot, they are presented with increased viscosity magnitudes, which is comparable to training trials. It is mentioned that the whole hand should be imagined to be emerged in the virtual fluid. As comparison, the user is able to switch back and forth between free space and viscous fluid.

Once the participant has understood the procedure and the feeling conveyed by the haptic interface, the experimenter indicated the participants the start of the experiments and the user studies are carried out. For Experiment 1, magnitude estimation and magnitude production are carried out in random order, but evenly divided. The same is applied for Experiment 2, in which the order of the viscosity groups is alternated. The magnitude estimation is carried out in three trials with 9 stimuli each, for which the experimenter documents the estimated value of the stimulus in %.



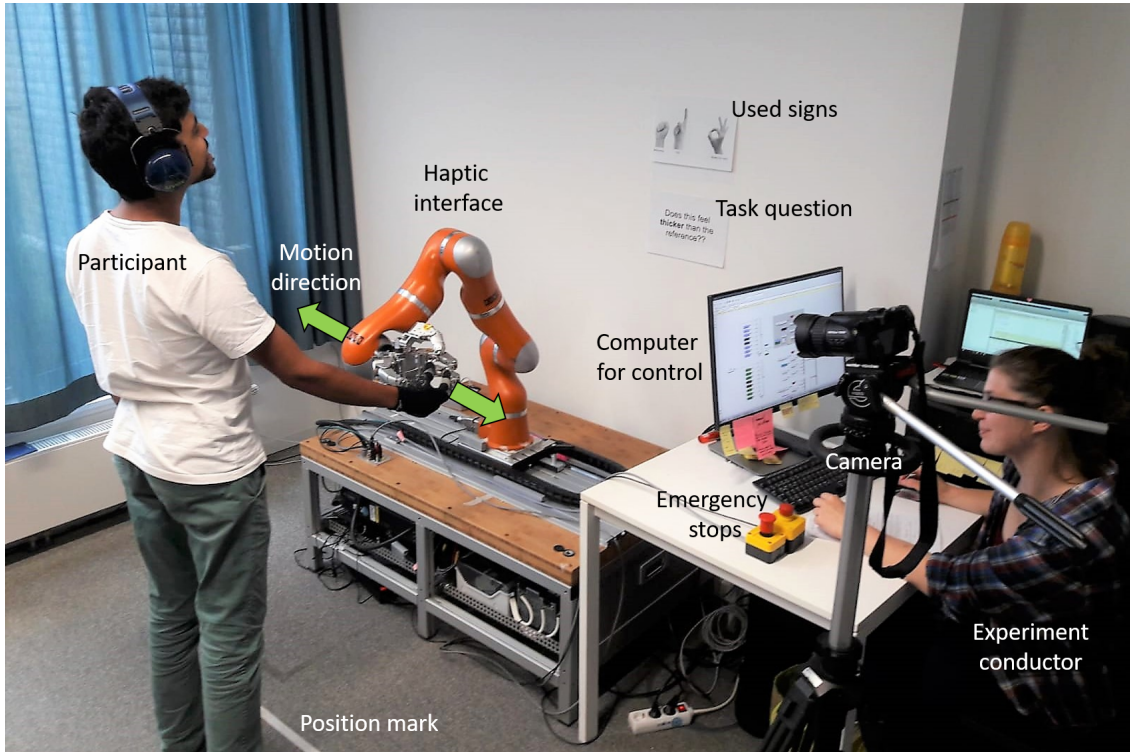


Figure D.7: Testing setup for the user studies with the participant being positioned in front of the robotic device. The human hand is attached to the hand exoskeleton, which is mounted on a KUKA LWR to extend the workspace. The green arrows indicate the specified direction of motion to investigate the virtual fluid.

Between each trial, the user is able to move around in free space again. For the magnitude production, the user is first asked to set the perceived stimulus to 100 %, equaling the feeling of virtual water, varying the start stimulus 9 times and documenting the scaling factor set by the participant. In the following, the participant has to set the stimulus to 50 % and eventually to 200 %. For Experiment 2, five trials are carried out, within each all possible test stimuli are presented once in pre-determined pseudo-randomized order. The participant is asked to answer the question "Does this test viscosity feel thicker than the reference", for which the experimenter documents the "Yes" and "No" answers. Between the magnitude estimation and production, as well as the different viscosity groups, a short break is taken, in which the user can detach from the robot to relax the hand. After approximately one hour, all data was collected. In the end the post-experiment is carried out, in which the participants are asked to touch a virtual stiff object and describe the feeling and if they can identify it to be solid. Lastly, the participant is asked to immerse their hand from free space in a viscous fluid and again describe the feeling. All answers are written down. Finally, participants are detached from the robot and asked to fill out a questionnaire (see E.4). If the participants had further questions concerning the data usage, they were answered and the participants afterwards dismissed.

### D.3.3 RESULTS EXPERIMENT 1

The first experiments was carried out with 13 participants and all the data for the psychometric analysis was recorded in written form. However, for the first participant, the recording of the device data did not work due to an unexpected computer crash. In the following, the results for the psychometric analysis are presented as well as the trajectories carried out by the participants to investigate the virtual fluid, which was obtained through the recorded device data. Lastly, the answers of the questionnaire are presented.

#### PSYCHOPHYSICS

As explained, for the magnitude estimation the participants were presented with a randomly scaled stimulus (scaling factor between 0 and 4 in steps of 0.5) and had to assign a percentage to each stimulus, the feeling of water being 100 %. Since the estimation was only repeated 3 times, in which every scaling factor was presented once, for each participant the correlation between the obtained curves of the three trials are analyzed. Exemplary, the obtained curves of participant 13 are shown in Figure D.8.

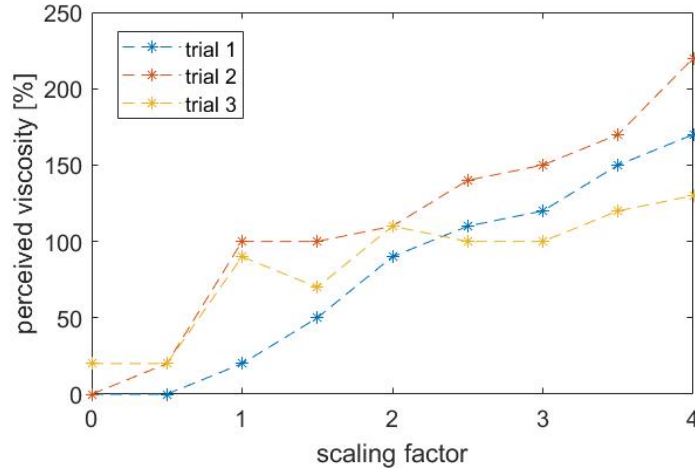


Figure D.8: Exemplary magnitude estimation curves for participant 13 for the three carried out trials.

Looking at the correlation between the curves for each participant shows with exception of participant 1, a moderate to strong correlation between the results of the trials (Tab. D.2). This indicates, that the similarities of the curves are not just random, but causal. The reason for the low correlation coefficients for participant 1 might be due to less clear instructions in the first run leading to more variety in the answers of the participant.

Table D.2: Calculated correlation coefficients between trial 1 (t1), trial 2 (t2) and trial 3 (t3) of the magnitude estimation part for each participant.

Correlation	Particip. 1	Particip. 2	Particip. 3	Particip. 4	Particip. 5	Particip. 6	Particip. 7
t1 - t2	0.0370	0.7224	0.8069	0.9773	0.8125	0.9403	0.8226
t1 - t3	0.3049	0.8667	0.6265	0.8478	0.6427	0.9109	0.8789
t2 - t3	0.7166	0.7142	0.7429	0.8446	0.7986	0.8242	0.7309

Correlation	Particip. 8	Particip. 9	Particip. 10	Particip. 11	Particip. 12	Particip. 13
t1 - t2	0.8777	0.7881	0.8097	0.8073	0.5379	0.9414
t1 - t3	0.7547	0.7868	0.8506	0.6668	0.8163	0.8864
t2 - t3	0.8239	0.9143	0.7847	0.7463	0.8165	0.9466

Taking the mean of the 3 trials of each participant and plotting the curve for all participants, shows a steadily increasing curve for all users D.9. Again it can be seen that the curve of participant 1 is higher than the others, which might also be due to the already mentioned reason. Nevertheless, a consistent trend can be observed for the perception of all participants for the magnitude estimation.

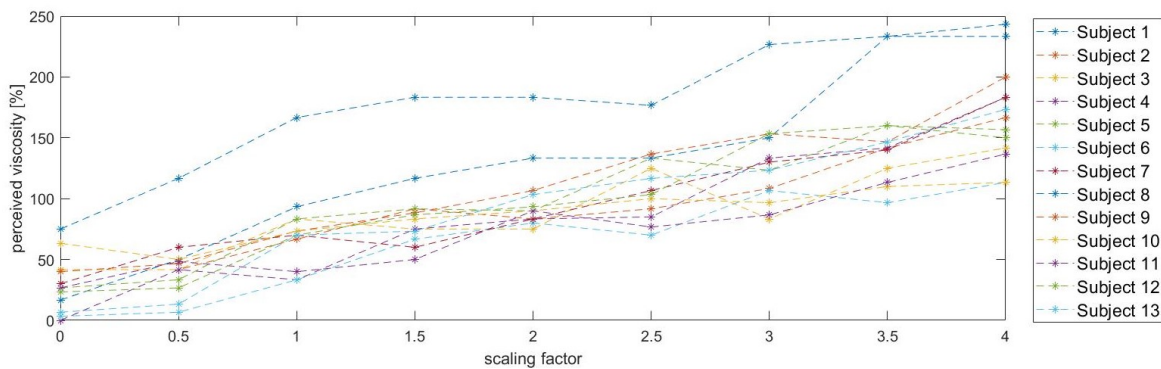


Figure D.9: Magnitude estimation curves for each of the 13 participants obtained by averaging the data of each trial ( $n = 3$ ).

The results of each participant averaged and then perception between the participants ( $n = 13$ ) compared in a boxplot in Figure D.10. The results of participant 1 can here be identified as outliers, but are still considered as they might also have occurred from natural perception variation of that participant and the effect is to be considered. Overall a very consistent increase of perceived viscosity can be observed with increasing scaling factor. The meaning of this relation will be analyzed further with the results obtained from the magnitude production, which are first to be presented.

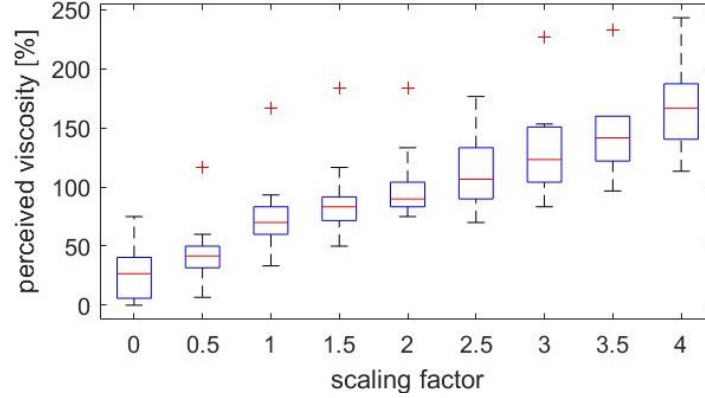


Figure D.10: Boxplot of the averaged perceived viscosity per participant ( $n = 13$ ) for the magnitude estimation.

For the magnitude production, the participants are asked to adjust the presented scaling factor until the investigated fluid can be identified to be as viscous as virtual water (100 %, trial 1), half as viscous as water (50 %, trial 2) and double as viscous (200 %, trial 3). Within each trial, each of the scaling factors between 0 and 4 is presented as a starting stimulus once, thus the production of each viscosity is repeated 9 times. Figure D.11 shows the boxplot for each participant in each of the trials. It can be seen that the spread of the set scaling factor in each trial is in a similar range for all the participants. However, it is noticeable that the median of the scaling factor for a viscosity of 50 % is in a similar range for all participants, while varying more for the higher viscosities reaching higher scaling factors as seen in the magnitude estimation. This is investigated further by plotting the mean of each participant in each trial and looking at the resulting curves (Fig. D.12).

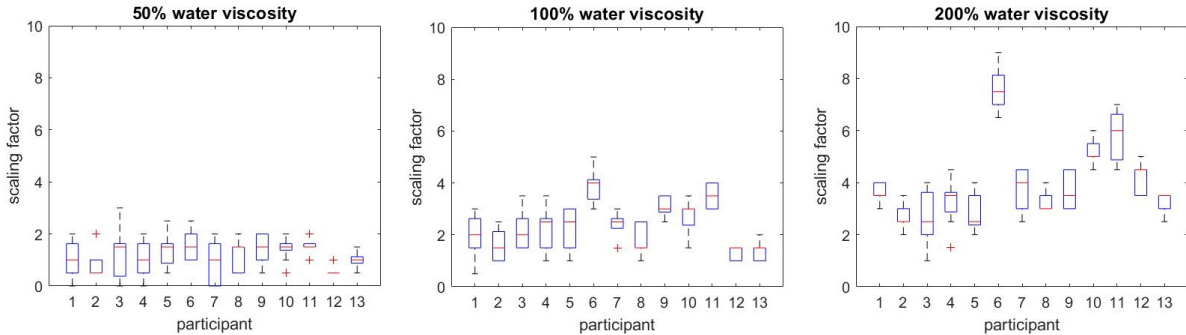


Figure D.11: Boxplots for the set scaling factor of each participant for the different trials (left: 50 %, middle: 100 %, right: 200 %) during magnitude production.

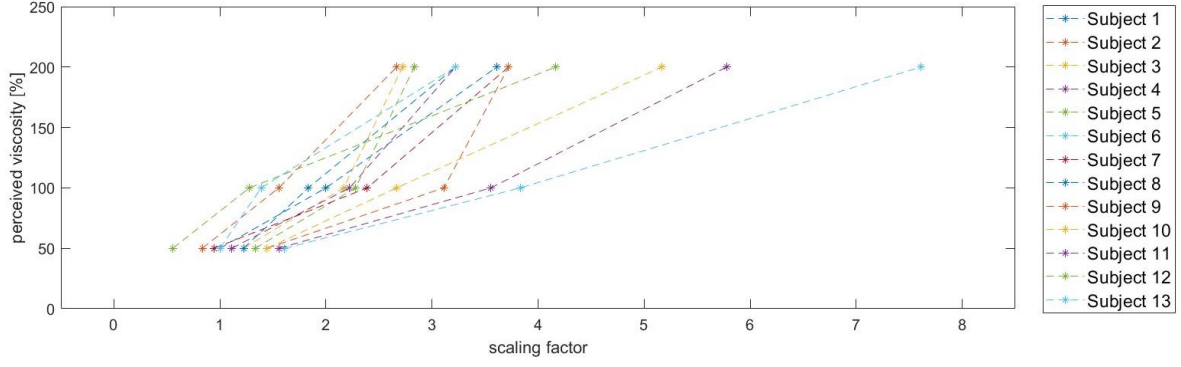


Figure D.12: Magnitude production curves for each of the 13 participants obtained for each trial (50, 100 and 200 %) by averaging throughout the repetitions ( $n = 9$ ).

For each participant once more a steadily increasing curve can be found. However, the mentioned increasing spread between the set scaling factor of the different participant becomes more prominent. Subject 6 for example set the scaling factor on average to 7.6, while participant 2 perceived the same viscosity with a scaling of 2.7. Nevertheless, a trend is noticeable, since for each participant the increased scaling is consistent within the trial. To investigate this further, the relative scaling between the trials for each participant are analyzed. As can be seen in Figure D.13, the ratio between the set scaling factor for 100 % viscosity compared to the one set for 50 % is in a similar range for all the participants ( $\bar{x}_1 = 1.97 \pm 0.34$ ). Likewise, the ratio between the set scaling for a perceived viscosity of 200 % compared to 100 % is in a similar range for all participants (except participant 12) with a mean ratio of  $\bar{x}_2 = 1.78 \pm 0.55$ . Despite this only being descriptive statistics, it indicates that, although the different participants perceived the scaling to be of varying intensity, the relationship between the questioned viscosities remains. Due to this a , while leading to a higher spread in the answers of the higher viscosity perception can be observed. The overall higher scaling factors compared to the ones seen in the magnitude estimation can be explained with the regression bias mentioned in section D.1.1 and were to be expected.

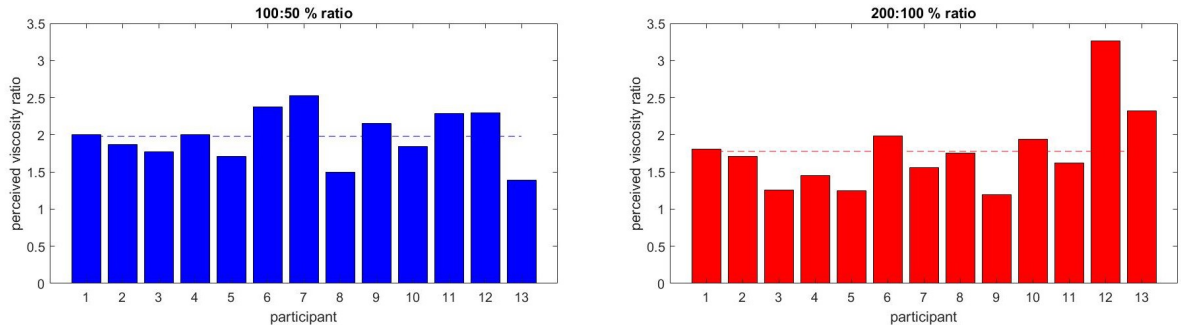


Figure D.13: Comparison of the ratios of the produced scaling factors for the matching of 100 % and 50 % (left) of virtual water viscosity and 200 % and 100 % (right), respectively.

To compare the results of the magnitude estimation and magnitude production, Steven's Power Law can be used as defined by equation D.1. Fitting a curve through the data points of the participants ( $n=13$ ) relates the set magnitude intensity  $I$ , being the scaling factor of the calculated forces, to the perceived viscosity (Fig. D.14). For the magnitude estimation (ME) the relationship is found to be

$$S_{ME} = 0.6663 \cdot I_{ME}^{0.6386} \quad (D.3)$$

The fitting of the data of the magnitude production (MP) yields the following equation

$$S_{MP} = 0.3761 \cdot I_{MP}^{1.206} \quad (D.4)$$

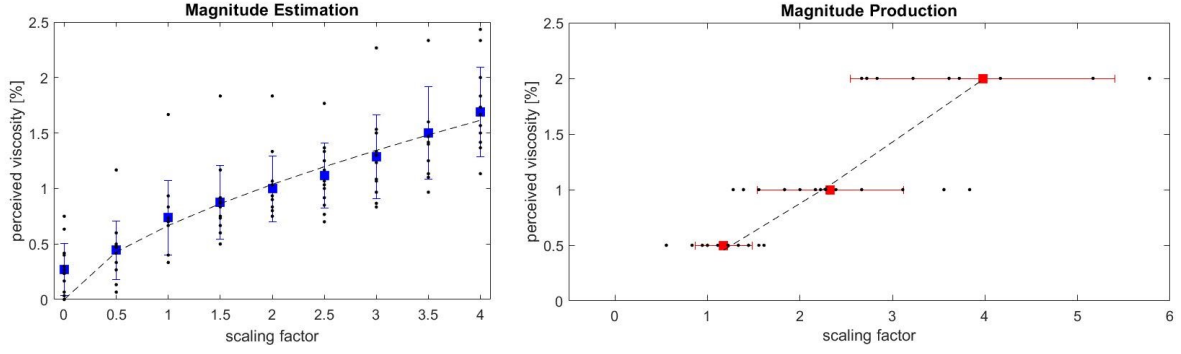


Figure D.14: Curve fitted through the averaged perceived viscosity for all participants ( $n = 13$ ) in the magnitude estimation (left) and production (right), additionally showing the average over all participants with the standard deviation in error bars

Comparing the fitted graphs in one plot on normal scale and log-scale (Fig. D.15) shows that the slope of the results from the magnitude production is steeper than the one of the magnitude estimation. This was expected due to the explained regression bias [48].

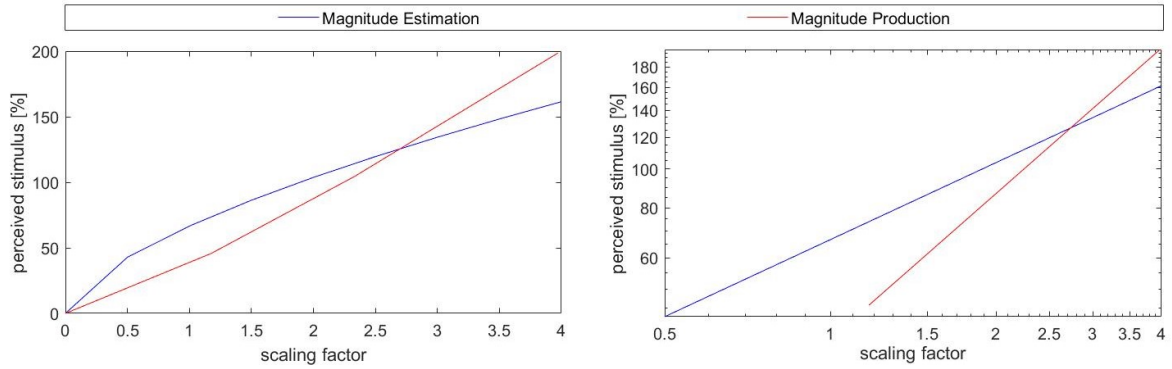


Figure D.15: Fitted curves obtained through magnitude estimation (red) and production (blue) with the fitted regression curve (dotted) between them to cancel out the occurring regression bias, shown in normal scale (left) and log-log-scale (right).

To cancel the bias, a regression curve is fitted between the two functions. The coefficient of determination for the found magnitude estimation is  $R_{ME}^2 = 0.9483$  and for the magnitude production  $R_{MP}^2 = 0.9706$  and therefore suggests to be a good fit. The finally found relationship between the scaling factor of the calculated forces for the interaction with virtual water and the perception of the human is then

$$S_{MP} = 0.5145 \cdot I_{MP}^{0.9021} \quad (D.5)$$

The exponent is thus found to be  $a = 0.9021$ , which indicates an almost linear relationship between the scaling factor and the viscosity, meaning a doubling of the given viscosity also leads to the doubling of the perceived one. However, it can be seen that when rendering virtual water with a scaling factor of 1, which should correspond to the forces felt in a realistic interaction with water, in the virtual environment, it is only perceived to have half the viscosity of water.



### TRAJECTORIES

Next to the psychophysical analysis, the data recorded through measurements of the haptic interface are considered. Since the theoretical correctness of the magnitude of the displayed forces has been shown in Appendix B, and the limitations of the read out data through the error is the torque sensor (Appendix A) make it hard to get meaningful information, the calculated and displayed forces are not analyzed in detail. However, since the calculation of the forces depends on the velocity with which the human user moves his hand/arm, the average maximum velocity of each participant are considered. Additionally, the trajectory made by the user's hand is analyzed, since only the general direction was specified to the participants, but not the precise execution. To see if the hand motion, stroke amplitude or height of the participants show a prominent effect on the psychometric data, those information are analyzed. Additionally, it is to be investigated, if the interaction procedure between magnitude estimation and magnitude production differed, since a break was taken in between the two parts. It is of interest, if the participant varied the procedure when positioned new, which might have effected the results presented above. As mentioned before, the data recorded by the device were lost for participant 1, so that this person is not considered for the following analysis.

To investigate the trajectories of the hand during the different trials of the magnitude estimation and production, the translation part of the end effector transformation matrix is plotted in space for participant 2 to 13. Exemplary, the resulting trajectories of participant 9 are shown in Figure D.16 for both magnitude matching methods. The trajectory is shown relative to a plane, which indicates the positioning of the human user. The origin is the base of the LWR, which is indicated by a black square. The comparison of the different trials shows an overlap of the hand trajectories with identical positioning in space for magnitude estimation and production. This can be observed for all participant. Only, the trajectory recording of participant 3 shows an odd behavior during the magnitude estimation in the third trial. Revisiting the the video recording for this participant, however, no abnormalities show in his hand motions. Since the other recordings for this trial also indicate errors, which cannot be supported with the video material, the recorded data of this trial is not considered and for this participant only the measurements of the first two trials are used for the further analysis.

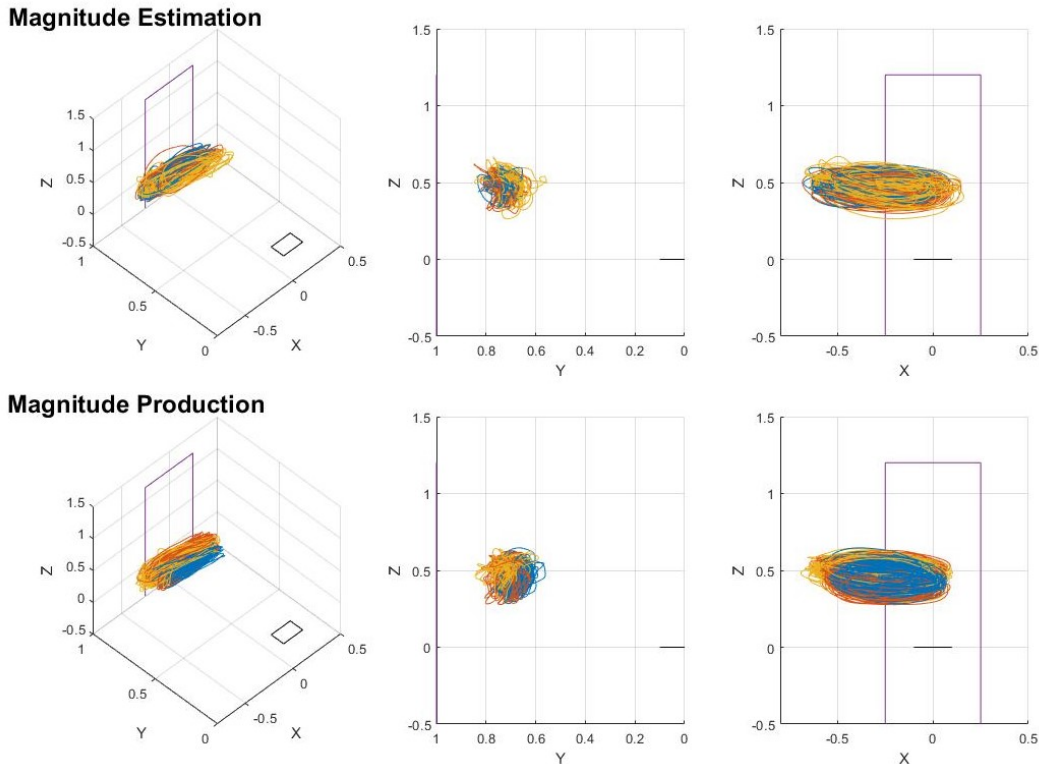


Figure D.16: Trajectories of the human hand, exemplary shown for participant 9, for the three trials (1-blue, 2-red, 3-yellow) during magnitude estimation and production in space plotted in reference to the position of the human user (purple square) and the base of the haptic interface (black square).



It can be observed, that most participant followed a circular trajectory, where the hand was lowered when moving forward (palm facing direction of motion), and then slightly raised when pulling back through the virtual fluid. Additionally the trajectory is shifted to one side of the participant, whose position is indicated in the graph with the purple rectangle. This is easily explained, since all participants used the haptic interface, with their right hand, therefore the the hand is moved on the right side of the participants body and is identical for all users. To better compare the trajectories of the magnitude estimation and production, the mean is taken between 100000 samples taken from the mid-section of each trial. The average height of the trajectory is calculated and related to the body height of each participant. For both magnitude methods similar results are obtained with the hand held at an average height of 52.03 % ( $\pm 9.94$  %) and 51.49 % ( $\pm 9.89$  %) compared to the total body height of the user for magnitude estimation and production, respectively.

The average stroke width and maximum velocity of each participant are shown in Figure D.17. It can be seen that with exception of participant 3 and 10, all participants applied a similar stroke width for the two tested methods. But even for participant 3, who showed the biggest deviation, the difference of the amplitude is only 0.11 m, which is considering the available range, not noteworthy. The plotted velocity is the average maximum velocity during the three trials. All participants stay well under 1 m/s and again apply a similar velocity throughout the different methods, thus validating the assumptions in A B. No relationship between the stroke width and the height of the person nor with the applied velocity can be observed. Furthermore, no gender-specific behavior is noticeable.

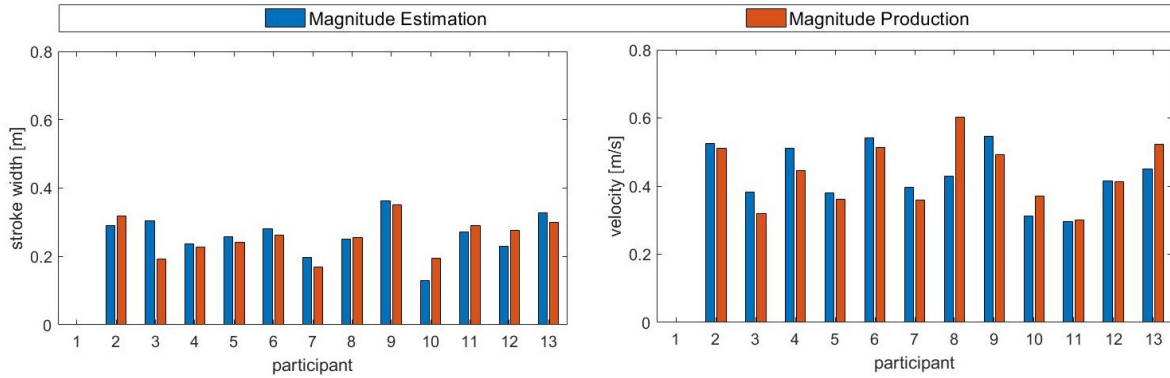


Figure D.17: Averaged values for the stroke amplitude (left) and maximum stroke velocity (right) of the human hand for magnitude estimation (blue) and production (red) throughout the recorded hand trajectories for all participants. Due to a saving error, the values of participant 1 could not be included.

To determine the importance of the exoskeleton during the interaction with a virtual fluid instead of a rigid end effector, the finger motions during the carried out trajectories are analyzed by plotting the joint angles for each exoskeleton finger D.18. Finger 1 and 2 refer to the points attached to the human palm, while finger 3, 4 and 5 correspond to the thumb, index and middle finger of the human, respectively. The recorded trajectory consists out of multiple strokes, where one stroke is defined as the motion of the human hand to a turning point and back. A stroke can either be started with a forward motion or backward motion of the hand. The plot shown in Figure D.18 depicts exemplary a stroke for participant 2 during the magnitude estimation and production part of the first experiment, where the starting point is defined to be in the middle of the human hand moving backwards. The turning point is indicated by a black line, where the human user changes the direction of motion to be forward until reaching the opposite turning point, where the hand moves back again ending approximately at the same position as started. Similar curves were found for all participants for both parts of the experiment. A characteristic pattern seems to be observable for the robotic fingers 1 and 2 of the exoskeleton, which are defined by the motion of the palm of the human hand. On the turning point from the backwards hand motion to the forward motion, the exoskeleton is pushed, resulting in a flexion of the robotic fingers. This is observable through increasing flexion angles. For most participants only the distal joint (Fig. D.18, blue) clearly moved, while for some the base joint D.18, red) flexed instead or additionally. The reason for this flexion of the robotic fingers is the inertia of the system to maintain the backwards motion, while the human presses against it to change the direction of motion, leading to forces exerted on the fingers. When the human hand and the LWR move in the same direction with the same speed, the angle remains constant. During the backwards motion, the opposite behavior can then be observed, where the human pulls the exoskeleton fingers against the motion of the system, leading to the extension of the robotic fingers

and thus a decrease in the distal joint angle.

This pattern, can only be observed for the robotic fingers attached to the palm of the human hand, which indicates, that the motion of the human is led by the palm. The human fingers are dragged behind being spread at the turning points to steer against the palm motion as indicated by the change of flexion angle of the base joint on the robotic finger 3, 4 and 5. This described behavior of the human user can be verified by looking at the corresponding video sequences. The angle behavior in the abduction base joint depended on how much the participants varied the height of their strokes and was not uniform.

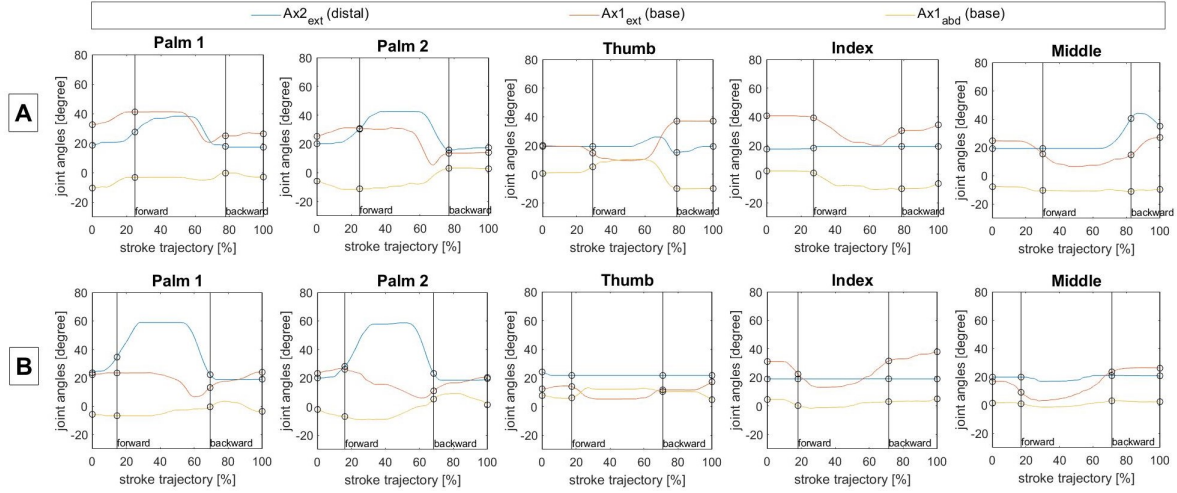


Figure D.18: Measured joint angles of each joint of the exoskeleton fingers during one stroke, exemplary shown for the hand trajectory of participant 2 for (A) magnitude estimation (upper row) and (B) production (lower row). Finger 1 and 2 correspond to the robotic fingers attached to the palm of the human hand, while Finger 3-5 attach to the thumb, index finger and middle finger of the human user, respectively. The vertical line indicates a change of direction of the hand motion.

In an attempt to look how much force is applied by the human to the haptic interface during the interaction, the measurements of the torque sensors of each joint in all robotic fingers are regarded (Fig. D.19). Again, exemplary the half stroke of participant 2 is shown, where the black dot indicates the starting point. It can be seen that the torque remains generally constant over the speed. However, since each robotic finger moves dynamically and thus the lever arm and direction of force continuously change, the torque measurements are hard to interpret and no useful information can be extracted. To better investigate this topic, a force sensor should be added to the human side, which would also help to improve the control algorithm.

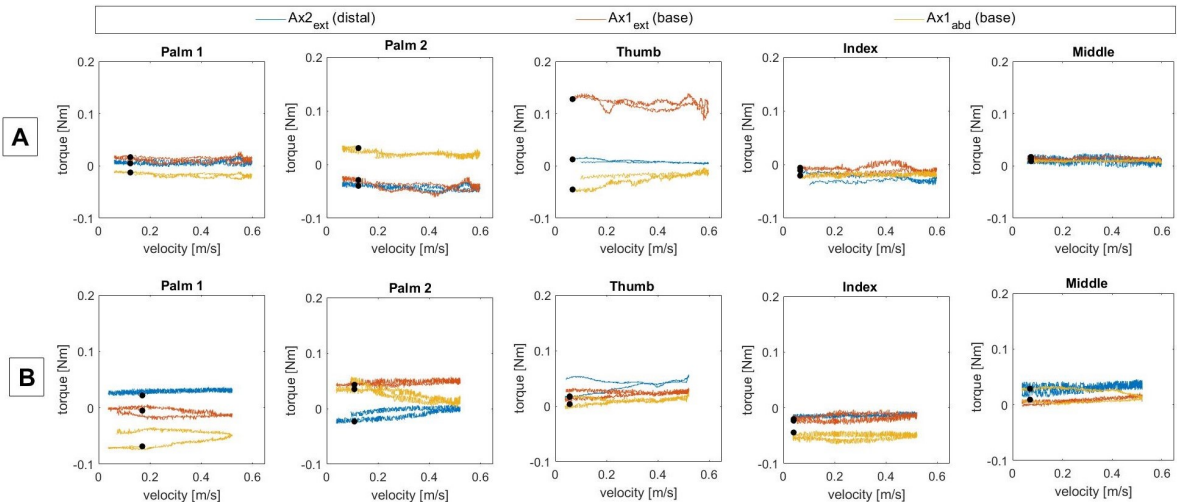


Figure D.19: Measured torques plotted over the velocity of the human hand exemplary shown for one stroke of the human hand trajectory of participant 2 for (A) magnitude estimation (upper row) and (B) magnitude production (lower row). The torques are plotted for each joint of each finger. Finger 1 and 2 respond to the robotic fingers attached to the palm of the human hand, while Finger 3-5 attach to the thumb, index finger and middle finger of the human user, respectively. The black dot indicates the starting point of the trajectory.

### QUESTIONNAIRE

The answers of the questionnaire are used as additional information about the carried out task and viscosity perception, but also to judge the general feeling of the participants during the interaction with the robot. The questionnaire therefore asks the users to rate the perceived safety, freedom and ease of the control out of 10. Furthermore, the task ease and interest are questioned relating to the necessary vigilance of the human as well as the perceived realism of viscosity of the virtual fluids. Additional open question leave room for suggestions of improve the system and experiment.

The results of the rating questions are summarized in Table D.3. It can be seen that with very little deviation, all participant felt very safe during the interaction with the robot, despite their hand being directly attached to the haptic interface with magnets. The range of hand freedom seemed quite satisfying and the control of the robots to interact with the virtual fluid relatively easy and intuitive. The task itself of matching the rendered viscosity to one that can be perceived as virtual water, however, was rather hard for the participants, indicating a high mental workload. Nevertheless, the taks was judged interesting, which is important to keep vigilance. The perception of the realism of the feeling of the virtual fluid varied: three out of the 13 participants gave the feeling a rating of below 5, but another eight users gave a rating of 8 or higher.

Table D.3: Averaged rating of the participants of experiment 1 (n = 13) for the rating questions in the questionnaire, where 1 is the worst rating and 10 the best rating with the standard deviation to indicate the spread in rating throughout the participants.

	SYSTEM related				TASK related		
	Robot Safety	Hand Freedom	Control Ease	Control Intuitivity	Task Ease	Task Interest	Realism
P1	10	7	6	8	3	10	5
P2	10	7	7	7	6	7	5
P3	10	5	8	9	5	8	7
P4	10	5	9	10	5	4	3
P5	10	5	7	9	3	9	8
P6	9	9	10	10	6	6	8
P7	10	7	8	8	6	7	4
P8	9	7	4	4	8	4	3
P9	10	10	10	10	9	10	9
P10	10	7	8	10	3	7	6
P11	9	7	7	9	3	6	8
P12	10	9	10	10	4	9	10
P13	9	6	6	8	3	7	7
avg.	9.69	7.00	7.69	8.62	4.92	7.23	6.38
sd.	0.48	1.58	1.80	1.71	2.02	1.96	2.26

In the open questions, the participants could indicate, which sensation they were missing to improve the realism. For this experiment a repeated answer was a better distribution of the forces over the hand. Two users mentioned, that the feeling of wetness cannot be perceived, however both also indicated, that they do not need it to identify the rendered material to be fluid. Five of the users indicated, that they expect a much better feeling, if the friction in the haptic interface can be lowered, which corresponds to the expectations.

### D.3.4 RESULTS EXPERIMENT 2

The second experiment was also carried out with 13 participants, who were however all different from the ones that participated in the first one, so the starting conditions concerning the knowledge about the system were identical. In this experiment, a computer failure lead to the loss the recorded data for viscosity group D of participant 11. The psychometric data was again not effected by this.

#### PSYCHOPHYSICS

For the viscosity discrimination, the participants were presented with a set of test stimuli alternating with a reference stimulus. This was carried out for two viscosity groups as defined in the work by Tiest et al (Tab. D.1). For each participant, the stimuli of each viscosity group were presented five times and for each the participant had to decide if it was thicker than the reference stimulus ("Yes") or not ("No"). Averaging the answers given, leads to data as exemplary shown in Figure D.20 for participant 2 (viscosity group E). Using equation D.2 a psychometric curve can be fitted, in which the Weber fraction is the free parameter.

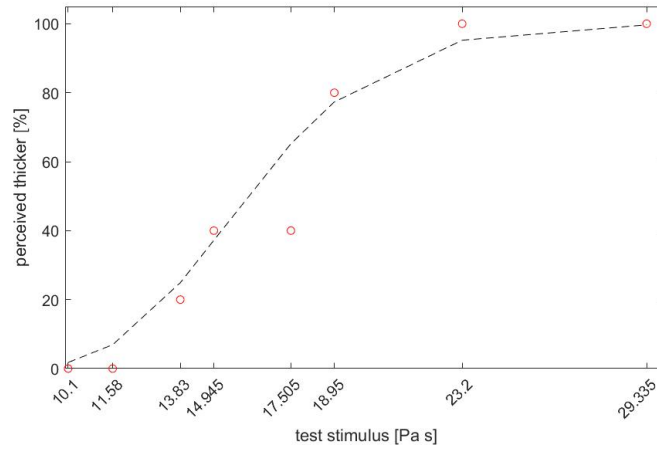


Figure D.20: Obtained data from the five trials of experiment 2, exemplary shown for participant 2 in viscosity group E with the determined Weber fraction indicated by the dotted line.

Through this fitting, the Weber fraction can be found for all participants in both viscosity groups. The found values are summarized in Figure D.21. It can be seen, that the Weber fractions for viscosity group D are significantly higher ( $p < 0.01$ ) than the ones obtained for viscosity group E. Noticeable is, that participant 3, 6 and 12 show a higher Weber fraction than the one of all other participants, even higher than the one obtained in viscosity group D.

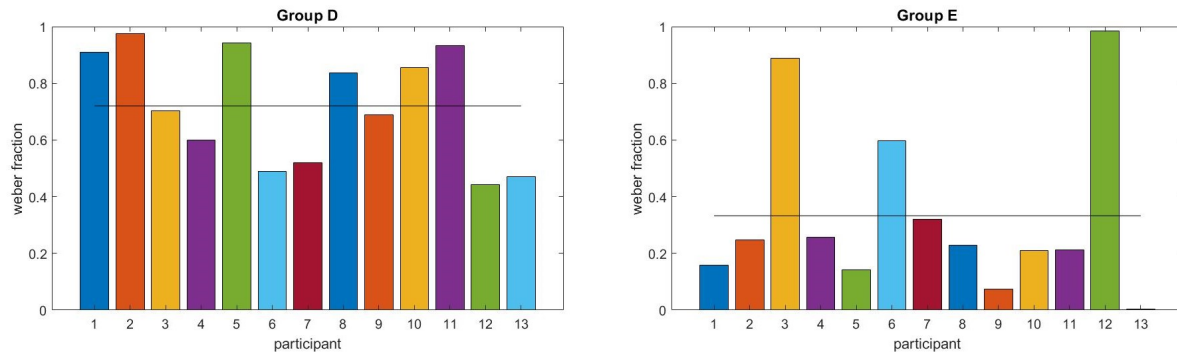


Figure D.21: Found Weber fraction for each participant in viscosity group D (left) and E (right) with the average value indicated by the horizontal black line.

Taking a closer look for those participants at the recorded device data and videos to exclude rendering mistakes and alike, shows no anomalies in comparison with the other participants. Therefore, the increased Weber fraction of those participants might solely be due to varying perceptive capabilities of the human users. By multiplying the found Weber fraction for each participant with the reference viscosity of each group, the absolute threshold can be calculated. Summarizing the values found for all participants in a boxplot is shown in Figure D.22. The mean threshold for group D is found to be  $\bar{x}_D = 1.33 \pm 0.37$  Pa·s and for group E  $\bar{x}_E = 5.53 \pm 4.68$  Pa·s. For the latter case, the very large standard deviation is caused by the seemingly outlying results of participant 3 and 12.

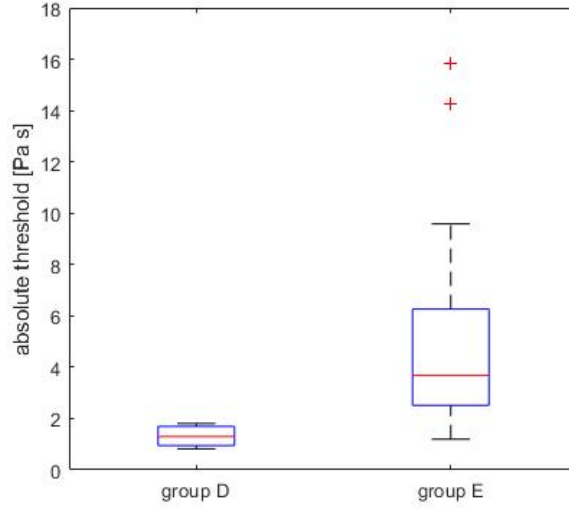


Figure D.22: Boxplot of the absolute threshold found for the two viscosity groups D and E for the 13 participants of experiment 2.

Averaging the results of all participants ( $n = 13$ ) for both viscosity groups and fitting a psychophysical curve through the data leads to the graph shown in Figure D.23. The Weber fraction obtained for group D can then be found to be  $w_D = 0.6970$  and for group E  $w_E = 0.2928$ .

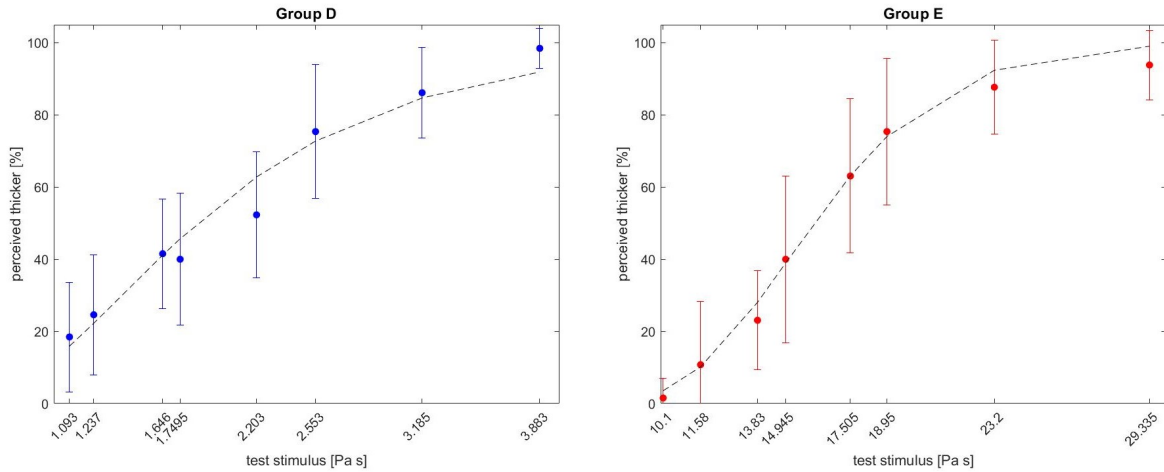


Figure D.23: Averaged data for all participants ( $n = 13$ ) of experiment 2 for viscosity group D (left) and E (right) with standard deviation and Weber fraction of the averaged data indicated by a dotted line.

### TRAJECTORIES

As for Experiment 1, the hand trajectories are also analyzed for this second user study. As aforementioned a saving error occurred for the data recordings of viscosity group for participant 11. Analysis showed additionally that the saved data of group D for participant 5 were damaged. Therefore, the trajectory data of those two participants cannot be considered for group D. Nevertheless, all other data can be analyzed as done for the first user study. However, for Experiment 2, all trials per viscosity group were recorded in one file and since experiment 1 has already shown a consistency of the carried out hand motion between trials, the data is not separated into trials but differences are only analyzed between the two viscosity groups. Figure D.24 exemplary shows the hand trajectories for both viscosity groups for participant 12. Similarly to the observations made in Experiment 1, the trajectories for both groups show strong resemblance. As already seen in Experiment 1, the trajectory is carried out on the right side of the human, relating to the use of the right hand. Overall, a pattern similar to the one described in Experiment 1 can be observed, that the users are carrying out a circular motion, with the hand lowering when the palm is facing the direction of motion and raising again on the way back. This feature can be identified for all participant, although with varying prominence.

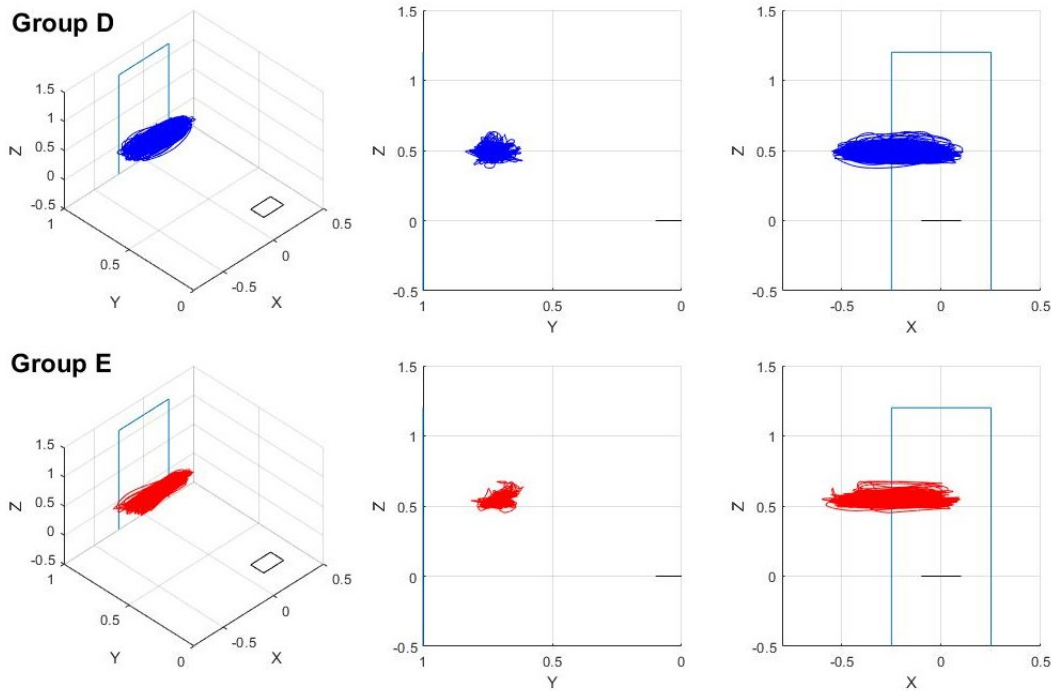


Figure D.24: Trajectories of the human hand, exemplary shown for participant 12, during the discrimination experiment for viscosity group D (blue) and E (red) in space plotted in reference to the position of the human user (light blue square) and the base of the haptic interface (black square).

Again, looking at the average height, in which the hand is held during the interaction with the virtual fluid, similar results for both viscosity groups are found for all participants. Averaging those results over the participants, it is found that the hand is held in a position at  $56.17\% \pm 3.23\%$  of the participants total body height for group D and  $56.35\% \pm 3.53\%$ . Looking at the average stroke width and maximum velocity for all participants leads to the plots shown in Figure D.25. Comparing the stroke width between the viscosity groups for each participants, does again show, that the users remained similar interaction procedures, although they were detached from the robot between the two parts of the experiment. It is noticeable, that the stroke width is significantly higher ( $p < 0.001$ ) for Experiment 2 ( $0.5135 \pm 0.1481$  m), than seen in the first one ( $0.2391 \pm 0.0882$  m). For the velocities no prominent difference to the one recorded in Experiment 1 can be seen. However, it is notable, that all participants show a lower maximum velocity for the exploration of the virtual fluids in viscosity group E than the one in D. This can be explained with the higher forces rendered for group E. Assuming, the user applies a similar amount of force to move the haptic interface in each part of the experiment, during the higher viscosity more force is counteracting the motion of the user, which consequently leads to a lower velocity.



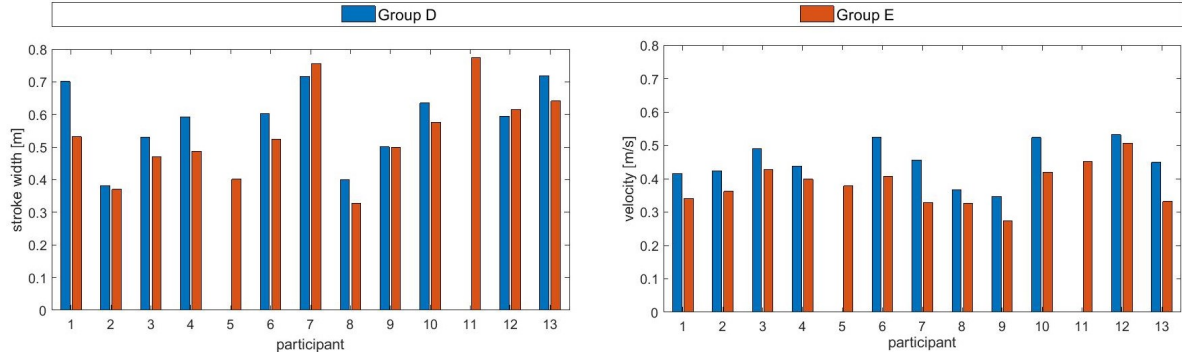


Figure D.25: Averaged values for the stroke amplitude (left) and maximum stroke velocity (right) of the human hand for viscosity group D (blue) and E (red) throughout the recorded hand trajectories for all participants. Due to a saving error, the values of group D could not be analyzed for participant 5 and 11.

As done for the first experiment, the motion of each robotic finger during the interaction with the virtual fluid is to be investigated. Figure D.26 exemplary shows a trajectory for participant 12, where the starting point is again in the middle of the backwards motion. A similar pattern can be observed as found for experiment 1. A clear flexion/extension of the robotic fingers 1 and 2 attached to the palm of the human user can be observed during the direction turn. Again, mostly the distal joint was moved, but in some cases the extension base joint moved instead or additionally. Furthermore, the robotic fingers attached to thumb, index and middle finger showed a more prominent motion of the extension base joint, opposing the direction of the fingers attached to the palm. This indicates, that the human used the spread of attached fingers to counteract the palm motion, as can also be seen in the video material. Overall, a similar behavior was observed throughout all participant, but varieties occurred throughout the trajectories per participant.

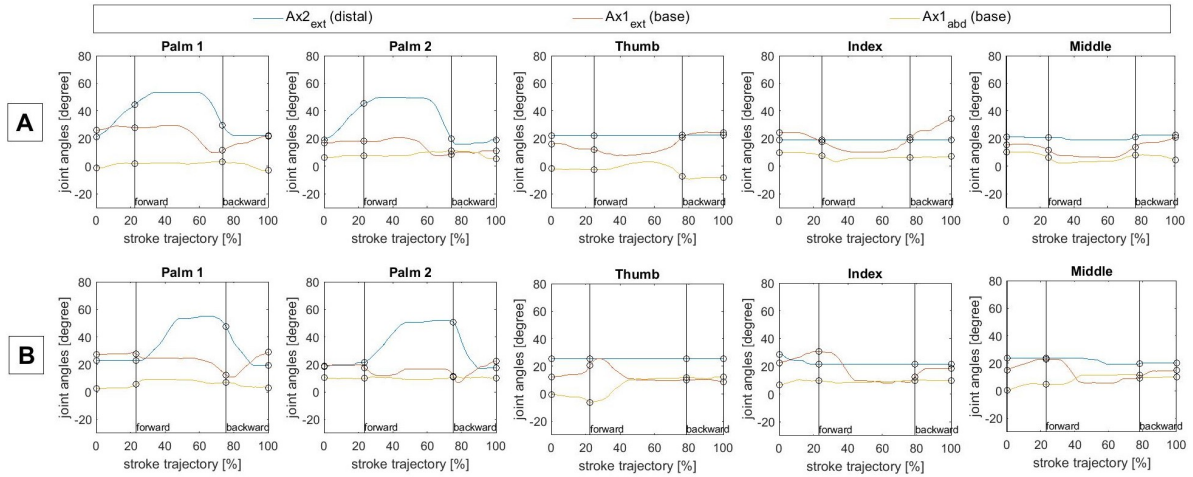


Figure D.26: Measured joint angles of each joint of the exoskeleton fingers during one stroke, exemplary shown for the hand trajectory of participant 12 in viscosity group D (upper row) and E (lower row). Finger 1 and 2 correspond to the robotic fingers attached to the palm of the human hand, while Finger 3-5 attach to the thumb, index finger and middle finger of the human user, respectively. The vertical line indicates a change of direction of the hand motion.

The torque measurements for the second experiment showed more noise and irregularities as well as higher values. This might indicate, that overall more force was applied by the human user, which corresponds to the increased value of the rendered forces for thicker virtual fluids. No uniform pattern could be observed throughout the participants and a general judgment is hard to make in light of the available torque measurements which depend on the robotic finger positions. Once more, the behavior should be investigated further by means of a force sensor on the human side.

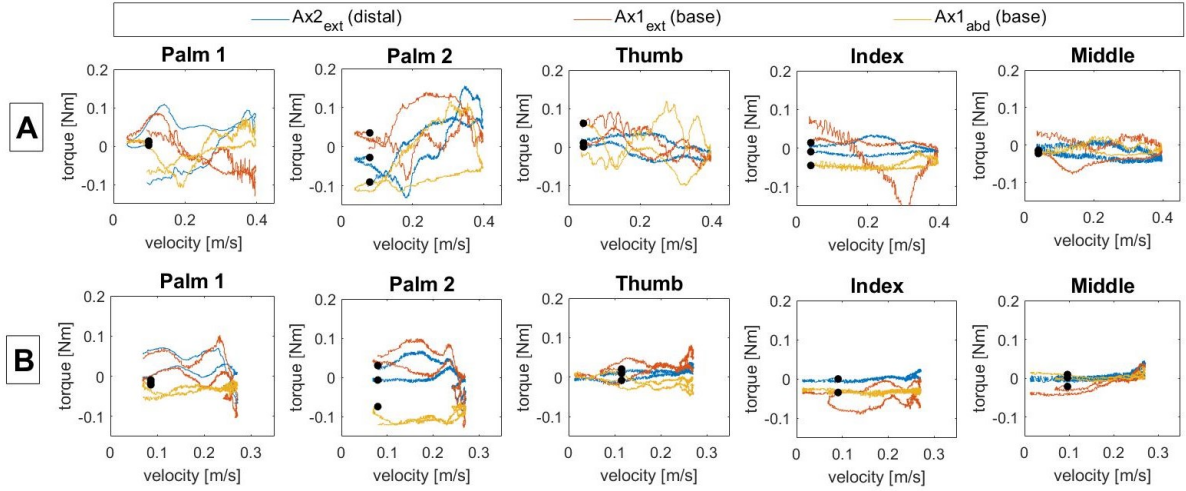


Figure D.27: Measured torques plotted over the velocity of the human hand exemplary shown for one stroke of the hand trajectory of participant 12 in viscosity group D (upper row) and E (lower row). The torques are plotted for each joint of each finger. Finger 1 and 2 correspond to the robotic fingers attached to the palm of the human hand, while Finger 3-5 attach to the thumb, index finger and middle finger of the human user, respectively. The black dot indicates the starting point of the trajectory.

#### QUESTIONNAIRE

As for the first experiment, the participants were given the questionnaire afterwards, of which the average results are presented in Table D.4. The users indicated to feel safe on the haptic interface. The ratings for the freedom of the hand were slightly lower than observed in the first experiment, which might relate to the given task. The control and intuitivity to move the robot during the haptic interaction were again judged to be good. The task of comparing a given viscosity to a reference was perceived to be a bit easier, but again the rating varied largely (between 2 and 8), indicating that it depends strongly on the individual. The interest in the task was still rather high. The perceived realism of the rendered fluid was on average similar to the one reported for the first experiment, with also 3 participants giving a rating below 5, but only two judging it to be 8 or higher.

Table D.4: Averaged rating of the participants of experiment 2 ( $n = 13$ ) for the rating questions in the questionnaire, where 1 is the worst rating and 10 the best rating with the standard deviation to indicate the spread in rating throughout the participants.

	SYSTEM related				TASK related		
	Robot Safety	Hand Freedom	Control Ease	Control Intuitivity	Task Ease	Task Interest	Realism
P1	10	4	7	8	3	8	8
P2	10	6	7	8	7	7	7
P3	8	4	4	10	4	9	7
P4	10	7	8	8	7	8	7
P5	9	6	5	9	3	7	8
P6	10	6	10	7	6	9	7
P7	10	9	8	10	8	7	6
P8	10	8	9	9	5	9	4
P9	7	4	7	5	8	7	7
P10	10	5	6	9	7	4	5
P11	10	8	10	10	3	7	4
P12	10	8	10	9	2	10	4
P13	8	4	5	7	5	5	6
avg.	9.38	6.08	7.38	8.38	5.23	7.46	6.15
sd	1.04	1.80	2.02	1.45	2.09	1.66	1.46

In this experiment, seven out of the 13 participants indicated that they were missing tactile information of the fluid flowing around the hand, which also relates to the force distribution. Four participants also indicated that temperature sensation could improve the perception of the fluid. Concerning the hardware, six mentioned that they would prefer to feel less constrained by the exoskeleton to move their hand more freely, which had not been mentioned specifically in the first experiment. Additionally, it was indicated, that the fingers themselves were not really needed to complete the task, since much was perceived through the motion of the human arm.

### D.3.5 RESULTS POST-EXPERIMENT

After the main experiment, the participants were asked to explore a solid surface that was rendered with the god-object method [11]. The visualization of this interaction is again not shown to the participant. Instead, instructions are given to arrange the human hand such that it is facing towards the ground and then to be lowered until the user feels something. This feeling is then to be explored and described to the experimenter. The investigated surface is identified to be "hard" or "solid" by 15 out of the in total 26 participants. Out of the remaining 11 people, 9 described it with words like "resistance" or "surface". Out of all, 15 user also explained the object to feel "elastic" or with similar words. Directly asked, if they can identify the object in a virtual environment to be solid, 23 answered "yes". The remaining three explained it felt more like a "balloon" or "foam". In a second part of this post experiment, the participant was asked to repeat the procedure of lowering the hand and describing what was felt. This time a highly viscous fluid was rendered ( $\mu = 16 Pa \cdot s$ ). All participants could identify a noticeable difference when changing the medium from free space to the rendered viscous fluid. The feeling was described as "emerging the hand" or "diving into something". The virtual fluid was described to feel like "honey", "mud" or "goo".

All interactions were observed to be stable with no occurring unwanted oscillations, for the rendered solid and fluid alike.

Almost all participants could identify the flat surface to be solid. However, the feeling was more similar to the one of rubber than a completely rigid object. The felt elasticity is probably caused by too low a commanded stiffness and damping factors, which can be tuned to obtain better results. The important point that was proven with this experiment, is that it was possible with the same control model that rendered the virtual fluid to enable a stable interaction with solid objects, since the update rates were kept high. To the knowledge of the author, this was the first time this was achieved.

## D.4 DISCUSSION

The main results of the user studies have already been discussed in the scientific paper and are therefore not analyzed in more detail in this Appendix. The extended results showed, however, more details about the applied trajectories of the human users. It can be seen that the general hand trajectory and thus exploration procedure are very similar for all participants and throughout both user studies. Even when detaching from the haptic interface in between experiment parts, the motion remained constant. It would be interesting to compare the procedure to the motion of the hand applied in real fluids. A comparable study has not been found in literature. In further studies on the topic of virtual fluids, it would be interesting to track the hand trajectories in real fluids to compare the results to the ones obtained in this study. This could help validate the hypothesis, that the used haptic interface allows an intuitive and more natural interaction with a virtual environment.

The questionnaires revealed, that the hardware was perceived to be safe and easy to control. The task to investigate the virtual fluid, however, was judged to be quite difficult. The perceived difficulty might again relate to the high inherent mechanical viscosity of the device as well as the novelty of the task. In further studies, it could be observed, if learning effects occur and if that can improve the performance. Despite the difficulty of the task and the very limited feedback possibilities, the interactions were judged to feel somewhat realistic, but most participants indicated that sensations like temperature and wetness were missing. Due to the lack of tactile sensations, it might not be possible to recreate the feeling of the interaction with a real fluid yet. Nevertheless, the identification of viscosity as a key property of fluids seems to be possible, which would already allow the interaction with a more elaborate virtual environment, even when solely using force-feedback devices. The importance of tactile senses as well as the interaction possibilities without them could also be investigated in further studies.

## D.5 ADDITIONAL EXPERIMENT

During the experiments carried out, the trajectory of the end effector of the LWR was not recorded. However, it was desired to compare the motion of each robotic finger in comparison to the motion of the robot arm to verify the hypothesis, that the use of the human fingers were of secondary importance, possibly finding a relationship to the rendered viscosity. Therefore, a quick additional study was carried out.

### D.5.1 EXPERIMENT SETUP

In this quick experiment, only five people participated. All were male and between 18 and 46 years old. One of them had no background in engineering nor in the use with robotic or haptic devices. The setup of the experiment was identical to the one explained for experiment 1 and 2 (see section D.3.2). The participants were positioned in front of the haptic interface with the human hand attached to the exoskeleton. They were asked to move their hand as described for the previous two experiments, stroking through the virtual fluid. The participants should not actively focus on the motion of their fingers and hand, in order to maintain natural exploration procedures as would be applied in a real fluid. Therefore, the participants were mentally distracted by the experimenter through talking. The motion of the participants were recorded, in free space, rendered water and higher viscosity where  $\mu$  was set to be 1 and then increased up to 30 Pa·s in steps of 5 Pa·s. Thus, a total of nine viscosities is presented. During each viscosity, 30 seconds are recorded with 1 kHz. For the analysis, the euclidean distance between the LWR end effector and each robotic finger is calculated. Neglecting the constant average distance between each finger tip and the end effector point and visualize the change in distance throughout the stroke, the average distance is additionally subtracted. This results in values around zero, where a positive number indicates an extension of the robotic fingers, meaning a greater distance, and a negative number the flexion of the fingers. It is to be investigated if a pattern can be found between the participants.

### D.5.2 RESULTS

As described in the previous section, the change of distance between the LWR end effector and each robotic finger tip are calculated. The progression is observed over multiple strokes and seems to be repeating itself for all participants. However, due to the short duration of recording (30 sec), only few strokes can be observed and a more dedicated study should be carried out investigating the behavior when interacting with the haptic interface over longer time. However, the focus in this experiment was to compare the motion of the robotic fingers to the one of the LWR end effector per participants for different viscosities. Therefore, for each person a random trajectory out of the recorded data is plotted for each viscosity as shown in figure D.28. As for the joint angles shown for the first two experiments, the beginning of each stroke shown in the graph is in the middle of the backwards motion of the human hand. The first black line indicates the turning point, where the human user changed the motion from backward to forward until reaching the next turning point. It is to be mentioned, that the percentage of the stroke at which the turn occurred in each viscosity differed slightly, due to the natural motion and thus free choosing of trajectory speed and amplitude throughout this experiment. For this reason, the local minima and maxima do not exactly overlap, but were chosen to be shown this way to analyze if a overall pattern can be observed between the viscosities and the participants. The turning points indicated in the figure are the average percentage of the trajectory at which the turn occurred and is only meant to help interpreting the observed data. It can be seen, that the progression for the exoskeleton fingers 1 and 2, which correspond to the palm attachment points, show a similar pattern for participant 1 and 2 for all tested viscosities. The palm point were flexed during when changing the direction from backwards to forward, thus decreasing the distance to the LWR end effector. This fits the findings from the joint angle observation for experiment 1 and 2 (Fig. D.18 and D.26). However, the thumb and index finger of the human hand for participant 2 barely moves during the stroke, while for participant 1 a change can be seen for different viscosities. However, no trend is visible, as change in finger motion seems to occur at random throughout the tested viscosities. For participant 4 and 5, it can be seen that the palm of the human hand was used less, while the human fingers attached to the exoskeleton showed more motion. The curves found for participant 3 seem to be overall more random in their progression. Nevertheless, a similar or at least reoccurring pattern can be observed for all participants, seemingly independent of the rendered viscosity.



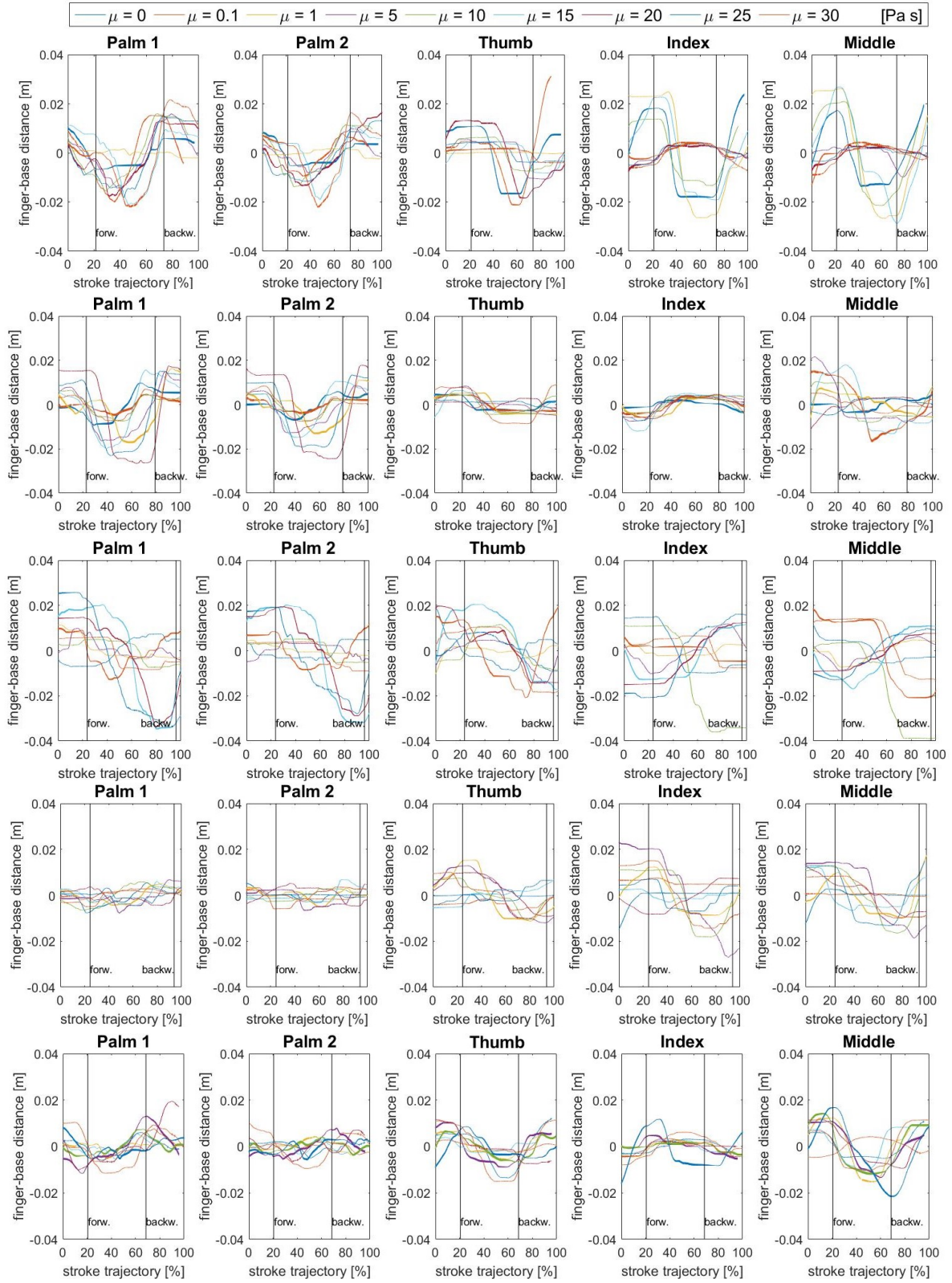


Figure D.28: Distance between exoskeleton fingers 1-5 and LWR end effector point for one exemplary trajectory in different viscosities for participant 1 (first row) to 5 (last row). Finger 1 and 2 respond to the robotic fingers attached to the palm of the human hand, while Finger 3-5 attach to the thumb, index finger and middle finger of the human user, respectively. The black vertical lines indicate a change of moving direction with the associated direction taken after the turn.

### D.5.3 DISCUSSION

No overall pattern can be observed valid for all the different participants. Considering, that a similar hand motion was observed for all participants during the two main experiments, this result is surprising. However, while in the main experiments the users had to investigate the virtual fluid and identify properties, in this additional study, they were only asked to continuously move through the fluid. This might indicate, that a characteristic exploratory procedure is applied when given an investigation task, that is not generally true for interactions in fluids. It appears when only asked to move through the fluid without purpose, every participants applies an individual pattern. This pattern seems to be consistent per person, however, and cannot be observed to be influenced by the rendered viscosity. However, to investigate this further, a larger sample size and more controlled investigation procedures are necessary.



## CRITICAL EVALUATION AND OUTLOOK

The research carried out in this thesis project is bound to limitations of the hardware and force simplifications. The reader should be aware of these constraints when interpreting the findings of this work. The given and chosen assumptions should be reflected upon in the case of future work on the rendering of virtual fluids. Therefore, all identified limitations of this study are summarized in the following.

### E.1 EVALUATION OF THE HAPTIC INTERFACE

The exoskeleton used as haptic interface is a novel device that has not been investigated in any application scenario. To evaluate the research carried out, the issues explained in Appendix A should be considered.

- The dynamics of the system, especially the **remaining friction**, were a limiting factor in the rendering of virtual fluids, as it was impossible to simulate fluids below a certain threshold. Improving the hardware and control model to exclude all friction would enable the comparison with the corresponding physical stimulus, such as water. Creating a system with no perceivable dynamic effects of the hardware would be an important step to enable perfect telepresence. An improvement could be made by implementing a force sensor, preferably in the glove worn by the human. This sensor could measure the exact forces applied by the human. The force measurements could be used to apply a more sufficient feed-forward gain than now by using approximations based on faulty torque measurements.
- The **dynamics of the LWR** should be considered. The robot arm has already been used for haptic interactions and its control implements effective measures to counteract much of the dynamic behavior. Again a threshold remains limiting the ability to render fluids with low viscosity such as water. Additionally, the experiments showed that the friction in each of the LWR's joints seemed to vary slightly. This variation leads to different perceptions of the same viscosity depending on the carried out motion. In hindsight it might have been a better choice to lock the LWR joints and define the human hand motion in more detail to obtain more comparable results. However, the results showed a coherent hand trajectory throughout the experiment for all participants. The variation in the perception were constant and not effect the results of the study. So far it is impossible to fabricate ideal and identical hardware components. Such variations remain and when they are known, the expected influence is very low. It was also noticed that the dynamic deficiencies of the LWR can actually enhance the perception of the virtual fluids. As mechanical viscosity is perceived similar to the one of fluids, it can add realistic effects.

Additionally, the user study revealed some design flaws, that need to be improved in a later revision.

- It is observed, that the **hardware is not yet robust enough** for extensive use. Regularly, connections in the individual fingers became loose, causing them to stop working. Even though, such problems were mostly fast fixes, they delayed some of the experiments. Occasionally, the robot kernel connecting the hardware and software, broke down without identifiable reason. In that case the experiment had to be interrupted for a restart.

- Another flaw are the **magnets of the attachment mechanism**. They were chosen to ensure easy detachment and thus safety in case of an emergency. However, especially when rendering higher viscosity, the user needs to apply more force to the device and the magnetic attachments tend to become loose. In that case, the human user had to adjust the attachment, which interrupted the flow of the experiment.

None of those issues opposed a risk to the user, but did lead to delays. Since this was the first extensive user study with this haptic device, such problems were not foreseeable, but can be prevented for future applications.

## E.2 EVALUATION OF THE FLUID INTERACTION FORCE

The calculation of forces in a fluid is a complicated task (Appendix B). Many factors influence the forces, such as the shape of the emerged body, the kind of fluid, the speed of motion and even the size of the container in which the interaction is carried out. Additionally, external disturbances can occur, e.g leading to wave effects. Taking into account all mentioned effects makes calculations very resource expensive. The interactions were strongly simplified in this project.

- To enable high update frequencies of the rendering loop, **only drag forces are taken into account**. While this is assumed to be sufficient to render viscosity, it neglects important effects, such as lift. This force is noticeable on the human hand when naturally interacting with water. It is possible to calculate the magnitude of the lift forces using equation B.1, but substituting  $C_D$  with the lift coefficient  $C_L$ . The lift coefficient has also been investigated for the interaction with water [25], so that a sufficient curve can be fitted, as explained for  $C_D$ . The calculation of the lift force magnitude has already been implemented in the current rendering algorithm. However, defining the direction of the lift is complicated as it dynamically changes with orientation and pose of the hand. Some authors even distinguish on different kinds of lift (2D- and 3D-lift). The necessity to implement those forces for implementation should be investigated further as it might play a role for manipulations under water. Overall, a study should be carried out to define the forces in a fluid interaction that are important for realistic perception or sufficient application. With such results a sufficient balance can be found between complexity and accuracy of the algorithm and high rendering frequencies.
- For **viscous fluids the force magnitude cannot be verified**. While investigated well for the interaction with water, no literature was available analyzing the forces acting on the human hand in fluids with higher viscosity. Due to the simplifications of the hand shape to a spheroid, it remains unclear if the rendered forces in this scenario are realistic and match the perception of the real fluids. To verify the calculated forces acting on the hand in viscous fluids, a CFD simulation or an experiment should be carried out. This was initially intended in this project, but could not be realized due to missing hardware. However, a hand model has already been fabricated (Fig. E.1). It could be used in further studies to compare the calculated forces with the one occurring in real interactions. The forces can then be scaled accordingly.



Figure E.1: Fabricated hand model to test the validity of the force calculations

- Due to the use of an exoskeleton, the user has **many possibilities to choose a fitting hand position**. The pose, the finger spread as well as the sweepback angle and pitch angle all influence the forces occurring in a fluid interaction. None of those have been investigated in detail in this project, but might also be important. They should therefore be considered in further research.

## E.3 EVALUATION OF THE IMPLEMENTATION

The exoskeleton is a novel system and has not yet been tested as a haptic device. The control algorithm was altered and improved throughout this project and bugs are still being identified. The control loop shown in Appendix A is strongly simplified.

- **No additional gain was added** to the forces calculated in the virtual environment, as it was suspected that the mechanical friction already acted as a gain. This should, however, be validated, e.g. using force sensors on the human side.
- It **remains to prove unconditional stability**. To prove this, a stability analysis should be carried out, taking into account the rendering of the virtual fluids as well as the LWR. Especially the quadratic dependency on velocity should be investigated.

## E.4 EVALUATION OF THE USER STUDIES

The user studies showed consistent perception throughout the participants leading to meaningful results for both carried out experiments. Nevertheless, the findings should be regarded critically and potential pitfalls are to be identified.

- **Biasing of the participants should be avoided**. Despite the intention, to give clear verbal instructions to the users and define procedures beforehand, it cannot be ensured that the participants were not subconsciously influenced since the experimenter knew the goal of the study. To guarantee that the users are not being biased, the experiments should be carried out double-blinded.
- The **hand motion of the users are not defined in detail** to allow a natural exploration procedures. Instead, only a vertical motion of the hand and arm is instructed. This gave the participants freedom to adjust their hand trajectory. Despite observing a consistent motion for all participants within their trial, some of the users mentioned during the experiment, that they perceived the stimulus to be different, depending how they used their hand. This is suspected to be caused by slight varying mechanical properties in the theoretically identical LWR joints. To enable a more consistent perception, it should be considered to lock the LWR joints in a defined position. However, locking the joints would restrict the hand-arm motion of the human. A trade-off between freedom and repeatability exists in this case.
- It was neglected to **record the position of the LWR end effector** during the experiments. This could have offered additional information about how the LWR moved in comparison to the human hand and exoskeleton. In an attempt to still investigate this, an additional user study was carried out. However, only five people participated and no task was given. This lead to ambiguous results. Therefore, in further studies, more attention should be paid to the motion of the LWR. Overall, it would be interesting to investigate more closely, how much the human operator uses the arm for the interaction of a fluid; considering real as well as virtual stimuli.
- It has **not been investigated if the magnitude of the starting stimulus influenced the perception** of the participants during magnitude production part of the first experiment. It should be investigated if a bias exists as well as if the order in which the stimuli are presented play a role.
- The perceived viscosity of the rendered **virtual fluids should be directly compared to real ones**. Even, when system dynamics remain, the comparison should be possible for the higher forces rendered in the virtual viscous fluids of experiment 2. In that case, it is also desirable to carry out the magnitude estimation and production experiment with the virtual fluids of high viscosity. The results could then be compared to available literature [18].
- It is desired to carry out the experiment with a **bigger sample size** to verify the obtained findings. The user study did not show an influence of gender or age for the investigated properties, but the age range was limited and a common engineering background existed. To obtain more meaningful results, a wider variety of people should be tested.

## E.5 CONCLUSION

The carried out research was a first attempt at implementing a haptic rendering algorithm that can run on very high update frequencies. Such frequency is important, when the rendering of the virtual environment should not be limited to virtual fluids, but should also enable realistic perception of rigid bodies. Due to the novelty of the haptic interface design and applied simplification to allow fast force calculations, the findings of this study are bound to many limitations. An important aspect is the improvement of the hardware, which would enable better rendering of fluids with low viscosity and allow a direct comparison to real fluids. Adding more forces, such as lift, might lead to a more realistic feeling during the virtual interaction. Furthermore, the magnitude of the fluid forces is to be validated through (CFD) simulations or experiments to validate the applied simplifications. The haptic rendering loop should be investigated more closely, e.g. carrying out a stability analysis for the complete system to insure the safety of the human user. The user study should be extended to include a wider variety of people. Additionally, it is desired to investigate the magnitude perception for virtual fluids with higher viscosity to compare the findings to literature [18].

Despite all the possible improvements, in hindsight, the applied simplifications seem justifiable and necessary to implement real-time rendering of fluids on the novel haptic interface. The user studies showed, that fluid viscosity can be rendered on high update rates, even when multiple interface points are included. It could be shown that the human is able to stably perceive the virtual viscosity and even identify differences. Thus, the made simplifications show to be a sufficient approximations for first implementation try.

# BIBLIOGRAPHY

- [1] N. Y. Lii, G. Stillfried, Z. Chen, M. Chalon, B. Pleitinger, and A. Maier, *Handexoskelett sowie roboterarm mit solchem handexoskelett*, (23-11-2017), patent DE102017220996.8 (pending).
- [2] N. Y. Lii, J. Dietl, Z. Chen, and B. Pleitinger, *Modularer endeffektor*, (23-11-2017), patent DE102017220999.2 (pending).
- [3] T. Endo, H. Kawasaki, T. Mouri, Y. Ishigure, H. Shimomura, M. Matsumura, and K. Koketsu, *Five-fingered haptic interface robot: Hiro iii*, IEEE Transactions on Haptics **4**, 14 (2011).
- [4] Cyberglove-systems, <http://www.cyberglovesystems.com/cybergasp/overview>.
- [5] I. Sarakoglou, A. Brygo, D. Mazzanti, N. G. Hernandez, D. G. Caldwell, and N. G. Tsagarakis, *Hexotrac: A highly under-actuated hand exoskeleton for finger tracking and force feedback*, in *Intelligent Robots and Systems (IROS), 2016 IEEE/RSJ International Conference on* (IEEE, 2016) pp. 1033–1040.
- [6] X. Gu, Y. Zhang, W. Sun, Y. Bian, D. Zhou, and P. O. Kristensson, *Dexmo: An inexpensive and lightweight mechanical exoskeleton for motion capture and force feedback in vr*, in *Proceedings of the 2016 CHI Conference on Human Factors in Computing Systems* (ACM, 2016) pp. 1991–1995.
- [7] T. Hulin, K. Hertkorn, P. Kremer, S. Schätzle, J. Artigas, M. Sagardia, F. Zacharias, and C. Preusche, *The dlr bimanual haptic device with optimized workspace*, in *Robotics and Automation (ICRA), 2011 IEEE International Conference on* (IEEE, 2011) pp. 3441–3442.
- [8] I. Díaz, J. J. Gil, and T. Hulin, *Stability boundary and transparency for haptic rendering*, in *Advances in haptics* (InTech, 2010).
- [9] S. J. Lederman and R. L. Klatzky, *Hand movements: A window into haptic object recognition*, Cognitive psychology **19**, 342 (1987).
- [10] H. Liu, K. Wu, P. Meusel, N. Seitz, G. Hirzinger, M. Jin, Y. Liu, S. Fan, T. Lan, and Z. Chen, *Multisensory five-finger dexterous hand: The dlr/hit hand ii*, in *Intelligent Robots and Systems, 2008. IROS 2008. IEEE/RSJ International Conference on* (IEEE, 2008) pp. 3692–3697.
- [11] C. B. Zilles and J. K. Salisbury, *A constraint-based god-object method for haptic display*, in *Intelligent Robots and Systems 95. Human Robot Interaction and Cooperative Robots, Proceedings. 1995 IEEE/RSJ International Conference on*, Vol. 3 (IEEE, 1995) pp. 146–151.
- [12] G. Stillfried and P. v. d. Smagt, *Movement model of a human hand based on magnetic resonance imaging (mri)*, in *International Conference on Applied Bionics and Biomechanics (ICABB)* (2010).
- [13] G. Stillfried, U. Hillenbrand, M. Settles, and P. van der Smagt, *Mri-based skeletal hand movement model*, in *The human hand as an inspiration for robot hand development* (Springer, 2014) pp. 49–75.
- [14] A. Pereira, G. Stillfried, T. Baker, A. Schmidt, and N. Y. Lii, *Reconstructing human hand pose and configuration in a fixed-base hand-arm-exoskeleton*, Robotics and Automation Letters (2019), in preparation.
- [15] L. Le Tien, A. Albu-Schaffer, A. De Luca, and G. Hirzinger, *Friction observer and compensation for control of robots with joint torque measurement*, in *Intelligent Robots and Systems, 2008. IROS 2008. IEEE/RSJ International Conference on* (IEEE, 2008) pp. 3789–3795.
- [16] *Fraunhofer institute for computer graphics reserach - instantreality*, [doc.instantreality.org/documentation/getting-started/](http://doc.instantreality.org/documentation/getting-started/), accessed: 2018-07-25.
- [17] J. J. Gil and E. Sanchez, *Control algorithms for haptic interaction and modifying the dynamical behavior of the interface*, in *2nd international conference on Enactive Interfaces* (2005) pp. 17–18.

- [18] W. M. B. Tiest, *Tactual perception of liquid material properties*, Vision research **109**, 178 (2015).
- [19] M. Vines, J. Mora, and W.-S. Lee, *Real-time haptic display of fluids*, in *Proceedings of the 2nd Canadian Conference on Computer Science and Software Engineering* (ACM, 2009) pp. 149–153.
- [20] M. Vines, J. Mora, and W.-S. Lee, *Haptic display of 3d liquids for interactive applications*, in *Games Innovations Conference, 2009. ICE-GIC 2009. International IEEE Consumer Electronics Society's* (IEEE, 2009) pp. 140–148.
- [21] I. P. Herman, *Physics of the human body* (Springer, 2016).
- [22] A. Wacker Chemie, *Solid and liquid silicone rubber-material and processing guidelines*, (2011).
- [23] R. Charrondiere, D. Haytowitz, and B. Stadlmayr, *Faolinfoods density database version 2.0. 2012*, in *Food and agriculture organization of the United Nations technical workshop report* (2012).
- [24] B. Lautrup, *Physics of continuous matter: exotic and everyday phenomena in the macroscopic world* (CRC Press, 2004).
- [25] J. Van Houwelingen, S. Schreven, J. B. Smeets, H. J. Clercx, and P. J. Beek, *Effective propulsion in swimming: grasping the hydrodynamics of hand and arm movements*, Journal of applied biomechanics **33**, 87 (2017).
- [26] M. A. Berger, G. de Groot, and A. P. Hollander, *Hydrodynamic drag and lift forces on human hand/arm models*, Journal of Biomechanics **28**, 125 (1995).
- [27] K. Matsuuchi, T. Miwa, T. Nomura, J. Sakakibara, H. Shintani, and B. Ungerechts, *Unsteady flow field around a human hand and propulsive force in swimming*, Journal of biomechanics **42**, 42 (2009).
- [28] D. A. Marinho, A. I. Rouboa, F. B. Alves, J. P. Vilas-Boas, L. Machado, V. M. Reis, and A. J. Silva, *Hydrodynamic analysis of different thumb positions in swimming*, Journal of sports science & medicine **8**, 58 (2009).
- [29] M. Bilinauskaite, V. R. Mantha, A. I. Rouboa, P. Ziliukas, and A. J. Silva, *Computational fluid dynamics study of swimmer's hand velocity, orientation, and shape: contributions to hydrodynamics*, BioMed research international **2013** (2013).
- [30] H. Takagi, Y. Shimizu, A. Kurashima, and R. Sanders, *Effect of thumb abduction and adduction on hydrodynamic characteristics of a model of the human hand*, in *ISBS-Conference Proceedings Archive*, Vol. 1 (2001).
- [31] B. Bixler and S. Riewald, *Analysis of a swimmer's hand and arm in steady flow conditions using computational fluid dynamics*, Journal of biomechanics **35**, 713 (2002).
- [32] Y. Sato and T. Hino, *Estimation of thrust of swimmer's hand using cfd*, in *Proceedings of second international symposium on aqua bio-mechanisms* (2003) pp. 81–86.
- [33] S. Kudo, R. Vennell, B. Wilson, N. Waddell, and Y. Sato, *Influence of surface penetration on measured fluid force on a hand model*, Journal of Biomechanics **41**, 3502 (2008).
- [34] J. van Houwelingen, W. van de Water, and G. van Heijst, *Three-dimensional simulations of a swimmer's hand using an immersed boundary method*, Unpublished Master Thesis. Technische Universiteit Eindhoven (2013).
- [35] J. John D. Anderson, *Introduction to flight*, (1989).
- [36] E. M. White and I. Corfield, *Viscous fluid flow*, Vol. 3 (McGraw-Hill New York, 2006).
- [37] H. Toussaint and M. Truijens, *Biomechanical aspects of peak performance in human swimming*, Animal Biology **55**, 17 (2005).
- [38] J. van Houwelingen, D. H. Willemsen, R. P. Kunnen, G. F. van Heijst, E. J. Grift, W. P. Breugem, R. Delfos, J. Westerweel, H. J. Clercx, and W. van de Water, *The effect of finger spreading on drag of the hand in human swimming*, Journal of biomechanics **63**, 67 (2017).



- [39] Y. Sato and T. Hino, *A computational fluid dynamics analysis of hydrodynamic force acting on a swimmer's hand in a swimming competition*, Journal of sports science & medicine **12**, 679 (2013).
- [40] M. Samson, T. Monnet, A. Bernard, P. Lacouture, and L. David, *Hydrodynamic angles, orientation and velocity of the hand in front crawl swimming*, in *ISBS-Conference Proceedings Archive*, Vol. 33 (2016).
- [41] T. SANGYO, *Food products viscosity data chart*, (2018).
- [42] W. M. B. Tiest, A. C. Vrijling, and A. M. Kappers, *Haptic discrimination and matching of viscosity*, IEEE transactions on haptics **6**, 24 (2013).
- [43] H. M. Jaeger, S. R. Nagel, and R. P. Behringer, *Granular solids, liquids, and gases*, Reviews of modern physics **68**, 1259 (1996).
- [44] Y. Taamneh, *Cfd simulations of drag and separation flow around ellipsoids*, Jordan Journal of Mechanical and Industrial Engineering **5**, 129 (2011).
- [45] A. Richter and P. A. Nikrityuk, *Drag forces and heat transfer coefficients for spherical, cuboidal and ellipsoidal particles in cross flow at sub-critical reynolds numbers*, International Journal of Heat and Mass Transfer **55**, 1343 (2012).
- [46] J. W. Garrett, *The adult human hand: some anthropometric and biomechanical considerations*, Human factors **13**, 117 (1971).
- [47] G. A. Gescheider, *Psychophysics: the fundamentals* (Psychology Press, 2013).
- [48] S. S. Stevens, *Problems and methods of psychophysics*. Psychological Bulletin **55**, 177 (1958).
- [49] T. Engen, *Psychophysics*, in *States of brain and mind* (Springer, 1988) pp. 89–91.
- [50] S. Sudman and N. M. Bradburn, *Asking questions: a practical guide to questionnaire design*. (1983).
- [51] J. P. Robinson, P. R. Shaver, and L. S. Wrightsman, *Measures of personality and social psychological attitudes: Measures of social psychological attitudes*, Vol. 1 (Academic Press, 2013).

**F**

**ADDITIONAL DOCUMENTS**

## **F.1 CONSENT FORM - EXPERIMENT 1**

# Consent form for participants

---

## Magnitude perception of virtual fluid stimuli

### Researcher

Annika Schmidt - MSc student  
Email: [annika.schmidt@dlr.de](mailto:annika.schmidt@dlr.de)

### Location of the experiment

Modex Lab RM (1st floor, room 1428)  
Institute of Robotics and Mechatronics (Building 135)  
Deutsches Zentrum für Luft- und Raumfahrt  
Oberpfaffenhofen, DE

**Duration:** The experiment will take approximately 1 hour.

---

### Introduction

Please read this consent document carefully before you decide to participate. This document describes the purpose, procedures, and potential risks/discomforts. Your signature is required for participation. If you desire a copy of this consent form, you may request one.

### Background

Haptic User Interfaces have been investigated increasingly within the last two decades. Many systems have been developed, through which it is possible for a human user to interact with a remote or virtual environment, while not only getting audio and visual feedback, but also feeling reaction forces. In order to enable the human to explore a virtual or remote environment freely and with natural exploration procedures, haptic interfaces have been developed that are attached to the human hand. So called hand exoskeletons can render the reaction forces of the interaction with a virtual solid object, even incorporating friction and textures. However, it would also be desirable to also enable the interaction with virtual fluids. This can improve gaming experience, exploration of unknown remote areas and training simulations for medical applications.

### Purpose of Study

"Viscosity" refers to the resistance of a fluid, that is how "thick" it feels. Water has for example a rather low viscosity, while the viscosity of honey is higher. It is the goal of this study to investigate if, based only on the rendering of viscosity, humans can identify virtual fluids using a hand exoskeleton.

## General procedures and instructions

### Before the experiment

You will get a cleaning glove to put on your left hand. With this hand you stir in a bucket of water for approximately 1 minute. You are asked to compare the feeling of moving in water with the feeling of moving your hand around in free space. **The feeling of water in comparison to the free space will be your reference stimulus and set to be 100 %.** Afterwards, you will be equipped with a glove to attach your right hand to the exoskeleton. Additionally you will get hearing protection, so you do not get distracted.

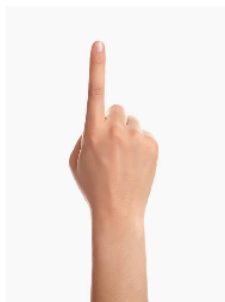
After being attached to the robot, you should move around freely for 2-3 minutes. During this time the robot will be simulating free space and everything you feel is due to the dynamics of the mechanical system. You will then be presented with some test viscosities to get a feeling for it. After accustoming to the feeling attached to the system, the experiment will start.

### Experiment

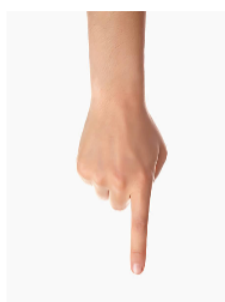
The experiment consists of two parts. The sequence of the two parts can differ. In between the two parts, you will get a short break, during which you can detach from the robot, relax your hand and feel the water bucket again. Your answers given during the the experiments, will be recorded.

In the first part, a variety of virtual fluids will be presented to you. For each fluid you are required to estimate its viscosity with reference to virtual water, where virtual water will be 100 % and free space will be 0 %. For example, if you feel the fluid to be twice as viscous as water, you should estimate 200 %, half as viscous would be 50 %. You have time to explore each viscosity as long as you wish, eventually giving a verbal answer of how you perceive the viscosity.

In the second part, you will be exposed to a virtual fluid of random viscosity and have to indicate (see figure below), if the viscosity should be raised or lowered until it matches the feeling of moving through water (100 %).



raise stimulus



lower stimulus



stimulus matches reference (water)

### After the experiment

After finishing the experiment, you are asked to fill out a short questionnaire.

## **Risks/Discomforts and Right to refuse/withdraw**

There are no known risks for you in this study. A feeling of discomfort might arise from wearing the glove with which you will be attached to the robot for too long. If at any point you begin to feel uneasy for any reason, please do not hesitate to inform the experimenter. We can then allow you to take a break. If you do not wish to continue the experiment for any reason, you are free to withdraw from it at any point in time as the participation is entirely voluntary.

## **Confidentiality**

All data collected in this study will be kept confidential and will be used for research purposes only. You will not be personally identifiable in any future publications based on this work.

I have read and understood the information provided above. I give permission to process the data for the purposes described above. I voluntarily agree to participate in this study.

---

Date

---

Name

---

Signature

---

Participant number (by experimenter)

For any questions, please email [annika.schmidt@dlr.de](mailto:annika.schmidt@dlr.de)



## F.2 CONSENT FORM - EXPERIMENT 2

# Consent form for participants

---

## Discrimination of viscosities of virtual fluids

### Researcher

Annika Schmidt - MSc student  
Email: [annika.schmidt@dlr.de](mailto:annika.schmidt@dlr.de)

### Location of the experiment

Modex Lab RM (1st floor, room 1428)  
Institute of Robotics and Mechatronics (Building 135)  
Deutsches Zentrum für Luft- und Raumfahrt  
Oberpfaffenhofen, DE

**Duration:** The experiment will approximately take 1 hour.

---

### Introduction

Please read this consent document carefully before you decide to participate. This document describes the purpose, procedures, and potential risks/discomforts. Your signature is required for participation. If you desire a copy of this consent form, you may request one.

### Background

Haptic User Interfaces have been investigated increasingly within the last two decades. Many systems have been developed, through which it is possible for a human user to interact with a remote or virtual environment, while not only getting audio and visual feedback, but also feeling reaction forces. In order to enable the human to explore a virtual or remote environment freely and with natural exploration procedures, haptic interfaces have been developed that are attached to the human hand. So called hand exoskeletons can render the reaction forces of the interaction with a virtual solid object, even incorporating friction and textures. However, it would also be desirable to also enable the interaction with virtual fluids. This can improve gaming experience, exploration of unknown remote areas and training simulations for medical applications.

### Purpose of Study

"Viscosity" refers to the resistance of a fluid, that is how "thick" it feels. Water has for example a rather low viscosity, while the viscosity of honey is higher. It is the goal of this study to investigate if, based only on the rendering of viscosity, humans can identify virtual fluids using a hand exoskeleton.

## General procedures and instructions

### Before the experiment

You will be equipped with a glove to attach your right hand to the hand exoskeleton. Additionally, you might get hearing protection, so you do not get disturbed.

After being attached to the robot, you should move around freely for 2-3 minutes. During this time there will be no forces acting and everything you feel is due to the dynamics of the mechanical system. After accustoming to the feeling attached to the system, the experiment will start.

### Experiment

First, a reference viscosity will be presented, which you can explore freely. Next, the first test viscosity will be presented. You need to decide on the viscosity by answering the question "Does this viscosity feel thicker than the reference viscosity?" with "Yes" or "No". In total, eight test viscosities will be presented in random order. Between each of them, the reference will be presented again.

The experimenter will signal a fist whenever the reference viscosity is presented and one finger pointing for the test viscosity. You can signal the experimenter that you are ready for the next stimulus by indicating okay (see figure below). Your "Yes" and "No" answers during the experiment will be recorded.



### After the experiment

After finishing the experiment, you are asked to fill out a short questionnaire.

## **Risks/Discomforts and Right to refuse/withdraw**

There are no known risks for you in this study. A feeling of discomfort might arise from wearing the glove with which you will be attached to the robot for too long. If at any point you begin to feel uneasy for any reason, please do not hesitate to inform the experimenter. We can then allow you to take a break. If you do not wish to continue the experiment for any reason, you are free to withdraw from it at any point in time as the participation is entirely voluntary.

## **Confidentiality**

All data collected in this study will be kept confidential and will be used for research purposes only. You will not be personally identifiable in any future publications based on this work.

I have read and understood the information provided above. I give permission to process the data for the purposes described above. I voluntarily agree to participate in this study.

---

Date

---

Name

---

Signature

---

Participant number (by experimenter)

For any questions, please email [annika.schmidt@dlr.de](mailto:annika.schmidt@dlr.de)

# F.3 PLAN OF PROCEDURE

# Plan of Procedure

---

## Before the userstudy

- ☐ check all fingers
- ☐ check the positions (fit Simulink to actual position)
- ☐ tighten all magnet holder
- ☐ print consent form
- ☐ print questionnaire
- ☐ start LN and robots

## During the userstudy

- ☐ greet participant
- ☐ let them sign form of consent
- ☐ show participant set up and robot
- ☐ explain the procedures
  - Magnitude Estimation / Magnitude Production
  - Method of constant stimuli
- ☐ explain hand gestures
- ☐ give the participant chance to ask questions and make sure they understand the procedure
- ☐ give participant cleaning glove and let them move their hand in water

*"Pay attention to how the viscosity feels, especially in comparison to moving in free space"*

- ☐ dress participant's hand in glove and attach to the exoskeleton
- ☐ position participant in front of the exoskeleton
- ☐ give participant adjustment time to move around freely (without any objects/forces) to get used to the system

*"Try out some different speeds and get familiar with the system."*

*"This is how the robot feels in free space. Therefore it cannot feel 1-1 like moving your hand in water. Imagine rather you are dragging something **THROUGH** a fluid"*

- ☐ go through different viscosities to give participant a chance to get used to the system (Training)

*"I will go through possible viscosities, so you get an idea of what you will feel during during the experiment"*

- ☐ activate virtual fluid

*"I want you to explore the fluid like you would a real fluid. Use this hand motion (s h o w) and a natural feeling velocity"*



- ☐ start video
- ☐ start data recording
- ☐ carry out user study
  - Magnitude: 9 stimuli (0:50:400 % of water, random order), 3 repetitions, break between Prod. and Est.
  - Viscosity: 1 reference stimulus, 8 test stimuli (random order), group D and E, each 5 repetitions
- ☐ **Post-experiment:**
  - present "solid" object to participant
  - participant can switch between solid and fluid
  - participant should give three words for each object
- ☐ detach participant from robot
- ☐ ask them to fill out questionnaire
- ☐ give them candy!!!!

#### **After the experiment**

- ☐ punch together sheets per participant
- ☐ put consent form into folder
- ☐ scan all sheets
- ☐ transfer recorded data to Matlab file
- ☐ transfer video data
- ☐ check that all recorded data are there
- ☐ make backup (after each day)

# F.4 QUESTIONNAIRE

Thank you for participating in this user study. To help interpret the results better, a little peak in your head might be helpful, so please fill out this short questionnaire. You have my eternal gratefulness and a small Thank-you-Snack afterwards. ☺

4. Do you possess background knowledge about the field of haptics? If so, which?
- ☐ Yes, \_\_\_\_\_
- ☐ No
5. Have you used a haptic user interface before? If so, what?
- ☐ Yes, \_\_\_\_\_
- ☐ No

**6. How did you feel during the interaction with the robot?**

very safe	<input type="checkbox"/> — <input type="checkbox"/> — <input type="checkbox"/> — <input type="checkbox"/> — <input type="checkbox"/> — <input type="checkbox"/> — <input type="checkbox"/> — <input type="checkbox"/> — <input type="checkbox"/> — <input type="checkbox"/>	very unsafe
very restricted	<input type="checkbox"/> — <input type="checkbox"/> — <input type="checkbox"/> — <input type="checkbox"/> — <input type="checkbox"/> — <input type="checkbox"/> — <input type="checkbox"/> — <input type="checkbox"/> — <input type="checkbox"/> — <input type="checkbox"/>	very free

**7. How was the motion control of the robot?**

very easy	<input type="checkbox"/> — <input type="checkbox"/> — <input type="checkbox"/> — <input type="checkbox"/> — <input type="checkbox"/> — <input type="checkbox"/> — <input type="checkbox"/> — <input type="checkbox"/> — <input type="checkbox"/> — <input type="checkbox"/>	very hard
very intuitive	<input type="checkbox"/> — <input type="checkbox"/> — <input type="checkbox"/> — <input type="checkbox"/> — <input type="checkbox"/> — <input type="checkbox"/> — <input type="checkbox"/> — <input type="checkbox"/> — <input type="checkbox"/> — <input type="checkbox"/>	very unintuitive

**8. How was the experiment task (to estimate the viscosity)?**

very easy	<input type="checkbox"/> — <input type="checkbox"/> — <input type="checkbox"/> — <input type="checkbox"/> — <input type="checkbox"/> — <input type="checkbox"/> — <input type="checkbox"/> — <input type="checkbox"/> — <input type="checkbox"/> — <input type="checkbox"/>	very hard
very interesting	<input type="checkbox"/> — <input type="checkbox"/> — <input type="checkbox"/> — <input type="checkbox"/> — <input type="checkbox"/> — <input type="checkbox"/> — <input type="checkbox"/> — <input type="checkbox"/> — <input type="checkbox"/> — <input type="checkbox"/>	very boring

**9a. In comparison with a real fluid, how did the virtual fluids feel?**

very realistic	<input type="checkbox"/> — <input type="checkbox"/> — <input type="checkbox"/> — <input type="checkbox"/> — <input type="checkbox"/> — <input type="checkbox"/> — <input type="checkbox"/> — <input type="checkbox"/> — <input type="checkbox"/> — <input type="checkbox"/>	very unrealistic
----------------	---	------------------

- ☺ THANK YOU!! ☺